Max-Planck-Institut für Polymerforschung

Max Planck Institute for Polymer Research

New dynamic bonds using Ru-ligand coordination for photoresponsive materials

Dissertation

Zur Erlangung des Grades

„Doktor der Naturwissenschaften"

am Fachbereich Chemie, Pharmazie und Geowissenschaften

der Johannes Gutenberg-Universität Mainz

Von

Jianxiong Han

geboren in Liaoning, P.R. China

Mainz, 2021

JOHANNES GUTENBERG UNIVERSITÄT MAINZ

Die vorliegende Arbeit wurde im Zeitraum von September 2017 bis September 2021 am Max-Planck-Institut für Polymerforschung in Mainz im Arbeitskreis von

und   angefertigt.

Dekan:

Prodekan:

Gutachter 1:

Gutachter 2:

Date of oral examination:

Table of Contents

Abstract

Photodynamic bonds are stable in the dark but reversibly dissociate/form under light irradiation. Photodynamic bonds are promising building blocks for responsive or healable materials, photoactivated drugs, nano-carriers, extracellular matrices, etc. However, reactive intermediates from photodynamic bonds usually lead to side reactions, which limit their application.

Here, I found that the Ru-Se coordination bond is a photodynamic bond that reversibly dissociates under mild visible light irradiation conditions (chapter 2). I observed that Ru-Se bonds form via the coordination of a selenoether ligand with [Ru(tpy)(biq)(H$_2$O)]Cl$_2$ (tpy = 2,2':6',2"-terpyridine, biq = 2,2'-biquinoline) in the dark, while the Ru-Se bond dissociates reversibly under visible light irradiation. No side reaction was detected in the formation and dissociation of Ru-Se bonds.

In chapter 3, I demonstrate that the Ru-Se bond is applicable to different operating environments. Therefore, I prepared photoresponsive amphiphiles, surfaces, and polymer gels using Ru-Se bonds. The amphiphiles with Ru-Se bonds showed reversible morphological transitions between spherical micelles and bowl-shaped assemblies in dark/light irradiation cycles. The surfaces modified with Ru-Se-bond-containing compounds showed photoswitchable wettability. Polymer gels with Ru-Se crosslinks underwent photoinduced reversible sol-gel transitions, which were used for reshaping and healing. These results demonstrate that the Ru-Se bond is a new dynamic bond for constructing responsive, reprocessable, switchable, and healable materials that work in a variety of environments.

Zusammenfassung

Photodynamische Bindungen sind im Dunkeln stabil. Unter Lichteinstrahlung jedoch, dissoziieren und bilden sich die Bindungen reversibel und ein neues Gleichgewicht stellt sich ein. Photodynamische Bindungen sind vielversprechende Bausteine für responsive oder selbstheilende Materialien, lichtaktivierbare Medikamente, Nano-Transporter, extrazelluläre Matrizen, etc. Allerdings führen reaktive Zwischenprodukte aus photodynamischen Bindungen in der Regel zu Nebenreaktionen, die den Einsatz einschränken.

In meiner Arbeit habe ich gefunden, dass die Ru-Se-Koordinationsbindung eine neue photodynamische Bindung ist, die unter milden Bestrahlungsbedingungen mit sichtbarem Licht reversibel dissoziiert (Kapitel 2). Ich habe beobachtet, dass sich Ru-Se-Bindungen durch die Koordination eines Selenoether-Liganden an [(Ru(tpy)(biq)(H$_2$O)]Cl$_2$ (tpy = 2,2':6',2"-Terpyridin, biq = 2,2'-Bichinolin) im Dunkeln bilden, während die Ru-Se-Bindung unter sichtbarer Lichtbestrahlung reversibel dissoziiert. Bei der Bildung und Dissoziation der Ru-Se-Bindung wurden keine Nebenreaktionen festgestellt.

In Kapitel 3 zeige ich, dass die Ru-Se-Bindung in verschiedenen Umgebungsbedingungen einsetzbar ist. Dazu habe ich photoresponsive amphiphile Moleküle, Oberflächen und Polymergele mit Ru-Se-Bindungen hergestellt. Supramolekulare Aggregate aus amphiphilen Molekülen mit Ru-Se-Bindungen zeigen reversible morphologische Übergänge zwischen kugelförmigen Mizellen und einer schalenförmigen Anordnungen in den Bestrahlungszyklen. Die mit Ru-Se-Verbindungen modifizierten Oberflächen ändern lichtabhängig ihre Benetzbarkeit. Polymergele mit Ru-Se-Vernetzungen durchliefen lichtinduzierte reversible Sol-Gel-Übergänge, die zur Formänderung und Selbstheilung genutzt werden konnten. Die Arbeit zeigt, dass die Ru-Se-Bindung eine neue dynamische Bindung für die Herstellung von responsiven, umformbaren,

schaltbaren und selbstheilenden Materialien ist, die sich in einer Vielzahl von Umgebungen einsetzen läßt.

Motivation

Stimuli-responsive materials have led to the advent of various fascinating applications, such as drug delivery systems, adaptive networks, re-healable materials and biosensing. However, some drawbacks still remain. 1) Side reactions may appear during the stimuli process result in harmful effects on the environment. 2) Most stimuli-responsive materials cannot be reversibly controlled with stimuli that are not adaptive with environments changing;

Developing reversible stimuli-responsive materials carrying new types of dynamic bonds without side effects is an intriguing topic for both fundamental researches and commercial applications. Among numerous dynamic bonds for improving stimuli-responsive materials, photodynamic bonds attract more attention owing to the high spatial and temporal resolution of light.

Although photoinduced reversible dynamic bond formation and dissociation based on cycloadditions/reversions have exhibited excellent performance in photoswitches, most of these photoreactions are triggered by UV light, which can cause photodamage to both organic and biological applications. Another type of photodynamic bond can undergo radical photogeneration for bond exchange, which is reactive and may cause side reactions. To develop the photodynamic bonds and avoid these drawbacks, the ruthenium (Ru) complex is a good choice. To date, several excellent works have proven Ru complexes have the promising dynamic photochemical property for constructing visible light-responsive materials. However, seldom works try to construct visible light-controlled reconfigurable materials based on photodynamic bonds containing Ru moiety. Therefore, the major challenge of photocontrolled materials is seeking a new configurable bond based on Ru backbones which do not lead to side products under visible light stimuli.

In this thesis, I report a new dynamic bond containing Ruthenium (Ru)-Selenium (Se) which can be controlled by visible light. The new photodynamic bond Ru-Se could form in the dark condition and break upon visible light irradiation. Moreover, this new bond could reversibly form and dissociate with dark and light irradiation transitions without any side reaction. Then, I further designed and synthesized a few reconfigurable photocontrolled complexes containing the Ru-Se bonds which are capable of different applications, including photoresponsive amphiphiles, surfaces, and polymer gels. I expect this work could open avenues for both fundamental studies of dynamic bonds and applications of functional materials

Chapter 1: Introduction

1.1 Stimuli-responsive dynamic bonds

1.1.1 The concept and mechanism of dynamic bonds

The molecular synthesis has been dominated traditionally by kinetically controlled reactions, which result in irreversible chemical bond formation. In this manner, it is impossible to reform the starting materials or convert them into another product, which could be a barrier to constructing smart materials. Therefore, recently, more insights have been put into a branch of chemistry where the chemical bonds can be capable of forming and breaking and indeed reversible reforming under thermodynamic control. These chemical bonds with dynamic nature are named dynamic bonds. Based on dynamic bonds, chemists extend and develop dynamic covalent chemistry and supramolecular chemistry which have been considered as powerful synthetic tools in organic synthesis, materials science and biotechnology.[1, 2]

In principle, at ambient conditions, a particular static molecular product can be obtained through an energetic pathway owing to the stability of the dynamic bonds. Under thermodynamic control, associative or dissociative pathways can occur on dynamic bonds.[3] In an associate pathway, dynamic bonds can reversibly break and reform at the same time. As for the dissociative pathway, new linkages should start to form after the previous linkages dissociate. Both pathways can exhibit response behaviors to different stimuli, and try to stay the lowest energy state of the system. The underlying idea of dynamic bond is that desired chemical, physical and biological properties can be achieved by selecting specific molecular species. These species can undergo reversibly assembly and disassembly based on dynamic bonds.

1.1.2 Types of dynamic bonds

According to the bonding type, dynamic bonds can be divided into two categories: dynamic covalent bond and noncovalent dynamic bond (Figure 1).[1]

Dynamic covalent bonds

The dynamic covalent bonds are a type of covalent bond with the sharing of electron pairs between atoms. This bond can undergo a breaking and reformation process under thermodynamic control. Typically, dynamic covalent bonds can be involved in two kinds of dynamic covalent reactions. One type is the formation of new dynamic covalent bonds, such as condensation and additions reactions. The other type of dynamic covalent reaction is the exchange reaction which undergoes the bond exchange process. So far, many groups try their best to develop dynamic covalent bonds in stimuli-responsive materials. For example, alkoxyamine bonds are designed for thermoresponsive self-assembly materials,[4, 5] hydrazones can be a classical chemosensitive functional group for drug delivery,[6] disulfide and diselenide bonds are usually constructed in multifunctional responsive materials, they can be activated by pH, redox and light irradiation for drug delivery, bioimaging and adaptive surface.[7-10] Dynamic covalent bonds can also be categorized into a few types based on atom connections, such as C-C bond,[4, 11-16] C-N bond,[17-20] C-O bond,[21, 22] C-S bond,[23, 24] B-O bond,[25] S-S bond and Se-Se bond.[8, 10, 26-28] However, drawback remains for the dynamic covalent bonds. For breaking dynamic covalent bonds in the reactions, reactive intermediates (free radicals) are always obtained, which lead to side reactions. This will affects the exploration of stimuli-responsive materials based on dynamic covalent bonds.

Noncovalent dynamic bonds

To be more specific, two kinds of molecular interactions are categorized into the noncovalent dynamic bond.

(1) A few supramolecular interactions, such as hydrogen bonding, host-guest interactions and molecular stacking interactions. Most of these interactions are formed by dipole-dipole or electrostatic interactions. For example, the hydrogen bond is formed by dipole-dipole interactions between a hydrogen atom and an electronegative atom with weak bond energies which are typically measured between 5 and 30 kJ/mol. In 1990, Lehn first reported a hydrogen bond for constructing a supramolecular system. So far, supramolecular interactions have already been applied for adhesion, drug delivery, biosensor and luminescent materials.[29-32]

(2) Metal-ligand coordination bonds. Metal-ligand coordination bonds are formed between acceptor metal ions and one or several donor atoms with electron pairs. Metal-ligand coordination bonds have attracted attention owing to their combination properties between functional ligands and the electronic, optical and catalytic potential of metals. Till now, these bonds can play an important role as molecular architecture backbone, polymer network crosslink and fluorescein for stimuli-responsive materials.[33-35]

Overall, compared with dynamic covalent bonds, noncovalent dynamic bonds typically have weaker bond energies, which might be easier formed or cleaved under thermodynamic control. Meanwhile, the use of noncovalent dynamic bonds can efficiently avoid reactive intermediates.
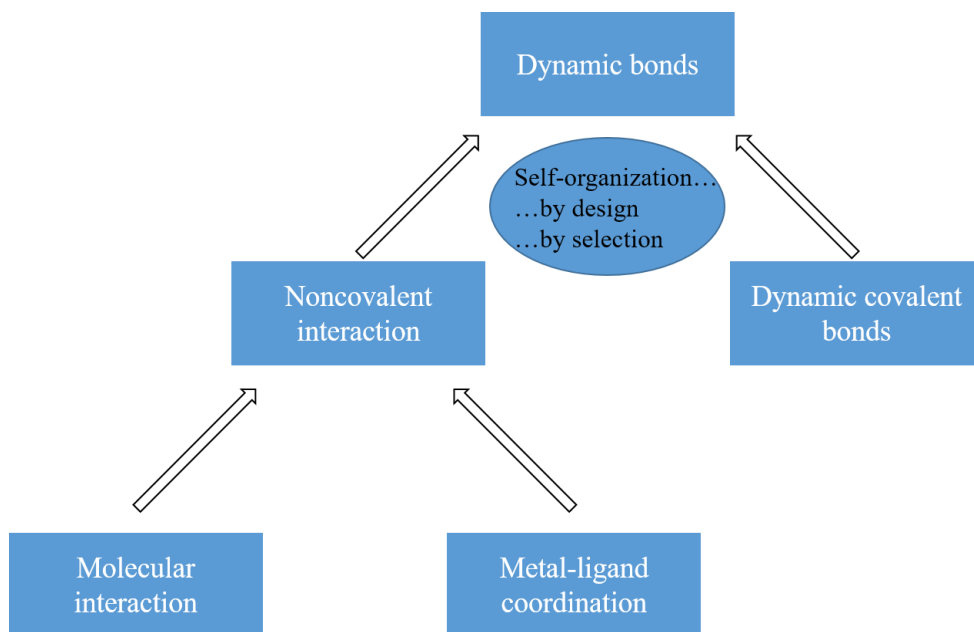
Figure 1. Overview of the structural order of dynamic bonds.

1.1.3 Types of stimuli

As abovementioned, dynamic bonds can be controlled by thermodynamic factors. This factor can be achieved by external environmental stimuli. To date, a series of external stimuli factors have been investigated for the dynamic system and applications, such as light, pH, force, heat and magnetic field. For example, pH-responsive dynamic bonds could reversibly undergo protonation or deprotonation process by changing environment pH value and the molecular structures can be changed for obtaining the desired properties of smart materials. As one of the easiest accessible stimuli, heat can produce energy for exciting the thermoresponsive molecules which further result in the dynamic bond formation or cleavage. Among these external stimuli, the light should be the most attractive according to its high spatial and temporal resolution. Meanwhile, light can be a stimulus with multiple levels of control, such as wavelength and intensity. Therefore,

photodynamic bonds can be an ideal choice for constructing stimuli-responsive materials. In the thesis, we further focus on the photodynamic bonds and their applications.

1.2 Photodynamic bonds for photoresponsive materials

The developments of photoresponsive materials are extremely important due to their controllable and predictable features which are mostly inspired by nature. Typically, response to light stimuli, formation or cleavage of the dynamic bonds could modify intrinsic chemical or physical properties of the materials.[36-40] Recently, photoresponsive materials have led to the advent of various fascinating applications, such as molecular machines,[41, 42] information storage,[37] 4D printing,[43] electronic devices,[38] recycling materials,[44] drug delivery,[45] self-healing[39] and porous materials,[46] etc. In this part, some excellent photosensitive materials containing photodynamic bonds for different applications are introduced.

1.2.1 Photodynamic covalent bonds for photoresponsive materials

To date, a series of light stimuli-responsive molecules have been reported containing photodynamic covalent bonds that can undergo photocycloaddition or photocleavage, such as coumarin,[47] cinnamate,[48] anthracene,[49] alkoxyamines,[4] hexaarylbiimidazoles,[50] spiropyran,[51] sulfides and selenides.[8, 10, 52] These molecules are constructed for various applications, such as self-assembly morphology control, functional surface, shape-memory hydrogels, etc.

For instance, spiropyran is one of the most popular classes of photochromic compounds owing to its photodynamic C-O bond. The reversible interconversion of spiropyran and merocyanine controlled by UV light are widely applied in sensor, photocontrolled actuator and photo-modulated

nanoparticle morphology. In 2015, Klajn and co-workers reported in the spiropyran solution, gold nanoparticles decorated with the carboxylic group could undergo a reversible assembly and disassembly under blue light control (Figure 2).[51] Owing to the photoaddition of the merocyanine derivatives, the deprotonation process could produce H^+ which further constructed intramolecular hydrogen bonds on gold nanoparticles. Therefore, the disassembly of these nanoparticles was achieved according to electrostatic repulsion. When stayed these nanoparticles in an acid environment in the dark, the spiropyran could reverse to merocyanine derivatives owing to the cleavage of dynamic C-O bond. The small gold nanoparticles could aggregate again to form larger particles.
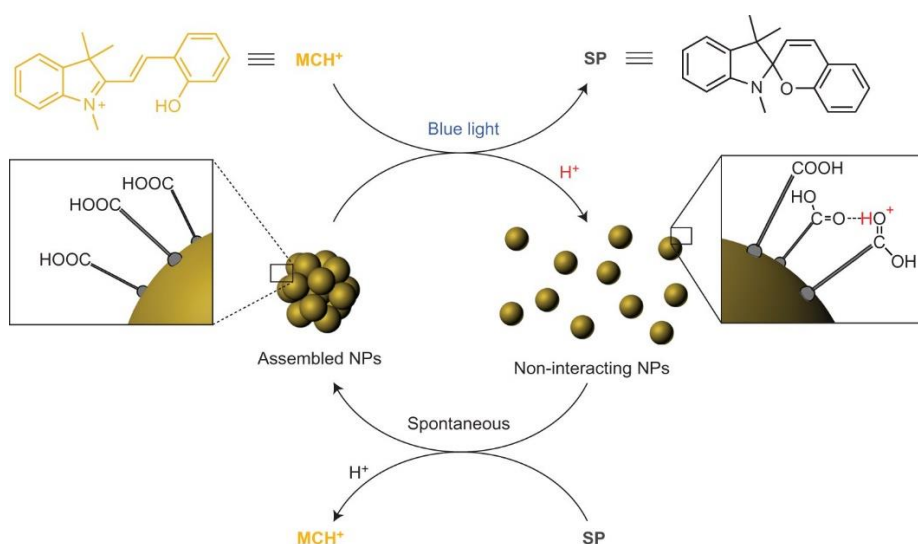
Figure 2. Schematic illustration of a reversible photoinduced nanoparticles aggregation based on the deprotonation and protonation of carboxylic ligands on the surfaces of gold nanoparticles. Adapted with permission from ref 51. Copyright 2015 Springer Nature.

The coumarin derivatives are fabricated as photocages, smart substrates and crosslinking for various photoresponsive applications, such as drug delivery, smart surfaces and hydrogels. Likewise, Wu's group chose coumarin units (C-C bonds) as crosslinks to fabricate reconstructable

gradient structure and reprogrammable 3D hydrogels (Figure 3).[53] The coumarin derivatives acted as crosslinks could reversibly undergo photodimerization/photocleavage under 365/254 nm light irradiation. Through photolithography, a series of gradient structures were reversibly performed on one hydrogel which could be utilized for different configurations. Based on this strategy, a hydrogel containing reversible photocrosslinking that enable reprogramming of the gradient structures and 3D deformations into various configurations.
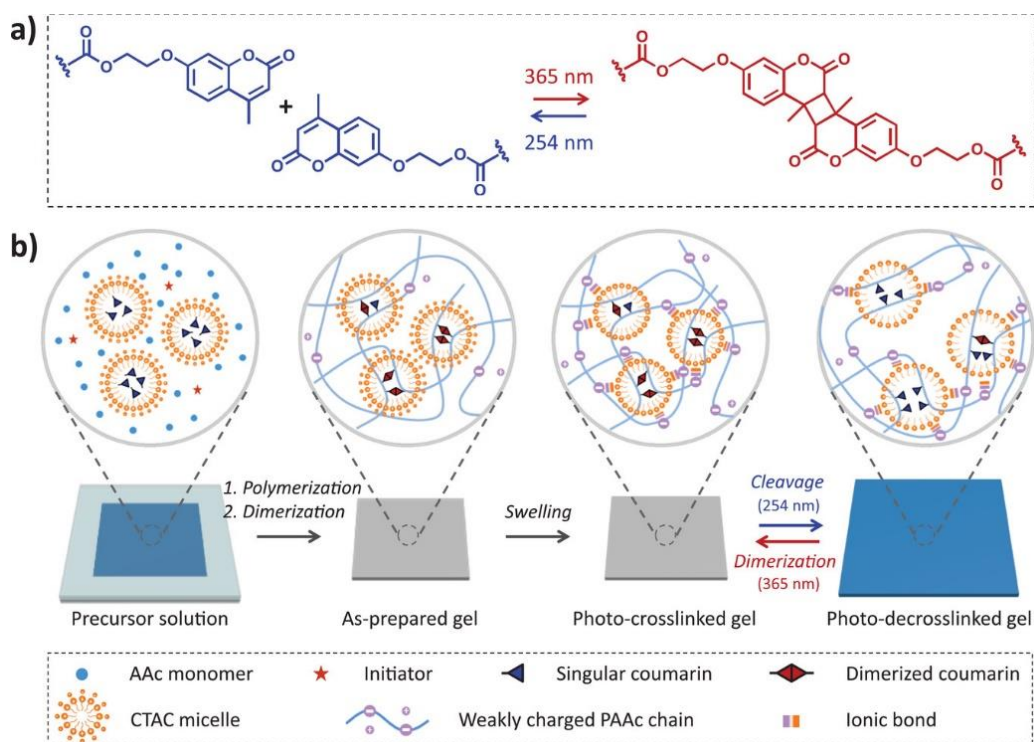
Figure 3. Chemical structure of coumarin units for photodimerization/photocleavage. Schematic illustration of the fabrication of photo-crosslinked and photo-decrosslinked gel. Adapted with permission from ref 53. Copyright 2021 WI LEY VCH Verlag GmbH & Co. KGaA.

Recently, according to visible light-responsive photodynamic S-S and Se-Se bond, sulfides and selenides catch more attention in constructing photoresponsive materials. For instance, in 2019,

Xu and co-workers used photodynamic diselenide bonds (Se-Se) to construct a reconfigurable photocontrolled surface (Figure 4).[54] By designing various diselenide molecules, controlling surface wettability and photopatterning functions were performed on surfaces under visible light control. To demonstrate photopatterning, a surface decorated-containing fluorescent molecule was irradiated by visible light with photomasks for photocleavage. The irradiated part showed darkness which could be observed less than 0.5 min. Furthermore, hydrophobic and hydrophilic diselenide molecules were fabricated for photoswitchable surfaces. Upon visible light irradiation, the breaking of the diselenide bond with functional groups resulted in surfaces losing their hydrophilic or hydrophobic properties. The surface wettability could be switched via the combination of diselenide molecules. This work demonstrated that surfaces based on photodynamic bonds can be reconfigurable and easily controlled.
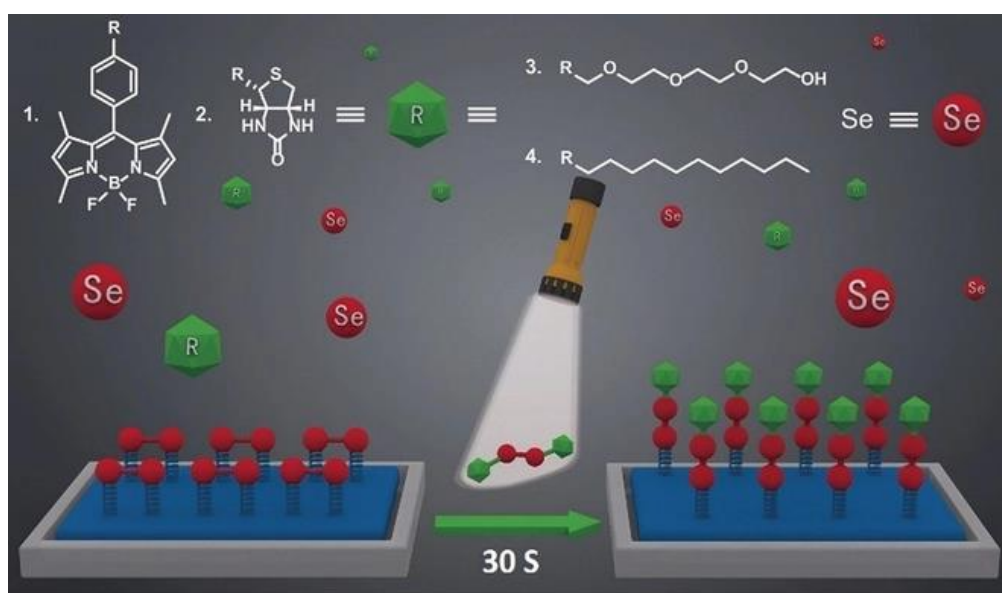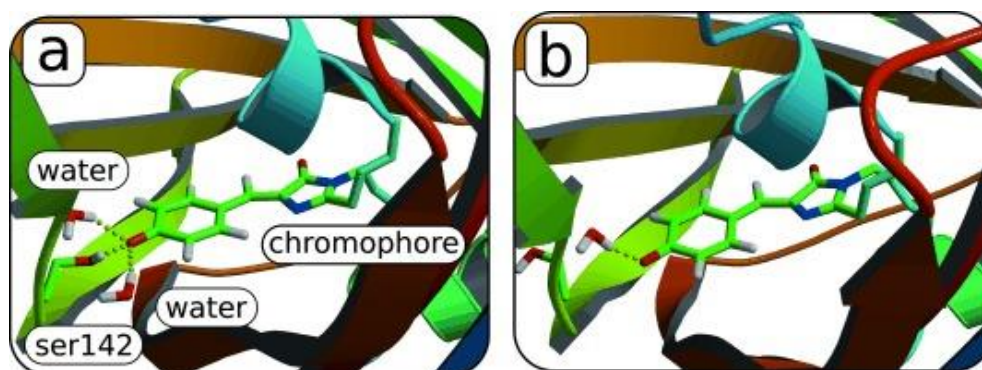

Figure 4. Schematic illustration of fast and reversible surface modification based on dynamic diselenide metathesis. Adapted with permission from ref 54. Copyright 2019 WILEY VCH Verlag GmbH & Co. KGaA.

1.2.2 Photodynamic noncovalent bonds for photoresponsive materials

Since 1987, Donald J. Cram, Jean-Marie Lehn, and Charles J. Pedersen were awarded the Nobel Prize in Chemistry for their excellent work in molecular recognition, which was further developed as supramolecular chemistry. As the main factor, noncovalent bonds or noncovalent interactions are systematically studied. Hence, photodynamic noncovalent bonds have proven that they have outstanding behaviors in sensors, drug delivery and photoelectronic devices.[55-57]

As classical noncovalent bond, the hydrogen bonds can be applied in sensor, drug delivery and bioimaging under the light control. For example, in 2015, Groenhof and co-workers divided the protein ensemble into fluorescent and non-fluorescent by photoisomerization of the chromophore molecules (Figure 5).[58] Upon UV light irradiation, the chromophore planar in the excited state could promote fluorescence which required the formation of the hydrogen bond network. In contract, the network was simply broken off the light.

Figure 5. Schematic illustration of chromophore pocket with the hydrogen bond intact and a transiently broken hydrogen bond network. Adapted with permission from ref 58. Copyright 2015 WI LEY VCH Verlag GmbH & Co. KGaA.

In addition, metal-ligand coordination bond also has great potential in hybrid materials, especially for hydrogels. In 2020, Johnson and co-workers reported a polymer gel containing

poly(ethylene glycol) connected with Cu(II) metal-ligand cages (Figure 6).[59] Coumarin acted as the photosensitized ligands to coordinate with Cu(II) center. In the presence of UV light, the photosensitizer could produce hydrogen to reduce the Cu(II) center to Cu(I) and Cu(0). The reduction process could efficiently break the metal-ligand coordination bond and further lead to network disassembly to solution state. Furthermore, the gelation could be reversibly achieved by oxidation in the dark to reform the metal-ligand cages.
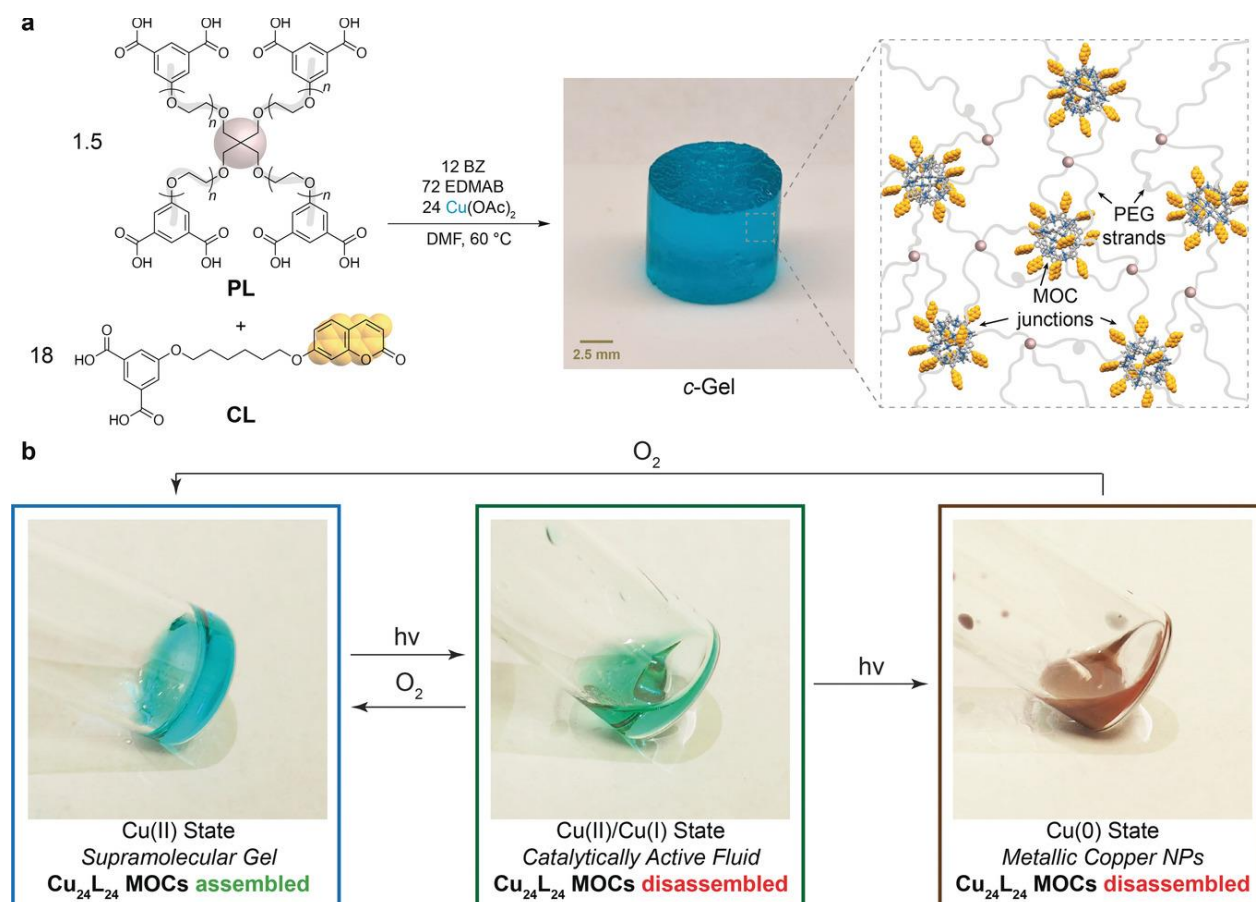
Figure 6. Chemical structure of Cu(II)-ligand complex for crosslinking polymer gel network. Photographs of reversible gel-to-sol transitions by metal-ligand cages. Adapted with permission from ref 59. Copyright 2020 WI LEY VCH Verlag GmbH & Co. KGaA.

**1.3 Ruthenium (Ru)-based dynamic bonds for constructing photoresponsive materials**

Among various photoresponsive materials, recently, Ru complexes are designed and synthesized for excellent photoresponsive materials owing to their photochemical property induced by the metal-ligand charge transfer (MLCT) mechanism. In principle, upon visible light irradiation, some Ru complexes can be photocleavaed through photolabile coordination bonds which result in free ligands and ruthenium residue. The visible light irradiation process could efficiently avoid the photodamage. Moreover, a few works reported that after photoreactions, some photocleaved ligands could reversibly coordinate with the Ru center under suitable conditions. These Ru complexes are even more attractive in stimuli-responsive materials.

1.3.1 Photochemistry of Ru complexes

The first introduction of Ru complexes exhibiting photoreactivity was presented by Dwyer and co-workers in 1963.[60] The photocleavage of ligands from Ru complexes $[Ru(bpy)_2XY]^{n+}$ (bpy = 2,2'-bipyridine, X, Y = monodentate ligand) was obtained upon light irradiation. After that, from 1978, Durham and co-workers systematically reported a few works to illustrated the photoreactions based on Ru complexes. They defined the photosubstitution to describe the process that other ligand spices L (L = water or some polar solvents) could coordinate with Ru backbone after the photocleavage of previous ligands.[61] As for the mechanism of the photosubstitution, a state diagram is clearly shown below (Figure 7). The MLCT band of most Ru complexes is observed from 400-800 nm which belongs to the visible and near-infrared region. Therefore, upon the visible or near-infrared light irradiation, the electronic charge of molecular orbital of Ru center is excited to the singlet MLCT excited state (^{1}MLCT). Then, an intersystem energy crossing transfer process happens from ^{1}MLCT to triplet MLCT excited state (^{3}MLCT). During the energy

transfer, the energy can be released by luminescence or non-radiative pathways or populates the non-bonding d-d state which can induce the cleavage of the ligand.

The first example based on photolytic $[Ru(bpy)_2XY]^{n+}$ complexes for applications was reported by Etchenique and coworkers in 2003.[62] They designed and synthesized a Ru complex $[Ru(bpy)_2(4AP)_2]^{2+}$ (4AP = 4-Aminopyridine) for neurochemical photodelivery. In a leech ganglion, the enhancement of neuron activity was detected attributed by photocleavage of ligands 4AP. Furthermore, different photoliable ligands were designed with type of $[Ru(bpy)_2XY]^{n+}$ complexes for more impressive applications, such as acetonitrile, nicotine and triphenylphosphine. McMillin and co-workers also provided the evidence for dissociative photoreaction of $[Ru(tpy)(bpy)(NCCH_3)]^{2+}$ (tpy = 2,2':6',2"-terpyridine, $NCCH_3$ = acetonitrile) which endowed the potential of photocages applications.[63]
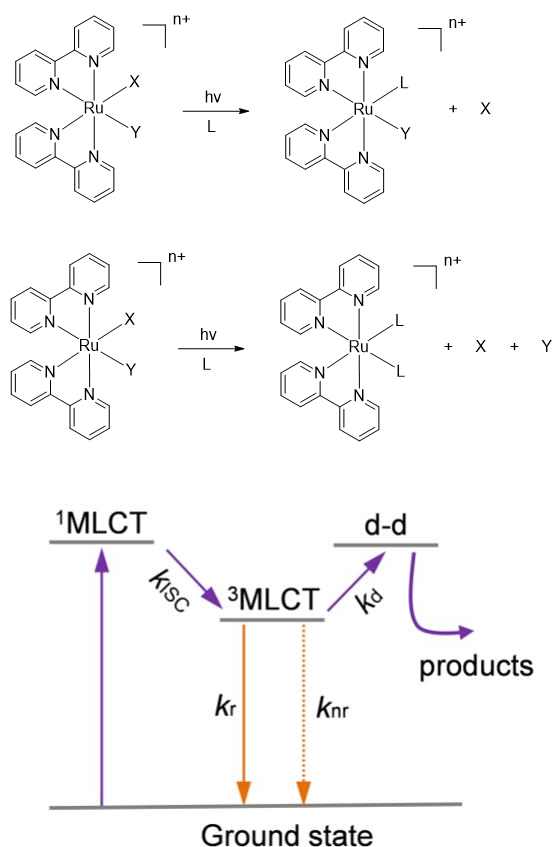
Figure 7. Photocleavage of ligands in the example type $[Ru(bpy)_2XY]^{n+}$ and energy diagram of a photochemical pathway of photolytic Ru complexes.

In addition, some Ru complexes could exhibit a reverse phenomenon between coordination and photosubstitution based on a family of $[Ru(tpy)-(N-N)(L)]^{2+}$ complexes. This was firstly reported by Takeuchi and co-workers in 1988, and further systematically studied in 1993.[64, 65] The first successful application based on the Ru dynamic bonds was reported by Sauvage and co-workers, they designed and synthesized [2]catenane could reversibly coordinate and dissociate with Ru center which was applied for dynamic photocages. Furthermore, a series of Ru-thioether complexes containing Ru-S photodynamic bonds have been systematically studied by Bonnet group.[66]

L = amine, nitrile, thioether

bpy

dcbpy

dmbpy

biq

phen

dmphen
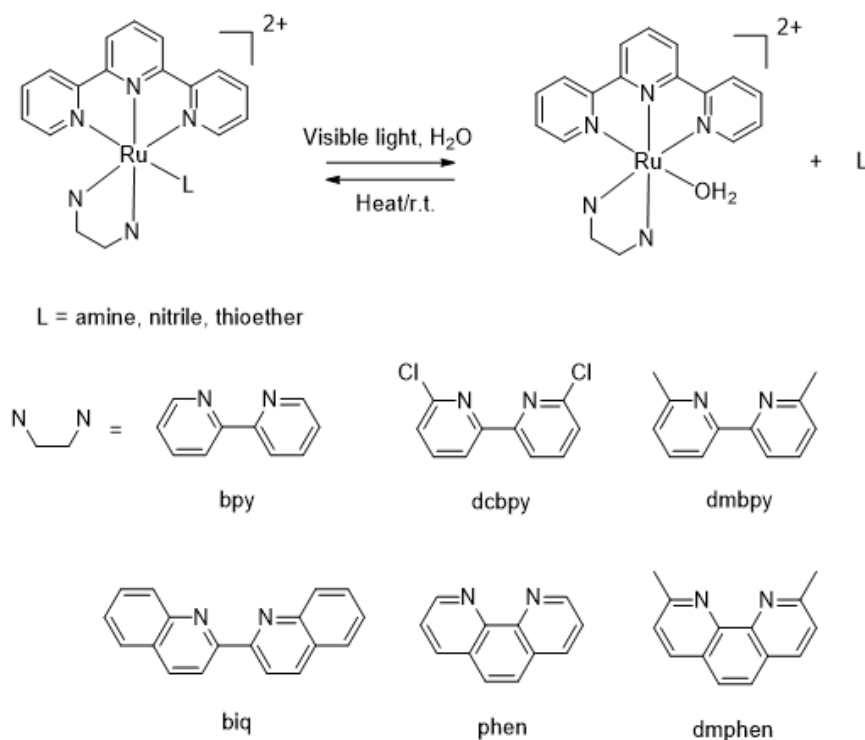
Figure 8. Classic reversible coordination and photosubstitution reaction based on Ru complexes.

1.3.2 Highlights of Ru-based photoresponsive materials

To date, Ru complexes have been successfully fabricated for photoresponsive materials, such as phototherapy, upconverting nanoparticles, switchable surfaces and polymer gels. With an intelligent structural design, these materials could stay stable in the dark and release the functional ligands and Ru moieties upon light irradiation.

1.3.2.1 Photolytic Ru complexes for photoresponsive materials

For instance, our group constructed red light responsive Ru complexes as the main chain into polymeric nanocarriers for phototherapy applications in 2017 and 2020 respectively.[67, 68] Upon red

light irradiation, photosensitized Ru complexes could produce $^1O_2$ which generates the extremely high toxicity to cancer cells. After the first work reported in 2017, we also constructed a bimetallic polymer containing Ru and Platinum (Pt) complexes to fight against drug-resistant tumors in 2020 (Figure 9). Under red light control, the Ru moieties were released for generating $^1O_2$. Meanwhile, the Pt(IV) moieties were reduced inside cancer cells to release cisplatin for chemotherapy. This is the first example of a stimuli-responsive multi-metallic polymer-drug for cisplatin resistance in both vitro and in vivo experiments.
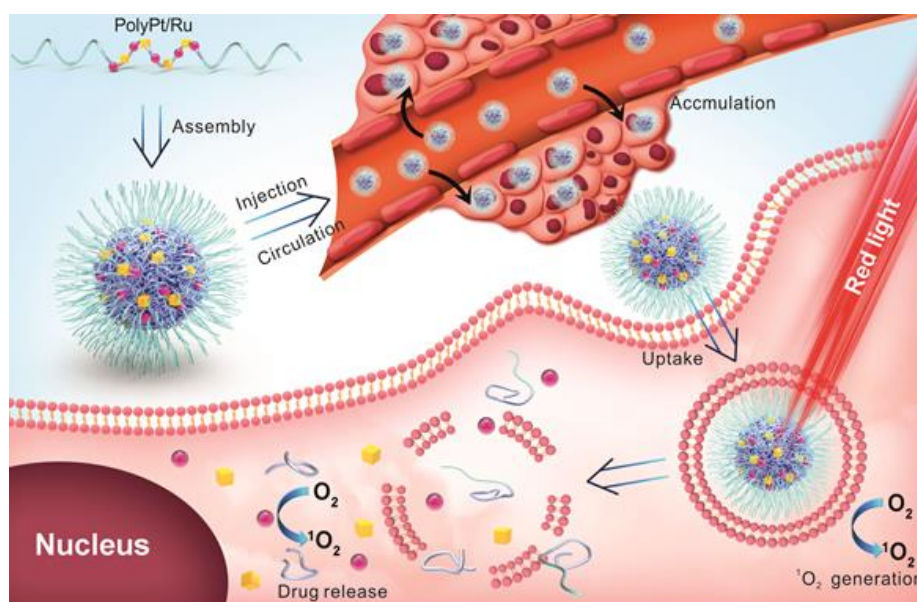
Figure 9. Schematic illustration of self-assembly, extracellular and intracellular processes for anticancer therapy using PolyPt/Ru. Adapted with permission from ref 68. Copyright 2020 WI LEY VCH Verlag GmbH & Co. KGaA.

Furthermore, Ru complexes have excellent performance in near-infrared (NIR) light-responsive upconverting nanoparticles (UCNPs) for drug delivery and photopatterning. In 2015, our group decorated a substrate with UCNPs, proteins and blue light-responsive Ru complexes (Figure 10).[69] Electrostatic interactions were used for adsorbing proteins on Ru-decorated substrate. Upon NIR

light irradiation with photomasks, in the exposed area, NIR light was converted into blue light by exciting UCNPs. The blue light could further induce the photocleavage of Ru complexes and the desorption of the proteins. Protein patterns could be fabricated in this photon upconversion lithography method. This work can open avenues for developing biomaterials, such as migration of cells control, extracellular matrices pattern, regulate inflammation and neurons guidance.
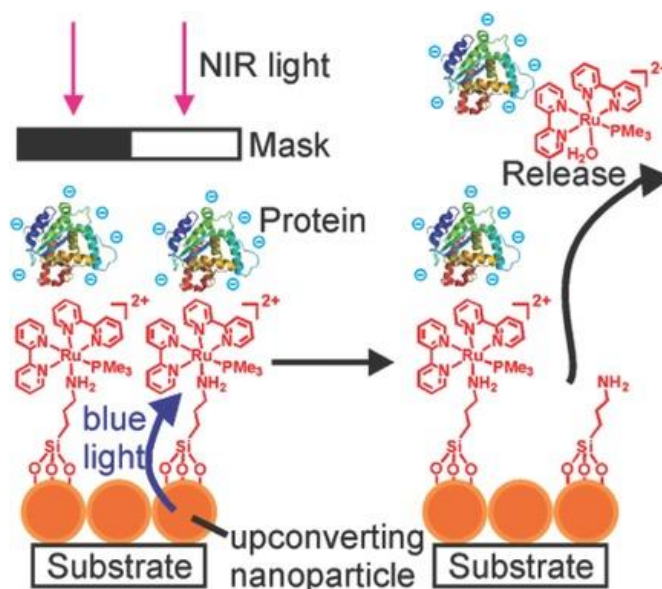
Figure 10. Schematic illustration of photon upconversion lithography by Ru complexes. Adapted with permission from ref 69. Copyright 2015 WI LEY VCH Verlag GmbH & Co. KGaA.

With the development of smart stimuli-responsive materials, more and more photodynamic bonds are introduced in this application. As an outstanding photoresponsive molecule, the construction of photodynamic bonds based on Ru moiety should be considerable. Inspired by the systematical study of Ru-S photodynamic bonds by Bonnet group, photocontrolled reconfigurable surface and anti-freezing polymer gels have been successfully introduced by our group in 2018 and 2020.[70, 71]

**1.3.2.1 Reconfigurable materials containing Ru-based dynamic bonds**

Manipulating surface properties have already been attractive in self-cleaning, flow guiding, protein adsorption, cell adhesion and many other applications.[10, 72-74] The Ru-S bonds are capable of reversible ligand substitution during the transitions between visible light irradiation and in the dark condition. Inspired by the connection between different functional bits and screwdrivers in decoration. We defined an aqueous compound [Ru(tpy-COOH)(biq)(H$_2$O)](PF$_6$)$_2$ (Ru–H$_2$O) (tpy-COOH =6-2,2':6',2"-terpyridin-4'-yloxyhexanoic acid, biq = 2,2'-biquinoline) coating on the glass substrate as the "multi-bit screwdriver", different functional group modified with thioethers could act as the molecular bits. In the dark condition, the mixture of Ru-H$_2$O and modified thioethers, the coordination process between Ru center and thioethers was observed attributed by the formation of Ru-S dynamic bond. Upon the light irradiation, the products of aqueous Ru-H$_2$O and free thioether ligands were obtained due to the photocleavge of Ru-S dynamic bond. Furthermore, these thioethers bits could be reversibly and dynamically connected with "multi-bit screwdriver" surface under light control. Based on this strategy, a series of surface applications, such as surface pattern rewriting, protein adsorption control, and reversible surface wettability was achieved by using different functional thioether bits via photodynamic Ru-S bond.

To demonstrate the reconfigurable functions of Ru–H$_2$O-modified surfaces, two fluoresceins were decorated for the thioether ligands, which further provide the Ru–H$_2$O-modified surfaces with rewriting patterns properties. In the transition from immersion to light irradiation to immersion, different fluorescences were detected on the surface.

Another application based on Ru–H$_2$O-modified surface is reversibly controlling surface wettability. After the fabrication of porous Ru–H$_2$O-modified silica coating, two functional hydrophilic and hydrophobic thioether ligands were selected and synthesized to coordinate on the

surface. The change of water contact angle from hydrophilic Ru-modified surface ($27 \pm 2°$) to hydrophobic Ru-modified ($154 \pm 2°$) illustrated the surface wettability by photosubstitution of Ru-S dynamic bonds.

In addition, the Ru–H_2O-modified surface can also be utilized for protein adsorption/resistance upon visible light irradiation. By coordination between poly(ethylene glycol) modified thioether and the Ru–H_2O, a fluorescence-labeled protein could not be adsorbed on the surface owing to high resistance to the protein property of ethylene glycol. Upon light irradiation with photomask and fluorescence-labeled protein decoration again, the function of protein adsorption/resistance was achieved by the Ru–H_2O-modified surface. Based on this work, we believe that our strategy is versatile for customizable surface functionalization.
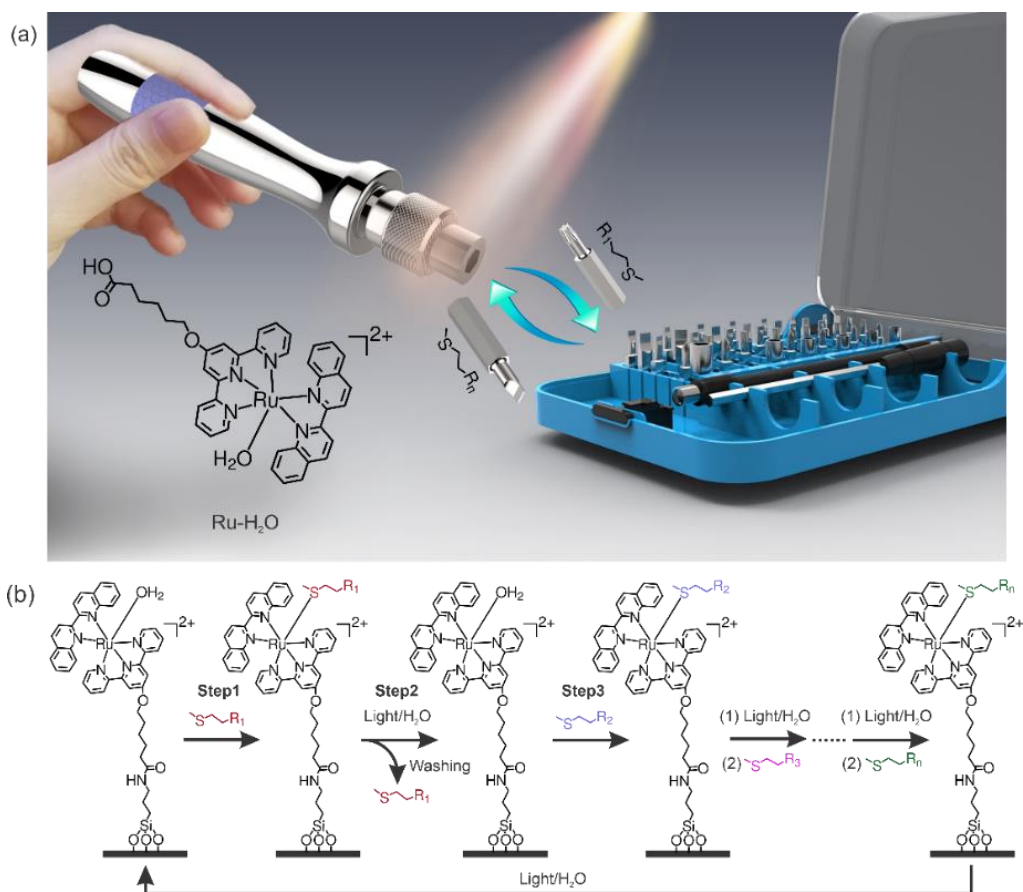
Figure 11. Schematic illustration of photocontrolled reconfigurable surface based on dynamic Ru-thioether coordination bond. Adapted with permission from ref 70. Copyright 2018 Springer Nature

Another reconfigurable application based on Ru dynamic bond is anti-freezing hydrogels. Although photoresponsive polymergels have been utilized in both fundamental researches and commercial applications, such as 3D extracellular matrices,[75] cargo release,[76] adhesion and actuators. Few works report that photoresponsive polymergels can function below freezing temperature owing to the inhibition of photoreactions below 0 °C. In 2020, our group constructed photoresponsive polymergels based on Ru-S dynamic bonds which could reversibly function below the freezing point for the first time.[71]

We fabricated the polymergels by using Ru-thioether complex as crosslinks and H_2O/glycerol as a binary solvent. With a suitable concentration ratio between crosslinks and monomer, the photoresponsive polymergels could undergo gel-to-sol transitions under light control at -20 °C. Upon visible light irradiation, the photocleavage of Ru-S dynamic bonds resulted in the liquefying of polymergels. Keeping the solution in the dark, the polymergels could reverse to the gel state again due to the Ru-S coordination bonds repair.

According to the reversible property of Ru-thioether based polymergels, self-healing and self-erasing were exhibited for applying in photopatterning. Photomasks were covered on a piece of free-standing polymergels film. Irradiating with green light, the pattern appeared due to the photocleavage of Ru-S dynamic bonds, which further transformed Ru-thioether to aqueous Ru complex. Afterward, keeping the film in the dark resulted in the disappearance of black patterns. Moreover, the photopatterning process could even function at −20 °C. Therefore, Ru-S

photodynamic bonds can construct anti-freezing photoresponsive polymergels with gel-to-sol transitions.
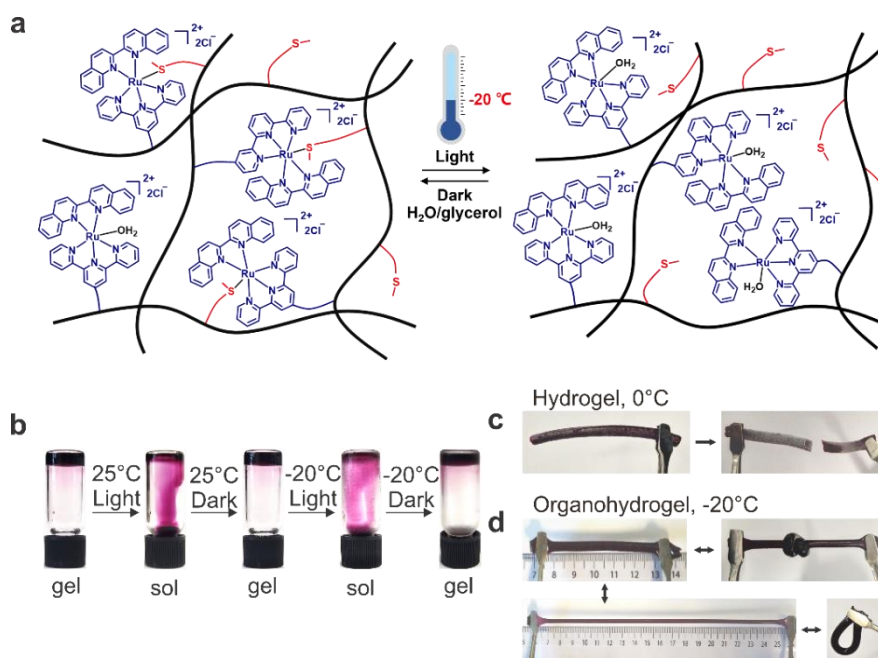
Figure 12. Scheme of photocontrolled organohydrogels based on Ru–thioether crosslinks which function at -20 °C. Adapted with permission from ref 71. Copyright 2020 WI LEY VCH Verlag GmbH & Co. KGaA.

1.3.3 Challenge of Ru-based photodynamic bonds

As abovementioned, a variety of photosensitive Ru complexes have been studied. However, seldom impressive Ru-based photodynamic bonds are used to fabricate reconfigurable photoresponsive materials. Desired exploring of new visible light triggered photodynamic bonds in reconfigurable photoresponsive materials is necessary. Therefore, the major challenges of Ru-based photodynamic bonds for photoresponsive materials are 1) design and synthesize new photodynamic bonds, 2) and the new constructed photodynamic bonds can be reversibly applied for multifunctional applications in different operating environments. In chapter 2, I will present a

new photodynamic Ru-Se bond containing Ru center and selenoether (Se) ligand, which have been fully characterized. To demonstrate that the Ru-Se bond is applicable to different operating environments, in chapter 3, I am going to prepare a variety of Ru-Se complexes for constructing reconfigurable photoresponsive amphiphiles, surfaces, and polymer gels.

1.4 References

[1] Lehn, J.-M., From supramolecular chemistry towards constitutional dynamic chemistry and adaptive chemistry. *Chemical Society Reviews* **2007,** *36* (2), 151-160.

[2] Zhang, W.; Jin, Y., Dynamic covalent chemistry: principles, reactions, and applications. **2017**.

[3] Rowan, S. J.; Cantrill, S. J.; Cousins, G. R.; Sanders, J. K.; Stoddart, J. F., Dynamic covalent chemistry. *Angewandte Chemie International Edition* **2002,** *41* (6), 898-952.

[4] Herder, M.; Lehn, J.-M., The photodynamic covalent bond: sensitized alkoxyamines as a tool to shift reaction networks out-of-equilibrium using light energy. *Journal of the American Chemical Society* **2018,** *140* (24), 7647-7657.

[5] Zhang, M. Q.; Rong, M. Z., Application of alkoxyamine in self-healing of epoxy. *Journal of Materials Chemistry A* **2014,** *2* (18), 6558-6566.

[6] Sonawane, S. J.; Kalhapure, R. S.; Govender, T., Hydrazone linkages in pH responsive drug delivery systems. *European Journal of Pharmaceutical Sciences* **2017,** *99*, 45-65.

[7] Zheng, M.; Åslund, F.; Storz, G., Activation of the OxyR transcription factor by reversible disulfide bond formation. *Science* **1998,** *279* (5357), 1718-1722.

[8] Ji, S.; Cao, W.; Yu, Y.; Xu, H., Visible-light-induced self-healing diselenide-containing polyurethane elastomer. *Advanced Materials* **2015,** *27* (47), 7740-7745.

[9] Wang, Y.; Xu, H.; Zhang, X., Tuning the amphiphilicity of building blocks: controlled self-assembly and disassembly for functional supramolecular materials. *Advanced Materials* **2009,** *21* (28), 2849-2864.

[10] Du, X.; Li, J.; Welle, A.; Li, L.; Feng, W.; Levkin, P. A., Reversible and rewritable surface functionalization and patterning via photodynamic disulfide exchange. *Advanced Materials* **2015,** *27* (34), 4997-5001.

[11] Vongvilai, P.; Angelin, M.; Larsson, R.; Ramström, O., Dynamic combinatorial resolution: direct asymmetric lipase‑mediated screening of a dynamic nitroaldol library. *Angewandte Chemie* **2007,** *119* (6), 966-968.

[12] Masci, B.; Pasquale, S.; Thuéry, P., Supramolecular Control of a Fast and Reversible Diels− Alder Reaction. *Organic letters* **2008,** *10* (21), 4835-4838.

[13] Wang, L.; Zhao, J.; Zhang, P.; Yang, S.; Zhan, W.; Dai, S., Mechanochemical synthesis of ruthenium cluster@ ordered mesoporous carbon catalysts by synergetic dual templates. *Chemistry–A European Journal* **2019,** *25* (36), 8494-8498.

[14] Nakatsuka, S.; Watanabe, Y.; Kamakura, Y.; Horike, S.; Tanaka, D.; Hatakeyama, T., Solvent-Vapor-Induced Reversible Single-Crystal-to-Single-Crystal Transformation of a Triphosphaazatriangulene‑Based Metal–Organic Framework. *Angewandte Chemie International Edition* **2020,** *59* (4), 1435-1439.

[15] Zhang, K.; Zhang, M.; Feng, X.; Hempenius, M. A.; Vancso, G. J., Switching light transmittance by responsive organometallic poly (ionic liquid) s: control by cross talk of thermal and redox stimuli. *Advanced functional materials* **2017,** *27* (41), 1702784.

[16] Ogba, O.; Warner, N.; O'Leary, D.; Grubbs, R., Recent advances in ruthenium-based olefin metathesis. *Chemical Society Reviews* **2018,** *47* (12), 4510-4544.

[17] Orcel, U.; Waser, J., One‑Pot Three‑Component Synthesis of Vicinal Diamines via In Situ Aminal Formation and Carboamination. *Angewandte Chemie International Edition* **2016,** *55* (41), 12881-12885.

[18] Hoerter, J. M.; Otte, K. M.; Gellman, S. H.; Cui, Q.; Stahl, S. S., Discovery and mechanistic study of AlIII-catalyzed transamidation of tertiary amides. *Journal of the American Chemical Society* **2008,** *130* (2), 647-654.

[19] Stephenson, N. A.; Zhu, J.; Gellman, S. H.; Stahl, S. S., Catalytic transamidation reactions compatible with tertiary amide metathesis under ambient conditions. *Journal of the American Chemical Society* **2009,** *131* (29), 10003-10008.

[20] Belowich, M. E.; Stoddart, J. F., Dynamic imine chemistry. *Chemical Society Reviews* **2012,** *41* (6), 2003-2024.

[21] Otera, J., Transesterification. *Chemical reviews* **1993,** *93* (4), 1449-1470.

[22] Cacciapaglia, R.; Di Stefano, S.; Mandolini, L., Metathesis reaction of formaldehyde acetals: an easy entry into the dynamic covalent chemistry of cyclophane formation. *Journal of the American Chemical Society* **2005,** *127* (39), 13666-13671.

[23] Allen, C.; Fournier, J.; Humphlett, W., The thermal reversibility of the Michael reaction: IV. Thiol adducts. *Canadian Journal of Chemistry* **1964,** *42* (11), 2616-2620.

[24] Nair, D. P.; Podgorski, M.; Chatani, S.; Gong, T.; Xi, W.; Fenoli, C. R.; Bowman, C. N., The thiol-Michael addition click reaction: a powerful and widely used tool in materials chemistry. *Chemistry of Materials* **2014,** *26* (1), 724-744.

[25] Brooks, W. L.; Sumerlin, B. S., Synthesis and applications of boronic acid-containing polymers: from materials to medicine. *Chemical reviews* **2016,** *116* (3), 1375-1397.

[26] Chujo, Y.; Sada, K.; Naka, A.; Nomura, R.; Saegusa, T., Synthesis and redox gelation of disulfide-modified polyoxazoline. *Macromolecules* **1993,** *26* (5), 883-887.

[27] Fredga, A., Organic selenium chemistry. **1972**.

[28] Cremlyn, R. J.; Cremlyn, R. J. W., *An introduction to organosulfur chemistry*. John Wiley & Sons: 1996.

[29] Senthilkumar, T.; Lv, F.; Zhao, H.; Liu, L.; Wang, S., Conjugated Polymer Nanogel Binding Anticancer Drug through Hydrogen Bonds for Sustainable Drug Delivery. *ACS Applied Bio Materials* **2019,** *2* (12), 6012-6020.

[30] Gulzar, A.; Gai, S.; Yang, P.; Li, C.; Ansari, M. B.; Lin, J., Stimuli responsive drug delivery application of polymer and silica in biomedicine. *Journal of Materials Chemistry B* **2015,** *3* (44), 8599-8622.

[31] Giubertoni, G.; Burla, F.; Bakker, H. J.; Koenderink, G. H., Connecting the stimuli-responsive rheology of biopolymer hydrogels to underlying hydrogen-bonding interactions. *Macromolecules* **2020,** *53* (23), 10503-10513.

[32] Liu, Z.-F.; Chen, X.; Mou, Z. F.; Jin, W. J., Stimuli-responsive luminescent bithiophene-dicarbaldehyde molecular rotors by hydrogen bonding. *Journal of Materials Chemistry C* **2020,** *8* (45), 16100-16106.

[33] McConnell, A. J.; Wood, C. S.; Neelakandan, P. P.; Nitschke, J. R., Stimuli-responsive metal–ligand assemblies. *Chemical reviews* **2015,** *115* (15), 7729-7793.

[34] Zhan, J.; Li, Q.; Hu, Q.; Wu, Q.; Li, C.; Qiu, H.; Zhang, M.; Yin, S., A stimuli-responsive orthogonal supramolecular polymer network formed by metal–ligand and host–guest interactions. *Chemical Communications* **2014,** *50* (6), 722-724.

[35] Liu, Z.; Zhang, L.; Sun, D., Stimuli-responsive structural changes in metal–organic frameworks. *Chemical Communications* **2020,** *56* (66), 9416-9432.

[36] Endo, K.; Ube, H.; Shionoya, M., Multi-stimuli-responsive interconversion between bowl-and capsule-shaped self-assembled zinc (II) complexes. *Journal of the American Chemical Society* **2019,** *142* (1), 407-416.

[37] Holub, J.; Vantomme, G.; Lehn, J.-M., Training a constitutional dynamic network for effector recognition: Storage, recall, and erasing of information. *Journal of the American Chemical Society* **2016,** *138* (36), 11783-11791.

[38] Zhang, Z.; Chen, Z.; Wang, Y.; Zhao, Y., Bioinspired conductive cellulose liquid-crystal hydrogels as multifunctional electrical skins. *Proceedings of the National Academy of Sciences* **2020,** *117* (31), 18310-18316.

[39] Taylor, D. L.; in het Panhuis, M., Self-healing hydrogels. *Advanced Materials* **2016,** *28* (41), 9060-9093.

[40] Zhou, H.; Xue, C.; Weis, P.; Suzuki, Y.; Huang, S.; Koynov, K.; Auernhammer, G. K.; Berger, R.; Butt, H.-J.; Wu, S., Photoswitching of glass transition temperatures of azobenzene-containing polymers induces reversible solid-to-liquid transitions. *Nature chemistry* **2017,** *9* (2), 145-151.

[41] Krause, S.; Feringa, B. L., Towards artificial molecular factories from framework-embedded molecular machines. *Nature Reviews Chemistry* **2020,** *4* (10), 550-562.

[42] Wilson, M. R.; Solà, J.; Carlone, A.; Goldup, S. M.; Lebrasseur, N.; Leigh, D. A., An autonomous chemically fuelled small-molecule motor. *Nature* **2016,** *534* (7606), 235-240.

[43] Ding, L.; Wang, X.-d., Luminescent Oxygen-Sensitive Ink to Produce Highly Secured Anticounterfeiting Labels by Inkjet Printing. *Journal of the American Chemical Society* **2020,** *142* (31), 13558-13564.

[44] Li, W.-J.; Wang, W.; Wang, X.-Q.; Li, M.; Ke, Y.; Yao, R.; Wen, J.; Yin, G.-Q.; Jiang, B.; Li, X., Daisy chain dendrimers: integrated mechanically interlocked molecules with stimuli-induced dimension modulation feature. *Journal of the American Chemical Society* **2020,** *142* (18), 8473-8482.

[45] Sun, W.; Wen, Y.; Thiramanas, R.; Chen, M.; Han, J.; Gong, N.; Wagner, M.; Jiang, S.; Meijer, M. S.; Bonnet, S., Red-Light-Controlled Release of Drug–Ru Complex Conjugates from Metallopolymer Micelles for Phototherapy in Hypoxic Tumor Environments. *Advanced Functional Materials* **2018,** *28* (39), 1804227.

[46] Yu, K.; Wei, T.; Li, Z.; Li, J.; Wang, Z.; Dai, Z., Construction of Molecular Sensing and Logic Systems Based on Site-Occupying Effect-Modulated MOF–DNA Interaction. *Journal of the American Chemical Society* **2020**.

[47] Fan, W.; Tong, X.; Yan, Q.; Fu, S.; Zhao, Y., Photodegradable and size-tunable single-chain nanoparticles prepared from a single main-chain coumarin-containing polymer precursor. *Chemical Communications* **2014,** *50* (88), 13492-13494.

[48] Jin, B.; Song, H.; Jiang, R.; Song, J.; Zhao, Q.; Xie, T., Programming a crystalline shape memory polymer network with thermo-and photo-reversible bonds toward a single-component soft robot. *Science advances* **2018,** *4* (1), eaao3865.

[49] Gerling, T.; Dietz, H., Reversible covalent stabilization of stacking contacts in DNA assemblies. *Angewandte Chemie* **2019,** *131* (9), 2706-2710.

[50] Honda, S.; Oka, M.; Takagi, H.; Toyota, T., Topology-Reset Execution: Repeatable Postcyclization Recyclization of Cyclic Polymers. *Angewandte Chemie International Edition* **2019,** *58* (1), 144-148.

[51] Kundu, P. K.; Samanta, D.; Leizrowice, R.; Margulis, B.; Zhao, H.; Börner, M.; Udayabhaskararao, T.; Manna, D.; Klajn, R. Light-controlled self-assembly of non-photoresponsive nanoparticles. *Nature communications* **2015,** *7* (8), 646-652.

[52] Ji, S.; Cao, W.; Yu, Y.; Xu, H., Dynamic diselenide bonds: exchange reaction induced by visible light without catalysis. *Angewandte Chemie International Edition* **2014,** *53* (26), 6781-6785.

[53] Zhu, C. N.; Li, C. Y.; Wang, H.; Hong, W.; Huang, F.; Zheng, Q.; Wu, Z. L., Reconstructable Gradient Structures and Reprogrammable 3D Deformations of Hydrogels with Coumarin Units as the Photolabile Crosslinks. *Advanced Materials* **2021,** *33* (18), 2008057.

[54] Xia, J.; Zhao, P.; Zheng, K.; Lu, C.; Yin, S.; Xu, H., Surface Modification based on diselenide dynamic chemistry: towards liquid motion and surface bioconjugation. *Angewandte Chemie International Edition* **2019,** *58* (2), 542-546.

[55] Li, Z.; Davidson-Rozenfeld, G.; Vázquez-González, M.; Fadeev, M.; Zhang, J.; Tian, H.; Willner, I., Multi-triggered supramolecular DNA/bipyridinium dithienylethene hydrogels driven by light, redox, and chemical stimuli for shape-memory and self-healing applications. *Journal of the American Chemical Society* **2018,** *140* (50), 17691-17701

[56] Chen, S.; Leung, F. K.-C.; Stuart, M. C.; Wang, C.; Feringa, B. L., Dynamic assemblies of molecular motor amphiphiles control macroscopic foam properties. *Journal of the American Chemical Society* **2020,** *142* (22), 10163-10172.

[57] Hatai, J.; Hirschhäuser, C.; Niemeyer, J.; Schmuck, C., Multi-stimuli-responsive supramolecular polymers based on noncovalent and dynamic covalent bonds. *ACS applied materials & interfaces* **2019,** *12* (2), 2107-2115.

[58] Morozov, D.; Groenhof, G. Hydrogen bond fluctuations control photochromism in a reversibly photo-switchable fluorescent protein. *Angewandte Chemie* **2016,** *128* (2), 586-588.

[59] Oldenhuis, N. J.; Qin, K. P.; Wang, S.; Ye, H. Z.; Alt, E. A.; Willard, A. P.; Van Voorhis, T.; Craig, S. L.; Johnson, Photoswitchable Sol–Gel Transitions and Catalysis Mediated by Polymer Networks with Coumarin-Decorated $Cu_{24}L_{24}$ Metal–Organic Cages as Junctions. *Angewandte Chemie International Edition* **2020,** *59* (7), 2784-2792.

[60] Dwyer, F.; Goodwin, H.; Gyarfas, E., Mono-and bis-(2, 2'-bipyridine) and-(1, 10-phenanthroline) chelates of ruthenium and osmium. II. Bischelates of bivalent and tervalent ruthenium. *Australian Journal of Chemistry* **1963,** *16* (4), 544-548.

[61] Zayat, L.; Filevich, O.; Baraldo, L. M.; Etchenique, R., Ruthenium polypyridyl phototriggers: from beginnings to perspectives. *Philosophical Transactions of the Royal Society A: Mathematical, Physical and Engineering Sciences* **2013,** *371* (1995), 20120330.

[62] Zayat, L.; Calero, C.; Alborés, P.; Baraldo, L.; Etchenique, R., A new strategy for neurochemical photodelivery: metal-ligand heterolytic cleavage. *Journal of the American Chemical Society* **2003,** *125* (4), 882-883.

[63] Hecker, C.; Fanwick, P.; McMillin, D., Evidence for dissociative photosubstitution reactions of (Ru (trpy)(bpy)(NCCH$_3$))$^{2+}$. Crystal and molecular structure of (Ru (trpy)(bpy)(py))(PF$_6$)$_2$-(CH$_3$)$_2$CO. *Inorganic Chemistry;(United States)* **1991,** *30* (4).

[64] Leising, R. A.; Ohman, J. S.; Takeuchi, K. J., Ligand substitution studies of aquo (phosphine) ruthenium (II) complexes. *Inorganic Chemistry* **1988,** *27* (21), 3804-3809.

[65] Bessel, C. A.; Margarucci, J. A.; Acquaye, J. H.; Rubino, R. S.; Crandall, J.; Jircitano, A. J.; Takeuchi, K. J., Steric ligand effects of six bidentate bipyridyl ligands. *Inorganic chemistry* **1993,** *32* (25), 5779-5784.

[66] Bahreman, A.; Limburg, B.; Siegler, M. A.; Bouwman, E.; Bonnet, S., Spontaneous Formation in the Dark, and Visible Light-Induced Cleavage, of a Ru–S Bond in Water: A Thermodynamic and Kinetic Study. *Inorganic chemistry* **2013,** *52* (16), 9456-9469.

[67] Sun, W.; Li, S.; Häupler, B.; Liu, J.; Jin, S.; Steffen, W.; Schubert, U. S.; Butt, H. J.; Liang, X. J.; Wu, S., An amphiphilic ruthenium polymetallodrug for combined photodynamic therapy and photochemotherapy in vivo. *Advanced Materials* **2017,** *29* (6), 1603702.

[68] Zeng, X.; Wang, Y.; Han, J.; Sun, W.; Butt, H. J.; Liang, X. J.; Wu, S., Fighting against Drug-Resistant Tumors using a Dual-Responsive Pt (IV)/Ru (II) Bimetallic Polymer. *Advanced Materials* **2020,** *32* (43), 2004766.

[69] Chen, Z.; He, S.; Butt, H. J.; Wu, S., Photon Upconversion Lithography: Patterning of Biomaterials Using Near-Infrared Light. *Advanced Materials* **2015,** *27* (13), 2203-2206.

[70] Xie, C.; Sun, W.; Lu, H.; Kretzschmann, A.; Liu, J.; Wagner, M.; Butt, H.-J.; Deng, X.; Wu, S., Reconfiguring surface functions using visible-light-controlled metal-ligand coordination. *Nature communications* **2018,** *9*, 3842.

[71] Liu, J.; Xie, C.; Kretzschmann, A.; Koynov, K.; Butt, H. J.; Wu, S., Metallopolymer Organohydrogels with Photo-Controlled Coordination Crosslinks Work Properly Below 0° C. *Advanced Materials* **2020,** *32* (14), 1908324.

[72] Zhao, Y.; Wu, Y.; Wang, L.; Zhang, M.; Chen, X.; Liu, M.; Fan, J.; Liu, J.; Zhou, F.; Wang, Z., Bio-inspired reversible underwater adhesive. *Nature communications* **2017,** *8*, 2218.

[73] Xie, J.-B.; Li, L.; Knyazeva, A.; Weston, J.; Naumov, P., Mechanically robust, chemically inert superhydrophobic charcoal surfaces. *Chemical Communications* **2016,** *52* (62), 9695-9698.

[74] Hao, C.; Li, J.; Liu, Y.; Zhou, X.; Liu, Y.; Liu, R.; Che, L.; Zhou, W.; Sun, D.; Li, L., Superhydrophobic-like tunable droplet bouncing on slippery liquid interfaces. *Nature communications* **2015,** *6*, 7986.

[75] Kloxin, A. M.; Kasko, A. M.; Salinas, C. N.; Anseth, K. S., Photodegradable hydrogels for dynamic tuning of physical and chemical properties. *Science* **2009,** *324* (5923), 59-63.

[76] Yan, B.; Boyer, J.-C.; Habault, D.; Branda, N. R.; Zhao, Y., Near infrared light triggered release of biomacromolecules from hydrogels loaded with upconversion nanoparticles. *Journal of the American Chemical Society* **2012,** *134* (40), 16558-16561.

Chapter 2 Characterization of a new Ru-Se photodynamic bond

2.1 Introduction

Dynamic bonds can dissociate and reform via reversible reactions. Their dynamic features are used to construct responsive materials, biomaterials, healable materials, adaptive networks, and other smart materials.[1-9] Some dynamic bonds are stable in the dark and they can reversibly dissociate/reform upon photoexcitation; they are called photodynamic bonds.[10] The properties of materials containing photodynamic bonds may be controlled with light, which is a non-invasive stimulus with high spatiotemporal resolution.[11] In the past, dynamic bonds based on photoinduced reversible cycloadditions,[12] photoinduced radical generation and subsequent bond exchange,[13] and photo-controlled metal-ligand coordination,[14-15] have been developed.

Coumarin,[16] cinnamate,[8] thymine,[17] styrylpyrene,[18-19] and anthracene[1, 20] showed photoinduced reversible bond formation and dissociation based on [2 + 2] or [4 + 4] cycloadditions/reversions. A challenge for the development of photoinduced reversible cycloadditions is red-shifting excitation wavelengths.[12] Reversible cycloadditions are usually induced by UV light or in few cases induced by short-wavelength visible light.[21-22] Compared with UV light, visible light is more suitable for organic and biological systems to prevent photodamage; visible-light-induced reversible cycloadditions are also useful for wavelength-selective photochemical systems. Another challenge for photoinduced reversible cycloadditions is suppressing competitive side reactions. While light induces cycloadditions/reversions, it also induces isomerization, cyclization and other side reactions.[23-24]

As another type of dynamic bond, sensitized alkoxyamines,[10] hexaarylbiimidazoles,[25] disulfides,[26-27] allyl sulfides,[13, 28] thiuram disulfides,[29] trithiocarbonates,[30] and other sulfides[31-32]

can generate radicals upon light irradiation; photogenerated radicals can subsequently recombine or induce bond exchange. Such reactions are also induced by UV light or short-wavelength visible light. To red-shift the excitation wavelength, several dynamic bonds based on selenium (Se) such as diselenide (Se-Se),[33] selenide-sulfide (Se-S),[34] and selenide-telluride (Se-Te),[35] have been investigated. These Se-containing dynamic bonds can be excited by visible light because they exhibit lower bond energies than their sulfide analogs. For instance, Se-Se bond exchange can be induced by red light,[36] which makes such dynamic bond attractive to the applications that require long-wavelength light. Never the less, a general issue for photogenerated radicals is that they are very reactive, which may react with substances in operating environments and thus cause side reactions. Considering the issues for photoinduced reversible cycloadditions and photoinduced bond exchange via radical processes, it is desirable to develop alternative visible-light-controlled dynamic bonds that avoid side reactions.

Herein, we report that the Ru-Se coordination bond is dynamic and reversibly dissociates upon visible light irradiation via a non-radical process. The Ru-Se bond formed spontaneously via mixing the selenoether ligand SeM and the complex Ru1-H_2O; visible light irradiation induced reversible dissociation of the Ru-Se bond. Some Ru complexes are photocages,[37-40] which showed irreversible ligand photosubstitution.[41-43] Although photo-controlled reversible metal-ligand coordination exists,[15, 44-46] Ru-Se bond is a new dynamic bond that has not been studied previously; it can be excited under mild irradiation conditions using red, green, blue or solar light. In addition, coordination is a non-radical process and the photoproducts from the Ru-Se bonds are stable Ru complexes and selenoethers, which prevent side reactions.

2.2 Results and discussion

2.2.1 Characterization of Ru-Se bond formation

To fully study the formation of the Ru-Se dynamic bonds. Ru1-H$_2$O ([Ru(tpy)(biq)(H$_2$O)]$^{2+}$, tpy = 2,2':6',2"-terpyridine, biq = 2,2'-biquinoline) and SeM (4-(methylselanyl)butanoic acid) were synthesized and used as model compounds (Figure 1).
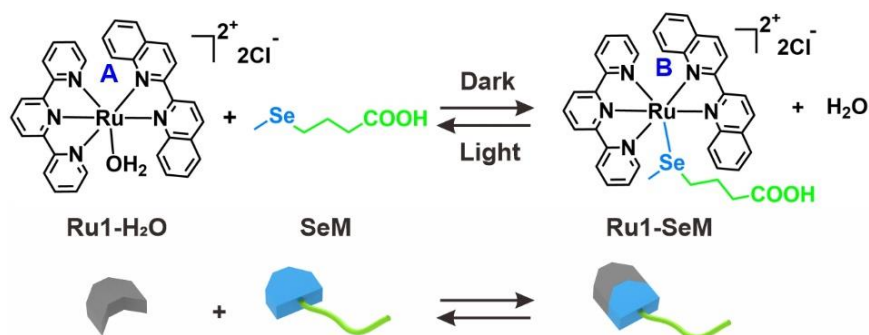
Figure 1. The reversible formation and dissociation of the Ru-Se coordination bond in the dark and upon light irradiation, which are demonstrated using Ru1-H$_2$O, SeM and Ru1-SeM. Different blocks represent different molecular group, black, Ru1-H$_2$O, blue, Se, green, functional group modified on Se.

First, we tried to use ^{1}H nuclear magnetic resonance spectroscopy (NMR) and nuclear overhauser effect spectroscopy (NOESY) to define the specific proton A1 and proton B1 position of [Ru(tpy)(biq)(Cl)]Cl. According to the NOESY spectrum (Figure 2), the red frame indicates the correlations of proton B1 with protons T4 and T5.We assigned that proton B1 belongs to the signal in the high field. The correlation signals in the red frame indicates B1 is closer to the tpy ligand, which agreed with the steric effect. On the other hand, chlorine atom is an electronegative atom that pulls electrons toward it and causes deshielding of the hydrogen nucleus. Hence, proton B1 which is far from the chlorine atom should be located in the high field and has a lower chemical

shift. When proton B1 was assigned, we excluded the possibility that the signal at 6.80 ppm belonged to proton A1 because there would not exhibit the correlation signals of A1 with protons T4 and T5 if A1 was assigned to the signal with a lower chemical shift.
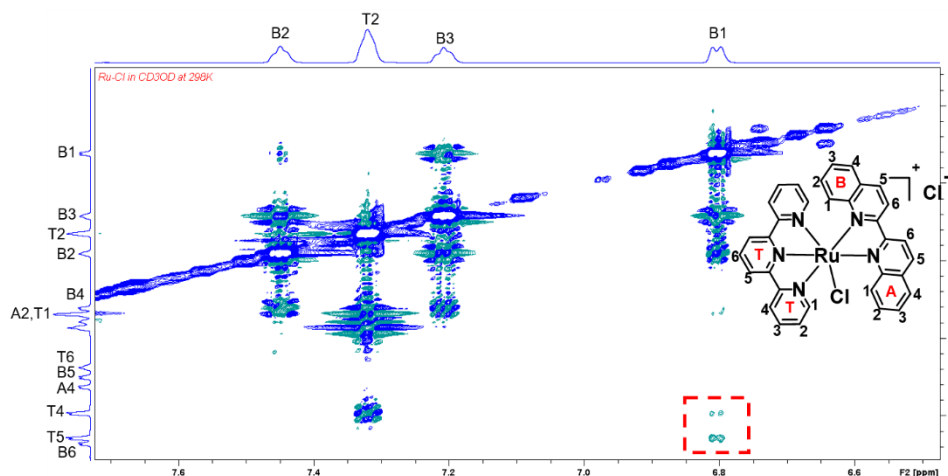
Figure 2. NOESY NMR spectrum (700 MHz, CD$_3$OD) of [Ru(tpy)(biq)(Cl)]Cl.

When Ru1-H$_2$O (6 mM) and SeM (30 mM) were mixed in D$_2$O with concentration ratio of 1:5 and kept in the dark for 2 h, the ^{1}H NMR singal of proton A at 6.8 ppm decreased and a new singal of proton B increased at 6.2 ppm (Figure 3a). This result suggests that a new coordination complex starts to yield owing to SeM coordinating with Ru1-H$_2$O.

To further demonstrate the formation of Ru-Se bond, we studied the mxiture of Ru1-H$_2$O with different concentrations of SeM in D$_2$O using ^{1}H NMR spectroscopy (Figure 3b). As the concentration of SeM increased, the signals from Ru1-SeM and Ru1-H$_2$O increased and decreased, respectively. The equilibrium constant K of Ru-Se bond measured using ^{1}H NMR spectroscopy was 206 ± 4 M^{-1} (Figure 3b and 13), which was higher than normal hydrogen bonding and van der

Waals interactions but lower than covalent bonds.[47] In the mixture of Ru1-H_2O (6 mM) and SeM(30 mM), more than 85% Ru(II) center was coordinated with SeM.
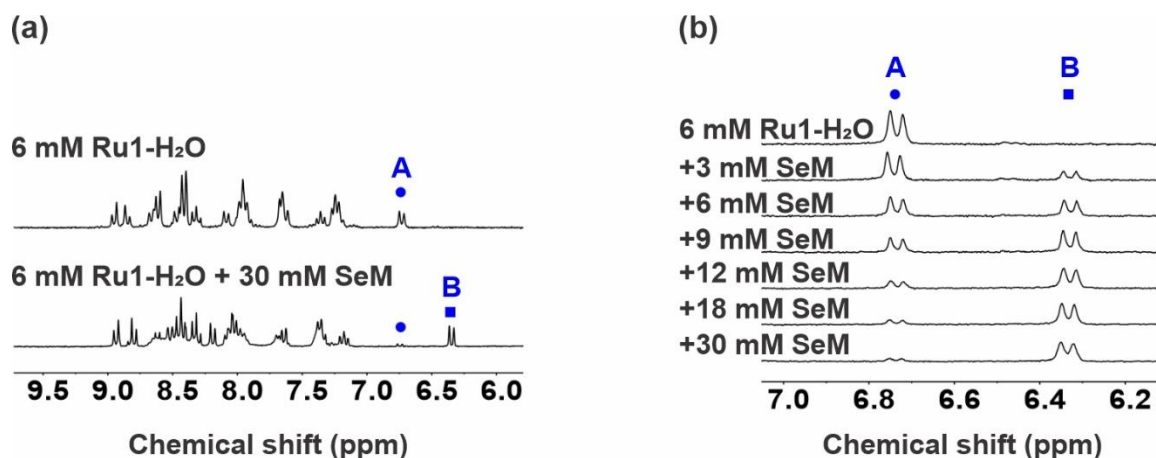
Figure 3. (a) ^1H NMR spectra of Ru1-H_2O (6 mM) and the mixture of Ru1-H_2O (6 mM) and SeM (30 mM). (b) ^1H NMR spectra of Ru1-H_2O (6 mM) with different concentrations of SeM.

In addition, the mixture of Ru1-H_2O (6 mM) and SeM(30 mM) was studied using ^{77}Se NMR spectroscopy (Figure 4a). Before added Ru1-H_2O, free SeM had a chemical shift at 54.6 ppm. Adding Ru1-H_2O to free SeM solution resulted in a new signal, which was assigned to the coordinated Ru1-SeM, appeared in the mixture of Ru1-H_2O and SeM. This result further confirms the formation of Ru-Se bond.

Furthermore, we studied the mixture of Ru1-H_2O and SeM in D_2O using diffusion order spectroscopy (DOSY) (Figure 4b). There were three main species in the mixture. The smallest species with the highest diffusion coefficient was HDO, indicating HDO had highest mobility in the mixture. The medium species was excess SeM. The largest species with the lowest diffusion coefficient contained the signals of both SeM and the Ru complex, which confirmed that SeM coordinated with the Ru complex.
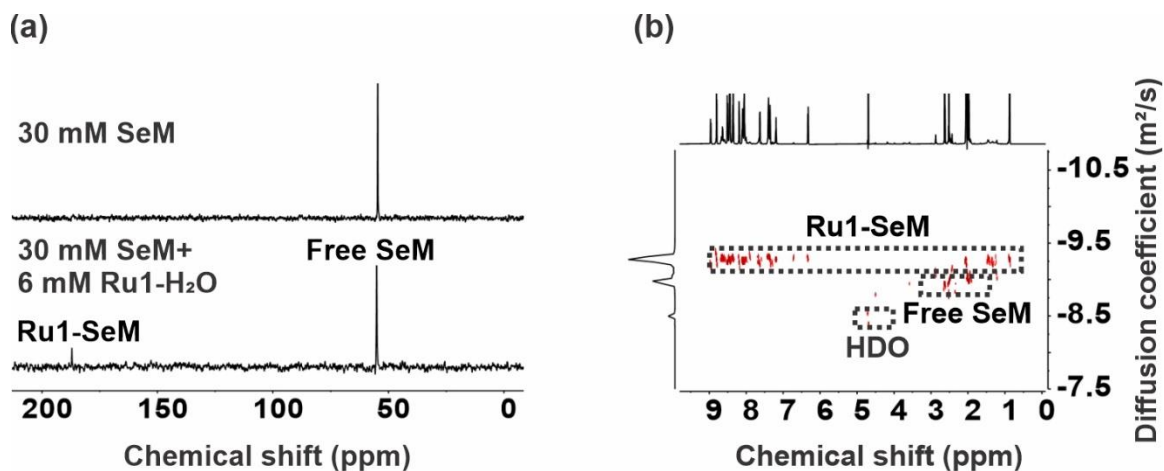
Figure 4. (a) ^{77}Se NMR spectra of SeM (30 mM) and the mixture of Ru1-H_2O (6 mM) and SeM (30 mM). (b) Diffusion order spectroscopy (DOSY) of the mixture of Ru1-H_2O (6 mM) and SeM (30 mM). The values of the diffusion coefficients were negative because logarithm was used.

Meanwhile, ^{1}H-^{77}Se heteronuclear multiple bond correlation (HMBC) NMR spectroscopy also verified the result (Figure 5). There was only one correlation signal for free SeM (30 mM) in D_2O from ^{1}H-^{77}Se HMBC spectrum (Figure 5a). When adding Ru1-H_2O (6 mM) to free SeM solution, a new correlation signal in the red frame appeared, indicating a new compound obtained containing Se element (Figure 5b). This result also agree with the ^{77}Se NMR spectra of SeM (30 mM) and the mixture of Ru1-H_2O (6 mM) and SeM (30 mM).
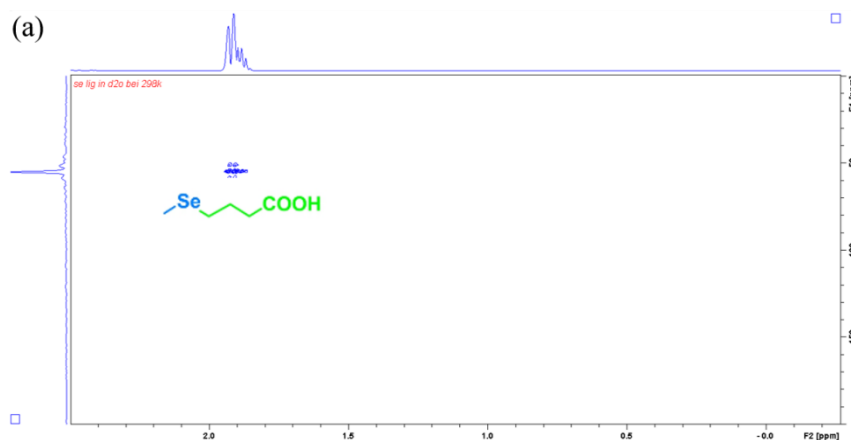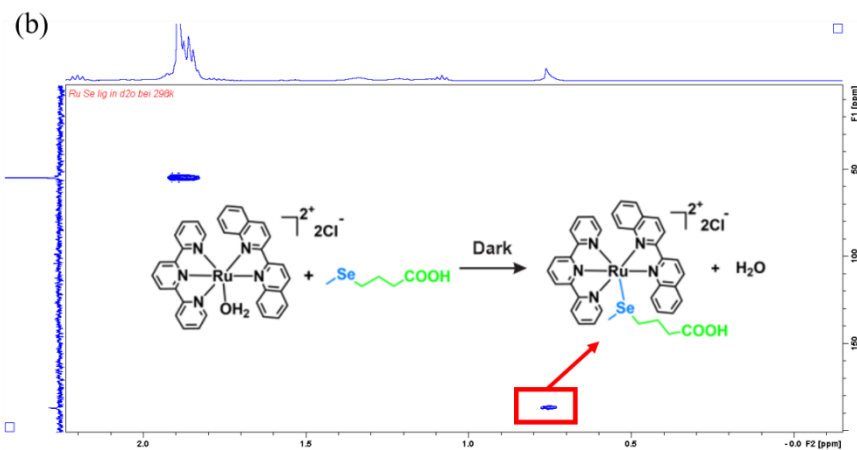
Figure 5. ^{1}H-^{77}Se heteronuclear multiple bond correlation (HMBC) NMR spectra for (a) SeM (30 mM) in D$_2$O, (b) the mixture of Ru1-H$_2$O (6 mM) and SeM (30 mM) in D$_2$O. The signal in red frame indicated that a new compound, which contained Se, appeared. The new compound was assigned as Ru1-SeM.

We still tried our best to detect the electrospray ionization (ESI) mass spectroscopy to confirm the coordination in the mixture of Ru1-H$_2$O (0.1 mM) and SeM (1.0 mM) (Figure 6). The molecular peak at 772.6 was observed, which agreed with value of calculated Ru1-SeM without chloride counterion.
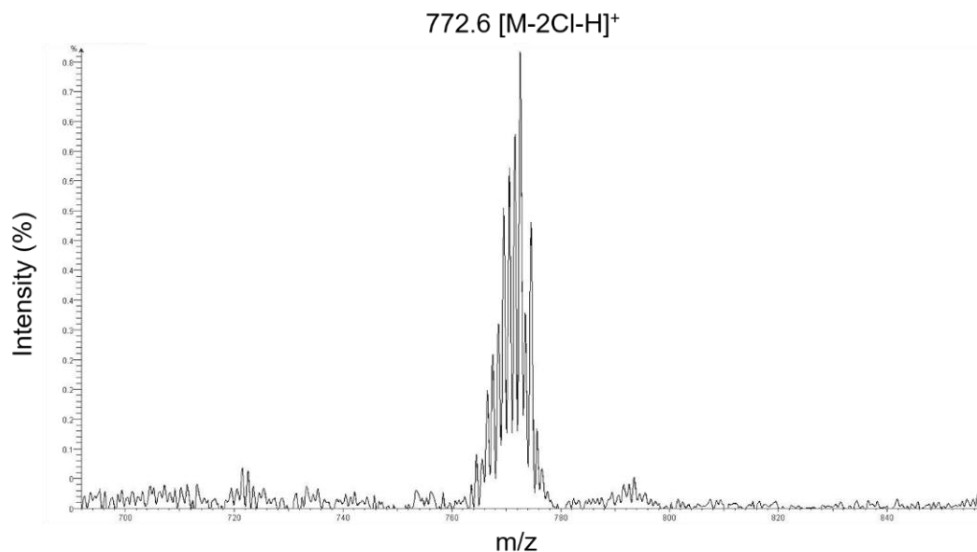
Figure 6. Electrospray ionization (ESI) mass spectroscopy of the mixture of Ru1-H$_2$O (0.1 mM) and SeM (1.0 mM). The molecular peak at 772.6 indicated the Ru1-SeM was formed ([M-2Cl-H]$^+$ calculated: 772.7).

2.2.2 Reversibility of Ru-Se bond

  After the characterization of Ru-Se bond formation, we further studied the reversibility of Ru-Se bond. We expect that the Ru-Se bond is a photodynamic bond, which reversibly form/dissociate in the dark/light irradiation cycles. As the mixture of Ru1-H$_2$O (6 mM) and SeM (30 mM) in D$_2$O was kept in the dark, ^{1}H NMR spectroscopy showed that Ru1-SeM was formed gradually and the coordination reaction reached an equilibrium in approximately 100 min (Figure 7). When the mixture was kept in the dark for 120 min, it was irradiated with green light (530 nm, 40 mW cm$^-$^{2}) for 10 min. ^{1}H NMR spectroscopy showed that light irradiation induced the dissociation of the Ru-Se bond. More than 85% Ru-SeM was converted to Ru1-H$_2$O. Afterwards, the sample was kept in the dark for 120 min; ^{1}H NMR data demonstrated that Ru1-SeM reformed.
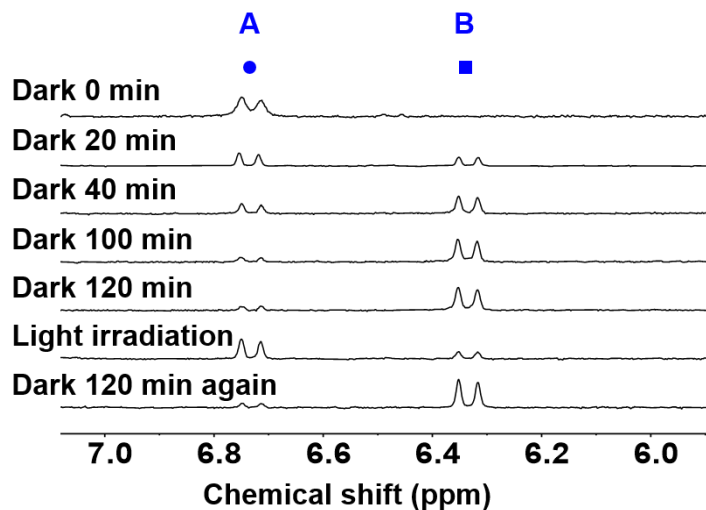
Figure 7. ^{1}H NMR spectra of the mixture of Ru1-H$_2$O (6 mM) and SeM (30 mM) in the dark for 0, 20, 40, 100 and 120 min, after green light (530 nm, 40 mW cm^{-2}) irradiation for 10 min, and subsequently kept in the dark for another 120 min.

The reversible formation and dissociation of Ru-Se bond were also confirmed using UV-vis absorption spectroscopy (Figure 8). Initially, the mixture of Ru1-H$_2$O (0.1 mM) and SeM (1 mM) had an absorption band at 550 nm, which was assigned to the metal-to-ligand charge transfer (MLCT) band of Ru1-H$_2$O. When the mixture was kept in the dark, the absorption band gradually blue-shifted to 528 nm. It is well known that ligand substitution resulted in similar spectral changes,[43-44] which indicates that the coordinated H$_2$O was substituted by SeM. The mixture was kept in the dark for 80 min and subsequently irradiated with green light for 1 min. The absorption spectrum reverted, suggesting that the formation and dissociation of the Ru-Se bond were reversible. Importantly, an isosbestic point at 532 nm was observed, which demonstrated that there was no side reaction during the formation and dissociation of the Ru-Se bond.

Moreover, the formation and dissociation of the Ru-Se bond were cycled for 20 times, which showed that the Ru-Se dynamic bond has excellent reversibility (Figure 9a). After the sample was cycled for 20 times, the isosbestic point was still observed (Figure 9b), which confirmed again that there was no side reaction during cycling.
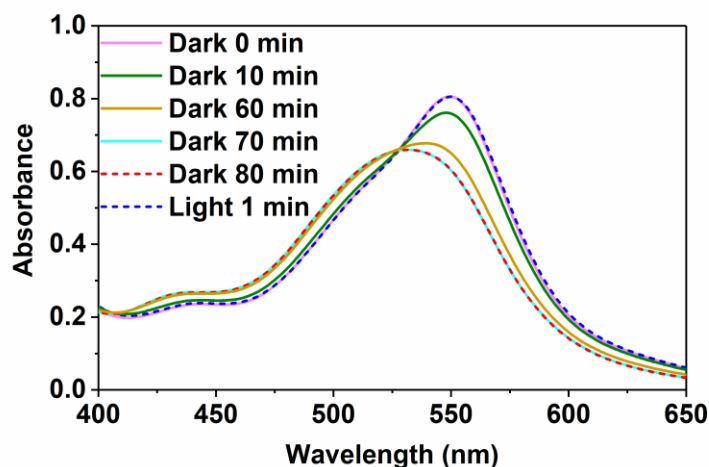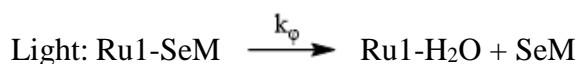

Figure 8. UV-vis absorption spectra of the mixture of Ru1-H_2O (0.1 mM) and SeM (1 mM) in the dark for different time periods and after green light (530 nm, 40 mW cm^{-2}) irradiation for 1 min.
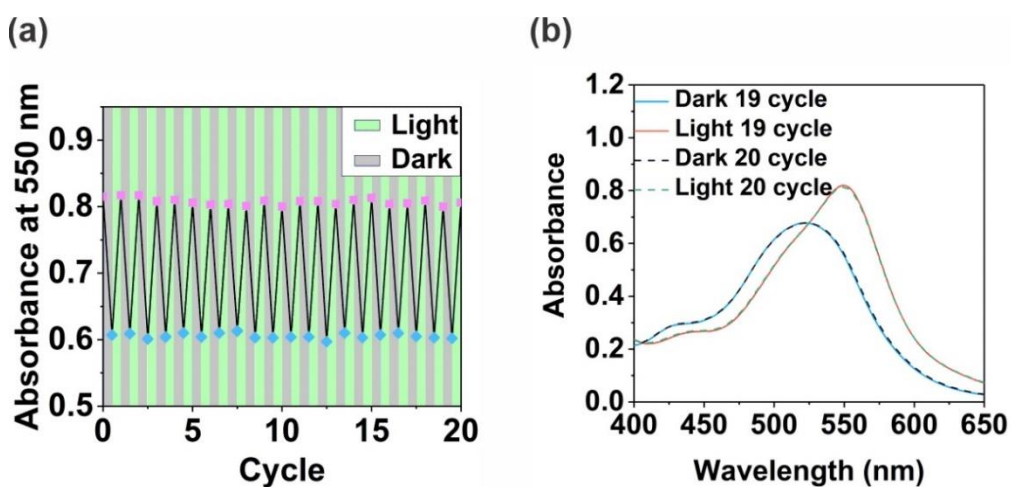
Figure 9. (a) Absorbance of the mixture of Ru1-H$_2$O (0.1 mM) and SeM (1 mM) at 550 nm under dark/light irradiation cycles. (b) UV-vis absorption spectra of the mixture of Ru1-H$_2$O (0.1 mM) and SeM (1.0 mM) cycled for 19 and 20 times. An isosbestic point still existed, which demonstrated that there was no side reaction during the dissociation/formation of the Ru-Se bond.

To investigate the "photodynamic" behavior of Ru1-SeM in other solvents, we chose normal organic solvent dichloromethane (DCM) to measure UV-Vis spectra. First, we measured UV-Vis absorption spectra of Ru1-H$_2$O (0.1 mM) in DCM solution in the dark condition, a blue shift of absorption peak from 544 nm to 572 nm demonstrated Ru1-H$_2$O could be substituted by DCM molecule (Figure 10a). When adding SeM (1 mM) to the Ru1-H$_2$O (0.1 mM) solution in the dark for at least 60 min, the absorption peak was located at 532 nm indicating the Ru-Se bond formed (Figure 10b). Then, after 4 min green light irradiation (530 nm, 40 mW cm^{-2}), the absorption peak blue shifted to 572 nm again which demonstrated the photocleavage of Ru-Se bond and the photosubstitution by DCM molecule appeared (Figure 10c). However, when kept the irradiated solution in the dark overnight, no obvious change from UV-Vis spectra indicating no coordination reaction happened. The results illustrate that Ru-Se bond could formed and be photocleaved in DCM solvent, but could not reversibly form.

Another feature of photosubstitution of the Ru-Se bond is that it can be induced by light with different wavelengths. Blue, green, red and solar light induced photosubstitution of the Ru-Se bond (Figure 11). Thus, Ru-Se bonds can be controlled by user-defined wavelengths. Moreover, the speed of Ru-Se bond formation could accelerate by increasing the temperature. When the mixture of Ru1-H$_2$O (0.1 mM) and SeM (1.0 mM) were heating to 40 °C, 60 °C and 80 °C, the formation of Ru-Se bonds reached equilibrium in 25 min, 8 min and 4 min, respectively (Figure 12).
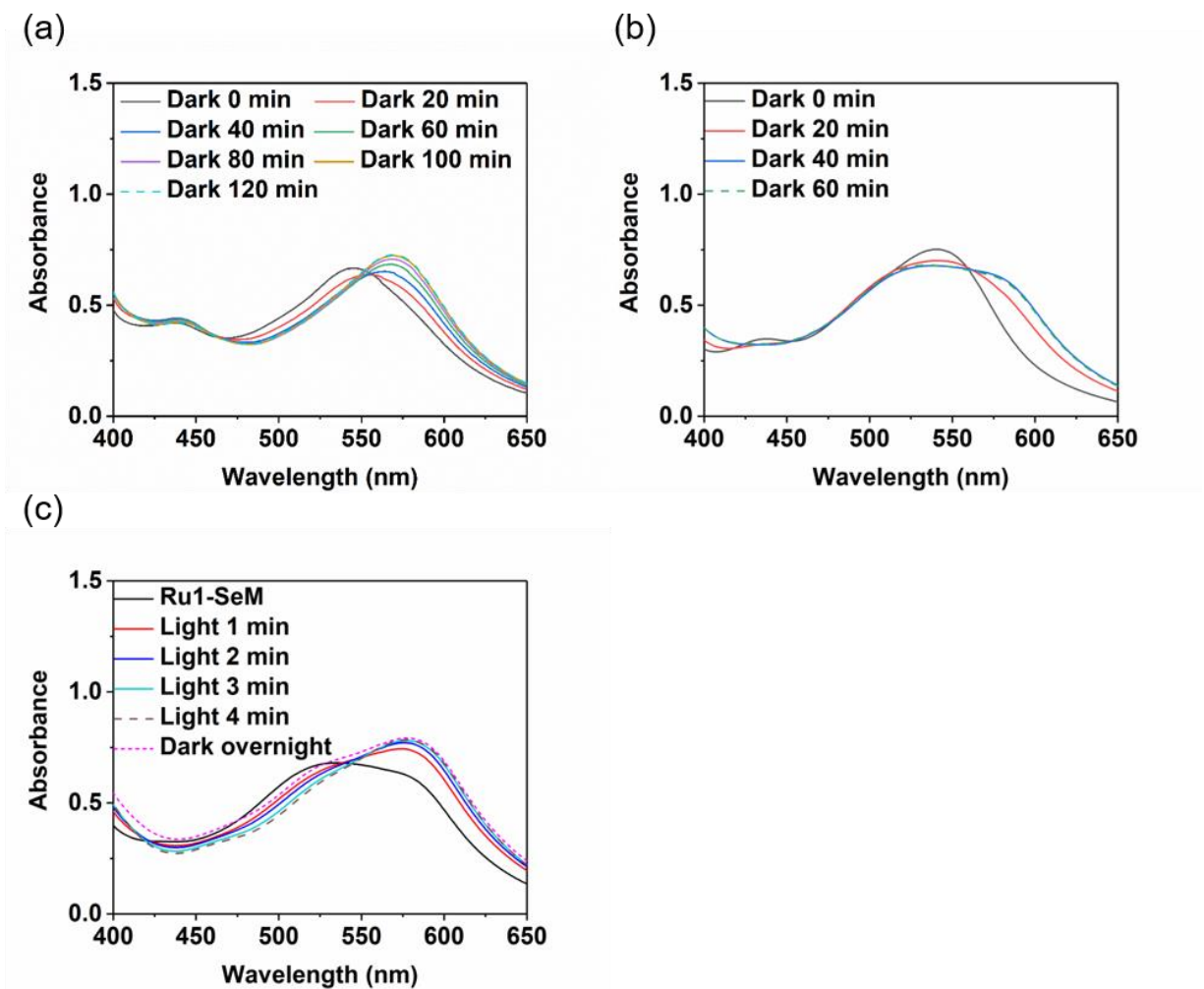
Figure 10. (a) UV-Vis absorption spectra for Ru1-H$_2$O (0.1 mM) in DCM kept in the dark for different time periods. (b) UV-Vis absorption spectra for a mixture of Ru1-H$_2$O (0.1 mM) and SeM (1 mM) in DCM kept in the dark for different time periods. (c) UV-Vis absorption spectra for the green light irradiation (530 nm, 40 mW cm^{-2}) of stable mixture of Ru1-H$_2$O (0.1 mM) and SeM (1 mM) in DCM and then kept in the dark overnight.
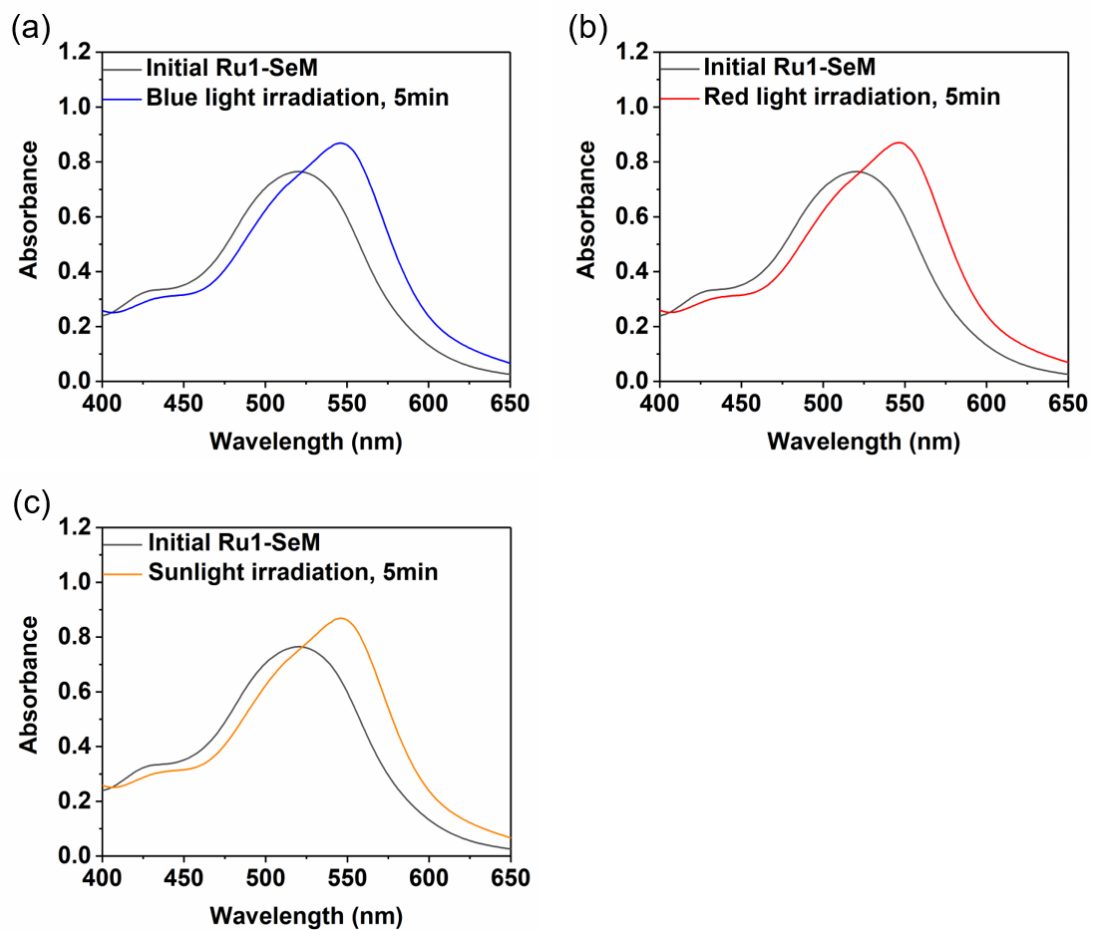
Figure 11. Photosubstitution of the Ru1-SeM complex induced by light with different wavelengths. UV-vis absorption spectra of the Ru1-SeM complex before and after (a) blue light (470 nm, 40.0 mW cm^{-2}, 5 min), (b) red light (656 nm, 40.0 mW cm^{-2}, 5 min) and (c) sunlight (50 mW cm^{-2}, 5 min) irradiation. Ru1-SeM was prepared by mixing Ru1-H$_2$O (0.1 mM) and SeM (1 mM) in the dark for 70 min.
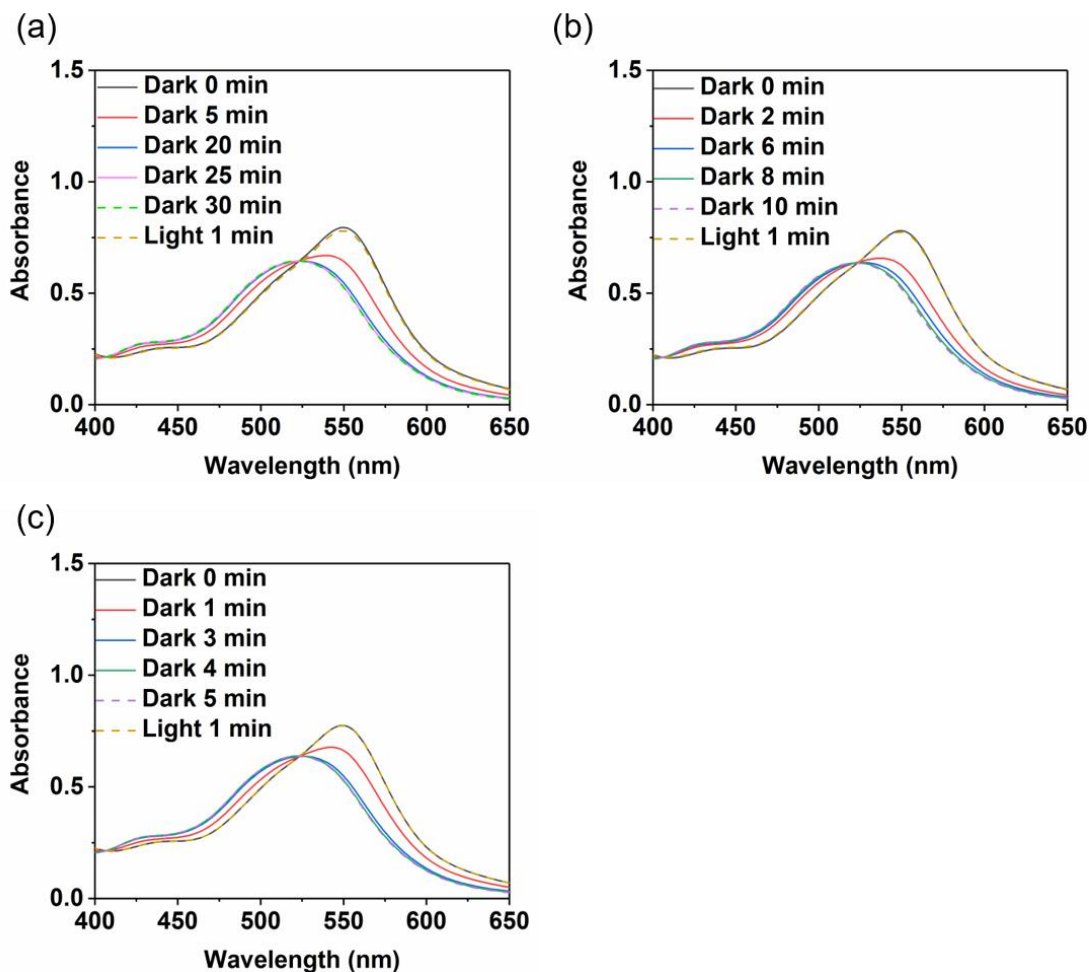
Figure 12. UV-vis absorption spectra of the mixture of Ru1-H$_2$O (0.1 mM) and SeM (1 mM) in the dark for different time periods with temperatures before and after green light (530 nm, 40 mW cm^{-2}) irradiation for 1 min. (a) 40 °C (b) 60 °C and (c) 80 °C.

2.2.3 Thermodynamic and kinetic parameter of Ru-Se bond

The Ru-Se bond has been verified as a photodynamic bond which can undergo reversible thermal coordination and photosubstitution. Therefore, we quantified the formation and dissociation of the Ru-Se bond using ^{1}H NMR and UV−vis absorption spectroscopy (Table 1). This part, the equilibrium constant K, the pseudo first-order rate constant k_1' for the thermal coordination, the

first-order constant k_{-1} for the thermal hydrolysis, first-order rate constant k_{φ} for photosubstitution and quantum yield φ for the photosubstitution were calculated and shown.

Table 1. Thermodynamic and kinetic data for thermal coordination and photosubstitution.

Dark: Ru1-H$_2$O + SeM $\underset{k_{-1}}{\overset{k_1'}{\rightleftharpoons}}$ Ru1-SeM

Light: Ru1-SeM $\xrightarrow{k_{\varphi}}$ Ru1-H$_2$O + SeM

K	k_1'	k_{-1}	k_{φ}	φ
206 ± 4 M^{-1}	5.7×10^{-4} s^{-1}	2.7×10^{-5} s^{-1}	1.0×10^{-4} s^{-1}	0.06

K: Equilibrium constant; k_1': Pseudo first-order rate constant for thermal coordination; k_1: Second rate constant for thermal coordination. ($k_1 = k_1' \cdot$[SeM], [SeM] = 0.1 M); k_{-1}: First-order rate constant for thermal hydrolysis; k_{φ}: First-order rate constant for photosubstitution; φ: Quantum yield for photosubstitution.

Measurements of the equilibrium constant

The equilibrium constant K was determined by the following equation:

$$\frac{[Ru1 - SeM]}{[Ru1 - H_2O]} = K \cdot [SeM] \qquad (Eq. 1)$$

Where [Ru1-H$_2$O] is the concentration of Ru1-H$_2$O; [Ru1-SeM] is the concentration of Ru1-SeM; [SeM] is the concentration of free SeM. To obtain K, SeM with different concentrations were mixed with 6 mM Ru1-H$_2$O in D$_2$O, respectively. After kept in the dark for more than 3 h to reach equilibrium, the samples were measured using ^{1}H NMR spectroscopy (Figure 3b). The ratio

between Ru1-SeM and Ru1-H$_2$O was determined by integration of the ^{1}H NMR signals of Ru1-SeM and Ru1-H$_2$O. K was the slope of the line in Figure 13, which was 206 ± 4 M^{-1}.
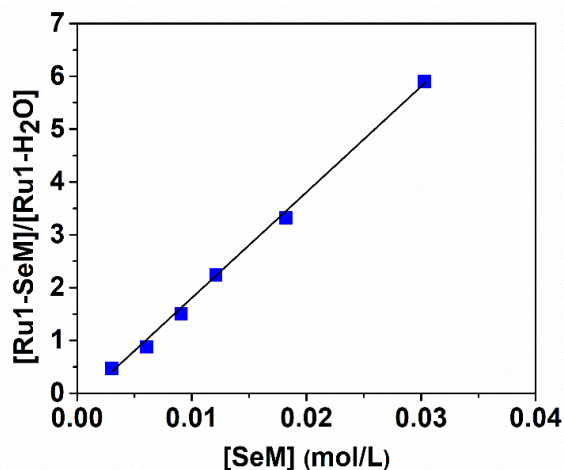
Figure 13. Plot of [Ru1-SeM]/[Ru1-H$_2$O] vs the equilibrium concentrations of free SeM at 298K. The total concentration of the Ru complexes was 6 mM in each sample. The equilibrium constant K was the slope of the line. K was 206 ± 4 M^{-1}. The details for the measurement of the equilibrium constant were described below.

Measurements of the rate constant of thermal coordination

The rate constant of thermal coordination was calculated according to the following two steps.

1) Extinction coefficients. The extinction coefficients of Ru1-H$_2$O and Ru-SeM were measured using UV-vis absorption spectroscopy. First, the aqueous solutions of Ru1-H$_2$O with different concentrations were prepared (2×10^{-5} M, 4×10^{-5} M, 6×10^{-5} M, 8×10^{-5} M and 1×10^{-4} M). Then, 3 mL of each solution was measured using UV-vis absorption spectroscopy. Finally, $\varepsilon_\lambda^{Ru1-H_2O}$ was obtained from the slope of the absorption vs concentration plot at selected wavelengths. The values of $\varepsilon_{550}^{Ru1-H_2O}$ and $\varepsilon_{528}^{Ru1-H_2O}$ are 9680 L mol^{-1} cm^{-1} and 7945 L mol^{-1} cm^{-1}, respectively.

The extinction coefficient of Ru1-SeM was obtained by a different method due to the thermodynamic equilibrium of Ru1-H_2O and Ru1-SeM in water. Firstly, aqueous solutions of Ru1-H_2O and SeM with four different concentrations were prepared ([Ru]$_{total}$ was 4×10^{-5} M, 8×10^{-5} M, 1.2×10^{-4} M and 1.6×10^{-4} M, respectively; [SeM] in each sample was 0.1 M). Concerning [SeM] was a constant, the ratio [Ru1-SeM]/[Ru1-H_2O] is a constant.

$$K' = \frac{[Ru1 - SeM]}{[Ru1 - H_2O]} = K \cdot [SeM] \qquad (Eq. 2)$$

According to the $[Ru]_{total} = [Ru1 - SeM] + [Ru1 - H_2O]$, the Eq.2 can be replaced by Eq. 3:

$$r = \frac{[Ru1 - SeM]}{[Ru]_{total}} = \frac{K'}{K' + 1} \qquad (Eq. 3)$$

The value r can be calculated from Eq.3, as $\varepsilon_\lambda^{Ru1-H_2O}$ was determined previously. The extinction coefficients of Ru1-SeM ($\varepsilon_\lambda^{Ru1-SeM}$) can be calculated by Eq.4:

$$\varepsilon_\lambda^{Ru1-SeM} = \frac{\varepsilon_\lambda^{Ru} - (1 - r) \cdot \varepsilon_\lambda^{Ru1-H_2O}}{r} \qquad (Eq. 4)$$

The values of $\varepsilon_{550}^{Ru1-SeM}$ and $\varepsilon_{528}^{Ru1-SeM}$ are 5857 L mol^{-1} cm^{-1} and 7100 L mol^{-1} cm^{-1}, respectively.

2) Rate constant. The rate constant was determined using UV-vis absorption spectroscopy. As the coordination reaction is thermodynamic, the absorption at two different wavelengths λ_1, λ_2 can be expressed with the two-wavelength method shown in Eq.5a and Eq.5b:

$$A_{\lambda 1} = \varepsilon_{\lambda 1}^{Ru1-H_2O} \cdot l \cdot [Ru1 - H_2O] + \varepsilon_{\lambda 1}^{Ru1-SeM} \cdot l \cdot [Ru1 - SeM] \qquad (Eq. 5a)$$

$$A_{\lambda 2} = \varepsilon_{\lambda 2}^{Ru1-H_2O} \cdot l \cdot [Ru1 - H_2O] + \varepsilon_{\lambda 2}^{Ru1-SeM} \cdot l \cdot [Ru1 - SeM] \qquad (Eq. 5b)$$

[Ru1-H_2O] can be converted to Eq.6 from Eq.5b:

$$[Ru1 - H_2O] = \frac{A_{\lambda2} - \varepsilon_{\lambda2}^{Ru1-SeM} \cdot l \cdot [Ru1 - SeM]}{\varepsilon_{\lambda2}^{Ru1-H_2O} \cdot l} \qquad (Eq.\,6)$$

Therefore, the [Ru1-SeM] can be expressed with the introduction of Eq.6 to Eq.5a as (l = 1 cm):

$$[Ru1 - SeM] = \frac{A_{\lambda1} \cdot \varepsilon_{\lambda2}^{Ru1-H_2O} - A_{\lambda2} \cdot \varepsilon_{\lambda1}^{Ru1-H_2O}}{\varepsilon_{\lambda2}^{Ru1-H_2O} \cdot \varepsilon_{\lambda1}^{Ru1-SeM} - \varepsilon_{\lambda1}^{Ru1-H_2O} \cdot \varepsilon_{\lambda2}^{Ru1-SeM}} \qquad (Eq.\,7)$$

Concerning the rate law of the coordination reaction, the rate constant can be expressed as:

$$\frac{d[Ru1 - SeM]}{dt} = -\frac{d[Ru1 - H_2O]}{dt} = k_1 \cdot [SeM] \cdot [Ru1 - H_2O] - k_{-1} \cdot [Ru1 - SeM] \quad (Eq.\,8)$$

As previously introduced, [SeM] is in large excess, where k_1 is the second-order rate constant, we can define the pseudo first-order rate constant k_1' as $k_1' = k_1 \cdot$ [SeM]. Hence, the Eq.8 can be expressed as:

$$\frac{d[Ru1 - SeM]}{dt} = -\frac{d[Ru1 - H_2O]}{dt} = k_1' \cdot [Ru1 - H_2O] - k_{-1} \cdot [Ru1 - SeM] \quad (Eq.\,9)$$

Because [Ru]$_{total}$ = [Ru1-H$_2$O] + [Ru1-SeM], the Eq.9 can be converted to Eq.10, and k_1' can be expressed by Eq.10, which is related to the slope of ln([Ru1]/[Ru]$_{total}$) vs time:

$$\frac{d[Ru1 - SeM]}{dt} = -\frac{d[Ru1 - H_2O]}{dt} = k_1' \cdot [Ru]_{total} - (k_{-1} + k_1') \cdot [Ru1 - SeM] \quad (Eq.\,10)$$

Concerning the rate constant of the thermal hydrolysis k_{-1} is negligible, the pseudo first-order rate constant k_1' is 5.7×10^{-4} s^{-1}.
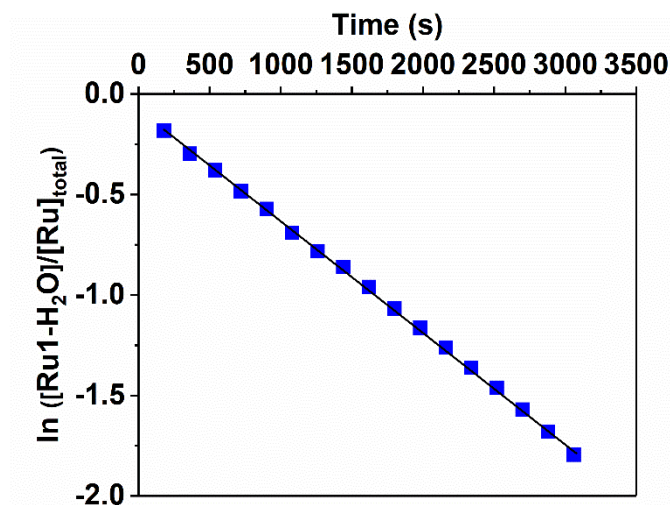
Figure 14. Plot of $\ln([Ru1\text{-}H_2O]/[Ru]_{total})$ vs time for the Ru1-SeM thermal coordination at 298 K. $[Ru]_{total} = 1 \times 10^{-4}$ M, [SeM] = 0.1 M. The pseudo first-order rate constant k_1' for the thermal coordination of Ru1-H_2O and SeM was 5.7×10^{-4} s^{-1}. The details for the measurements of the rate constant were described below.

As discussed above, [SeM] is 0.1 M, the second-order rate constant $k_1 = k_1' / [SeM] = 5.7 \times 10^{-3}$ M$^{-1} \cdot$s^{-1} (Table 1).

As for the first-order rate constant of thermal hydrolysis k_{-1}, it was based on the knowledge of the thermodynamic equilibrium constants K, and the second-order rate constants k_1, expressed as Eq.11:

$$k_{-1} = \frac{k_1}{K} \qquad\qquad (\text{Eq. 11})$$

The value of first-order rate constant of thermal hydrolysis k_{-1} is 2.7×10^{-5} s^{-1} (Table 1).

Measurements of photosubstitution quantum yield

The first-order rate constant for photosubstitution of Ru1-SeM was measured using UV-vis absorption spectroscopy. When Ru1-H$_2$O (10^{-4} M) and SeM (0.1 M) were kept in the dark for 3 h, the equilibrium state correspond to the "ON" state in Figure 15 and the ratio between Ru1-H$_2$O and Ru-SeM was defined as [Ru-SeM]$_{dark}$/[Ru1-H$_2$O]$_{dark}$, which can be expressed as Eq.12a:

$$\frac{[Ru - SeM]_{dark}}{[Ru1 - H_2O]_{dark}} = \frac{k_1'}{k_{-1}} \qquad (Eq.\,12a)$$

Then, the sample was irradiated by green light (530 nm, 6.8 mW cm^{-2}) for 60 s, and measured every 10 s, till the ratio reached a constant that corresponded to the "OFF" state in Figure 15. The ratio between Ru1-H$_2$O and Ru1-SeM was defined as [Ru1-SeM]$_{light}$/[Ru1-H$_2$O]$_{light}$. The irradiation state should concern the rate constant of photosubstitution. Therefore, the ratio was expressed as Eq.12b:

$$\frac{[Ru - SeM]_{light}}{[Ru1 - H_2O]_{light}} = \frac{k_1'}{k_{-1} + k_{\varphi}} \qquad (Eq.\,12b)$$

As we obtained the pseudo first-order rate constant for thermal coordination k_1' and thermal hydrolysis k_{-1} above, the first-order rate constant of photosubstitution was obtained as 1.0×10^{-4} s^{-1}.

The photosubstitution quantum yield of Ru-SeM φ can be expressed by Eq.13:

$$\varphi = \frac{k_{\varphi} \cdot n_{Ru_{total}}}{\emptyset \cdot (1 - 10^{Ae})} \qquad (Eq.\,13)$$

Where k_{φ} is the first-order rate constant of photosubstitution, $n_{Ru_{total}}$ is the number of moles of ruthenium in the sample, $\emptyset$ is the photon flux which was measured with a power meter, $1 - 10^{Ae}$

is the probability of photon absorption, Ae is the absorbance at the wavelength of the light source. Based on Eq.15, φ was 0.06 (Table 1).
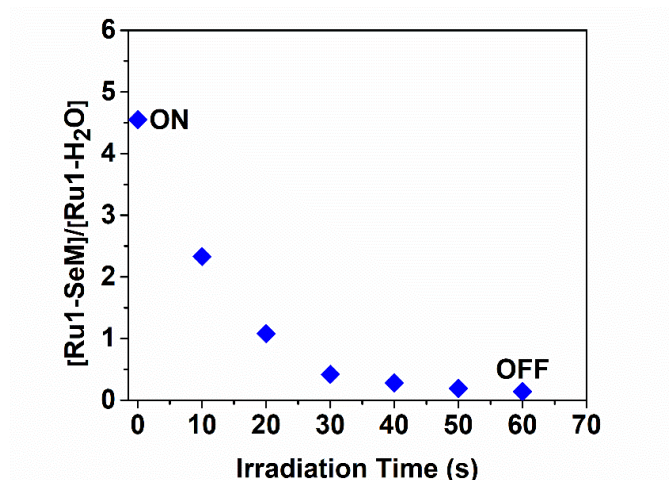
Figure 15. The first-order rate constant for photosubstitution of Ru1-SeM. Plot of the ratio [Ru1-SeM]/[Ru1-H$_2$O] vs irradiation time at 298 K. [Ru]$_{total}$ = 1×10^{-4} M, [SeM] = 0.1 M. The spectra were measured every 10 s. The first-order rate constant for photosubstitution k_φ was 1.0×10^{-4} s^{-1} (Table 1).

In summary, the equilibrium constant K for the Ru-Se bond was 206 ± 4 M^{-1} (Figure 13). The pseudo first-order rate constant k_1' for the thermal coordination was 5.7×10^{-4} s^{-1} and the first-order constant k_{-1} for the thermal hydrolysis was 2.7×10^{-5} s^{-1} (Figure 14). Upon green light irradiation (530 nm, 6.8 mW cm^{-2}), the first-order rate constant k_φ for photosubstitution was 1.0×10^{-4} s^{-1} and the quantum yield φ for the photosubstitution was 0.06 (Figure 15).

Comparison of Ru-Se bond and Ru-S bond with thermodynamic and kinetic data

(a)

(b)
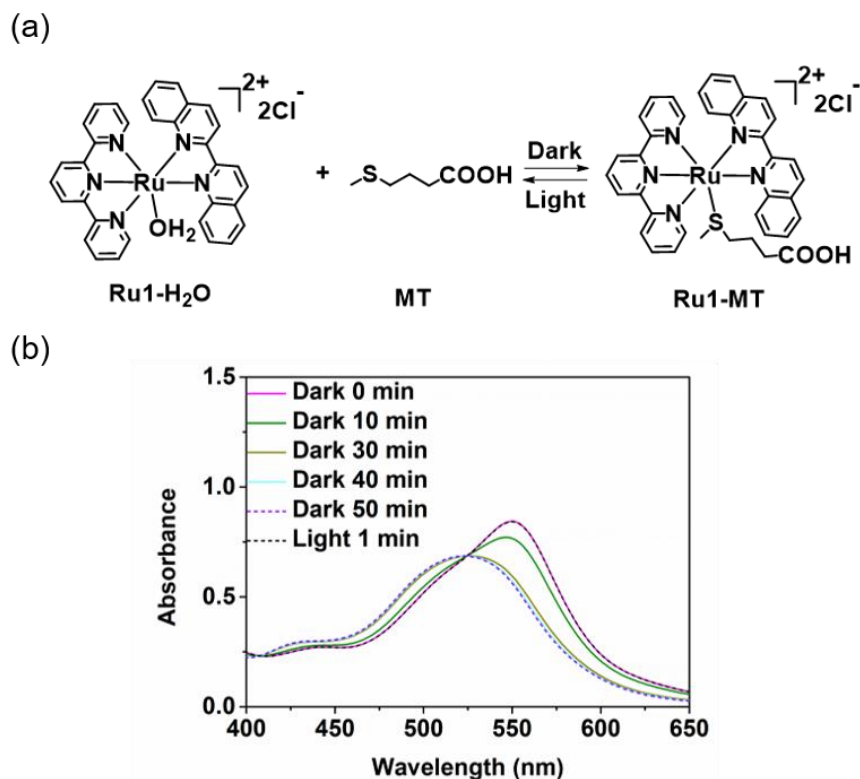
Figure 16. (a) The reversible formation and dissociation of the Ru-S coordination bond upon dark and upon light irradiation, as demonstrated using Ru1-H$_2$O, MT and Ru1-MT (b)UV-Vis absorption spectra for a mixture of Ru1-H$_2$O (0.1 mM) and MT (1 mM) kept in the dark for different periods and after irradiation with green light (530 nm, 40 mW cm^{-2}) for 1 min.

To investigate the thermodynamic and kinetic data for thermal coordination and photosubstitution of Ru-S bond vs. Ru-Se bond, we chose Ru1-H$_2$O and MT (4-(methylthio)butanoic acid) as model compounds to study the photochemical, kinetic and thermodynamic parameters of Ru-S dynamic bond (Figure 16a). The UV-Vis spectra for a mixture of Ru1-H$_2$O and MT kept in H$_2$O in the dark for different periods and after irradiation with green light were investigated (Figure 16b). The photodynamic behaviors of the Ru-S bond were similar to reported Ru-thioether complexes.
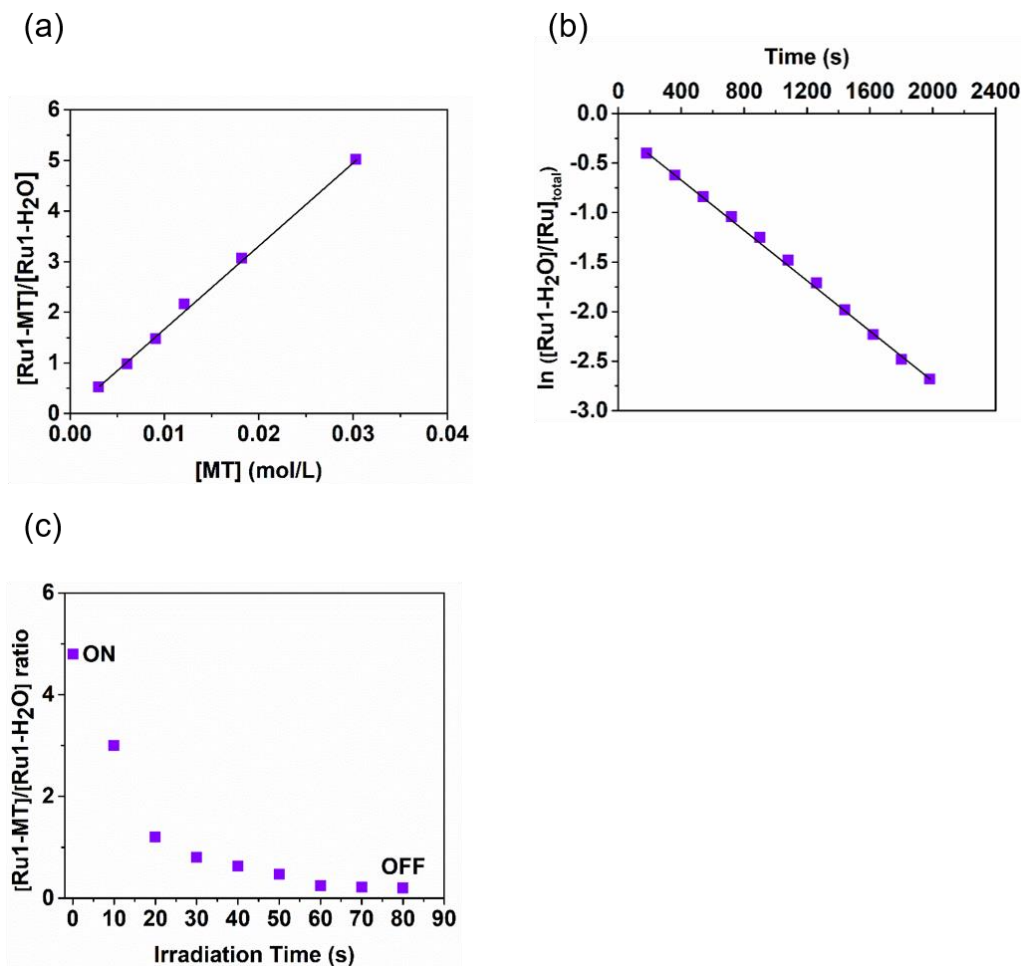
Figure 17. Thermodynamic and kinetic data for Ru-S bond thermal coordination and photosubstitution. (a) Plot of [Ru1-MT]/[Ru1-H$_2$O] vs the equilibrium concentrations of free MT at 298K. The equilibrium constant K was 160 ± 4 M^{-1}. (b) Plot of ln([Ru1-H$_2$O]/[Ru]$_{total}$) vs time for the Ru1-MT thermal coordination at 298 K. The pseudo first-order rate constant k_1' for the thermal coordination of Ru1-H$_2$O and MT was 1.1×10^{-3} s^{-1}. (c) First-order rate constant for photosubstitution of Ru1-MT. Plot of the ratio [Ru1-MT]/[Ru1-H$_2$O] vs irradiation time at 298 K. The first-order rate constant for photosubstitution k_φ was 1.6×10^{-4} s^{-1} and the quantum yield φ for photosubstitution was 0.09.

The calculations of the kinetic and thermodynamic parameters of Ru-S dynamic bond are totally as same as the Ru-Se bond. By using ^{1}H NMR and UV-Vis absorption spectroscopy, the equilibrium constant for thermal coordination, the pseudo first-order rate constant for thermal coordination, the first-order constant for thermal hydrolysis, the first-order rate constant for photosubstitution and the quantum yield for photosubstitution of Ru-S bond were exhibited in Table 2 and Figure 17. Compared with Ru-S bond, Ru-Se dynamic bond prefers to stay metastable state in the dark with weaker photosensitivity (Table 2).

Table 2. Thermodynamic and kinetic data for thermal coordination and photosubstitution of Ru-S bond and Ru-Se bond.

Bond type	K	$k_1{}'$	k_{-1}	k_φ	φ
Ru-S	160 ± 4 M^{-1}	1.1×10^{-3} s^{-1}	7.3×10^{-5} s^{-1}	1.6×10^{-4} s^{-1}	0.09
Ru-Se	206 ± 4 M^{-1}	5.7×10^{-4} s^{-1}	2.7×10^{-5} s^{-1}	1.0×10^{-4} s^{-1}	0.06

K: Equilibrium constant; $k_1{}'$: Pseudo first-order rate constant for thermal coordination; k_1: Second rate constant for thermal coordination; k_{-1}: First-order rate constant for thermal hydrolysis; k_φ: First-order rate constant for photosubstitution; φ: Quantum yield for photosubstitution.

2.3 Conclusion

In conclusion, we demonstrate that the Ru-Se coordination bond is a new photodynamic bond. When a Ru complex such as [Ru(tpy)(biq)(H$_2$O)]Cl$_2$ and a selenoether ligand are mixed, Ru-Se bond forms spontaneously in the dark. Ru-Se bond is dissociated upon visible light irradiation.

The formation and dissociation of the Ru-Se bond in the dark and upon light irradiation are fully reversible. Ru-Se bond is a new visible-light-controlled dynamic bond, which can prevent side reactions. Moreover, the thermodynamic and kinetic parameters of the coordination and photosubstitution reactions based on Ru-Se bonds have been calculated. We believe our work based on this new photodynamic bond can be impressive for the further fundamental researches.

2.4 Supporting Information

Materials

$RuCl_3 \cdot xH_2O$ (99.9%) and 2,2'-biquinoline (98%), 4-(methylselanyl)butanoic acid (95%) were purchased from Sigma-Aldrich. Terpyridine (97%) was purchased from Alfa Aesar. All other solvents (HPLC grade) were purchased from Sigma-Aldrich or Fisher Scientific. Milli-Q water with a resistivity of 18.2 $M\Omega \cdot cm$ was used in this study.

Instruments and characterization

NMR spectra were recorded on Bruker Spectrospin NMR spectrometers (300 MHz or 700 MHz). UV-vis absorption spectra were measured on a Lambda 900 spectrometer (Perkin Elmer). The molecular weights were determined using mass spectrometry (Bruker Time-of-flight MS Reflex III or Advion ASAP Atmospheric Solids Analysis). Photon flux was measured by Ophir 7Z02410 PD300 10pW-300mW power meter.

Synthesis
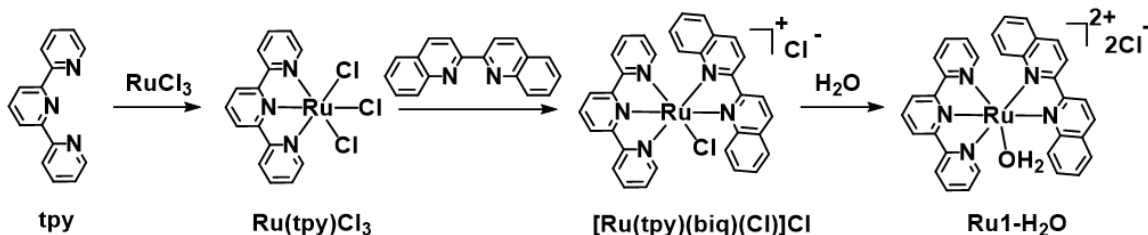
Figure S1. Synthetic route for compound Ru1-H_2O.

Synthesis of Ru(tpy)Cl₃ (Figure S1)

Ru(tpy)Cl₃ was synthesized according to literature. Brown powders were obtained.

Synthesis of [Ru(tpy)(biq)(Cl)]Cl (Figure S1)

[Ru(tpy)(biq)(Cl)]Cl was synthesized according to literature. Violet powders were obtained. ^{1}H NMR (700 MHz, CD₃OD) (Figure S2) δ (ppm): 9.66 (d, J = 8.6 Hz, 1H), 8.99 (d, J = 8.8 Hz, 1H), 8.93 (d, J = 8.8 Hz, 1H), 8.68 (d, J = 8.8 Hz, 1H), 8.65 (d, 8.3 Hz, 2H), 8.49 (d, J= 7.9 Hz, 2H), 8.32 (d, J = 8.7 Hz, 1H), 8.25 (d, J = 8.8 Hz, 1H), 8.19 (t, J = 8.3 Hz, 1H), 7.96-7.83 (m, 6H), 7.81 (d, J = 8.2 Hz, 1H), 7.44 (t, J = 8.8 Hz, 1H), 7.31 (t, J = 6.9 Hz, 2H), 7.20 (t, J = 8.8 Hz, 1H), 6.80 (d, J = 8.8 Hz, 1H). ^{13}C NMR (175 MHz, CD₃OD) (Figure S4) δ (ppm): 161.82, 159.31, 158.98, 158.58, 152.48, 151.79, 151.12, 138.36, 137.45, 136.33, 135.43, 130.66, 130.44, 130.38, 129.36, 129.05, 129.10, 128.56, 128.35, 128.24, 126.96, 123.53, 123.46, 122.55, 120.36, 120.29. MALDI-TOF (m/z): [M-Cl]$^+$, calculated for C₃₃H₂₃ClN₅Ru, 626.07, found, 626.12.

Synthesis of Ru1-H_2O (Figure S1)

Ru1-H$_2$O was prepared by hydrolysis of [Ru(tpy)(biq)(Cl)]Cl in water. The coordinated chloride was substituted by H$_2$O in an aqueous solution. ^{1}H NMR (700 MHz, D$_2$O) (Figure S5) δ (ppm): 8.89 (d, J = 8.7 Hz, 1H), 8.78 (d, J = 8.7 Hz, 1H), 8.65-8.55 (m, 3H), 8.40-8.32 (m, 4H), 8.27 (t, J = 7.8 Hz, 1H), 7.99 (d, J = 8.6 Hz, 1H), 7.96-7.84 (m, 4H), 7.57 (d, J = 5.3 Hz, 2H), 7.52 (d, J = 7.9 Hz, 1H), 7.27 (t, J= 8.7 Hz, 1H), 7.20-7.12 (m, 3H), 6.65 (d, J= 8.7 Hz, 1H).
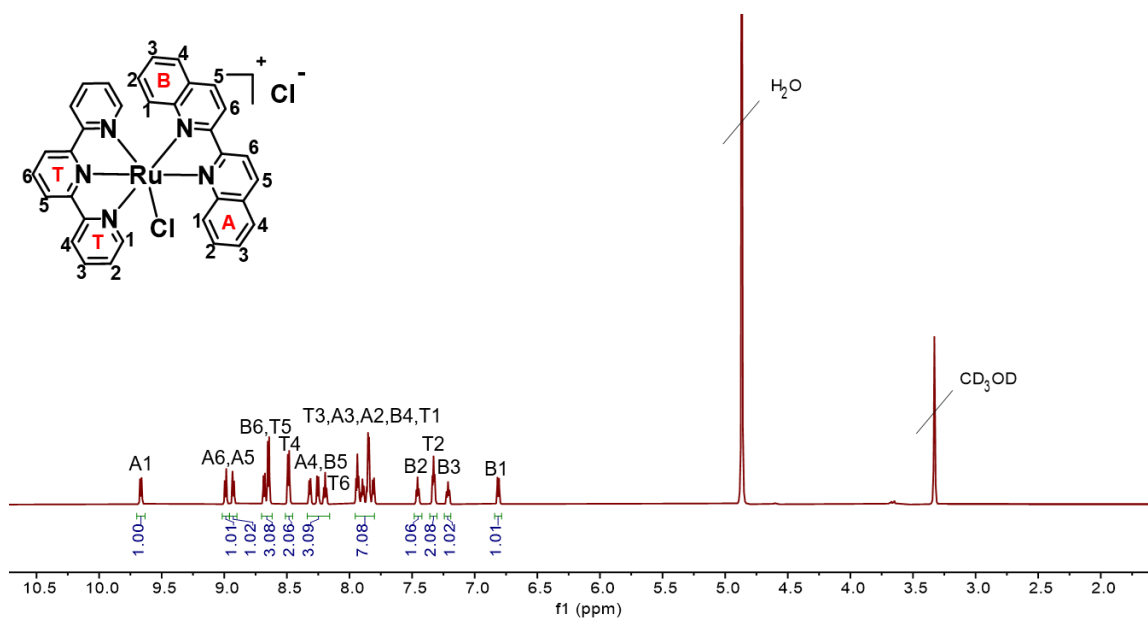
Figure S2. ^{1}H NMR spectrum of [Ru(tpy)(biq)(Cl)]Cl (700 MHz, CD$_3$OD).
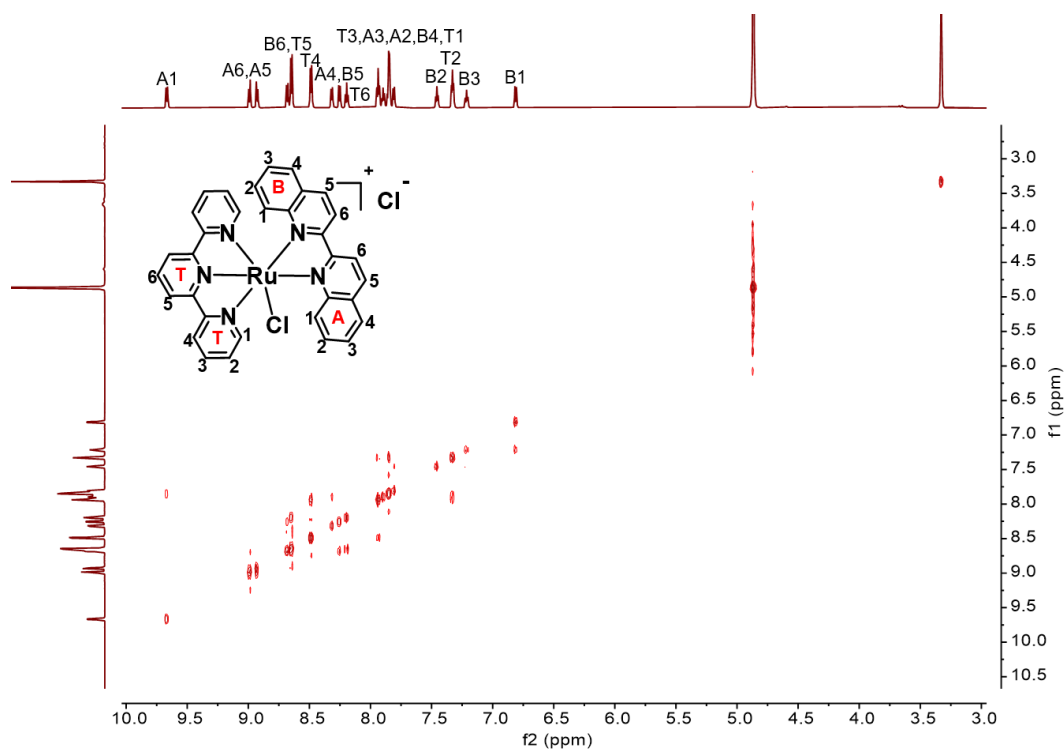
Figure S3. COSY NMR spectrum of [Ru(tpy)(biq)(Cl)]Cl (700 MHz, CD₃OD).
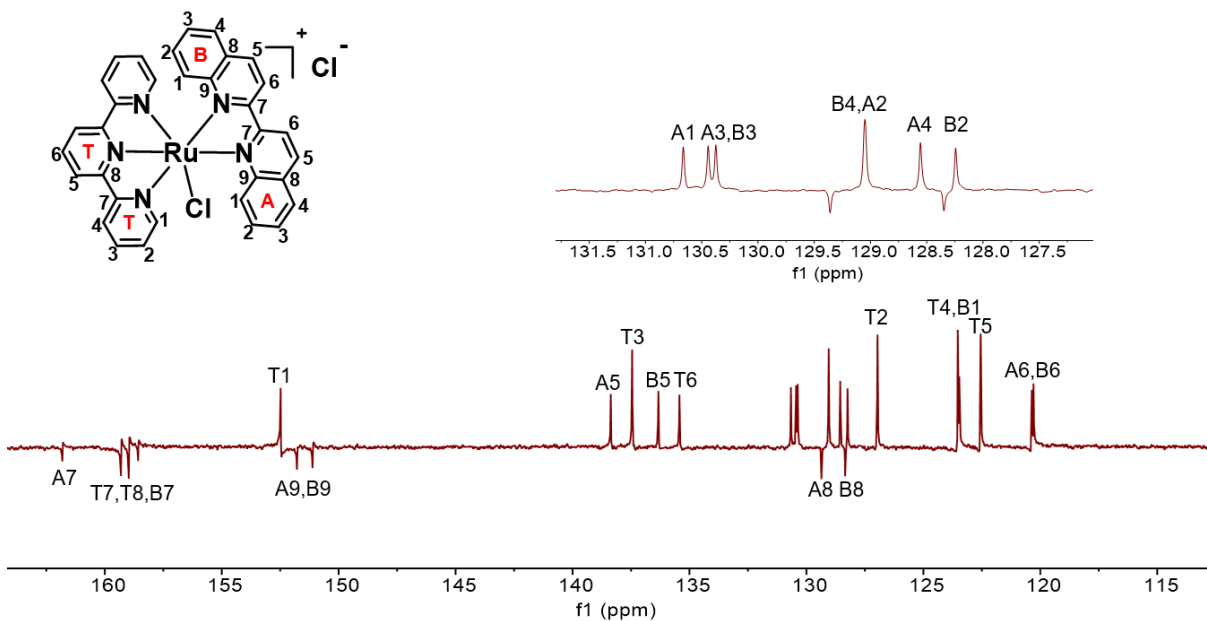
Figure S4. ¹³C NMR spectrum of [Ru(tpy)(biq)(Cl)]Cl (175 MHz, CD₃OD).
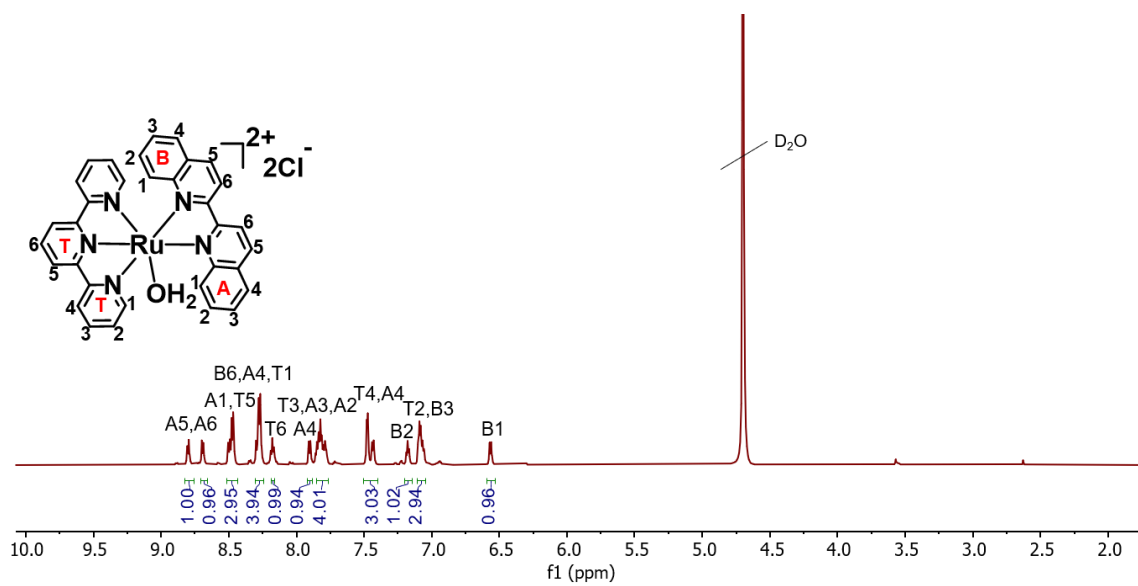
Figure S5. ^{1}H NMR spectrum of Ru1-H$_2$O (700 MHz, D$_2$O).
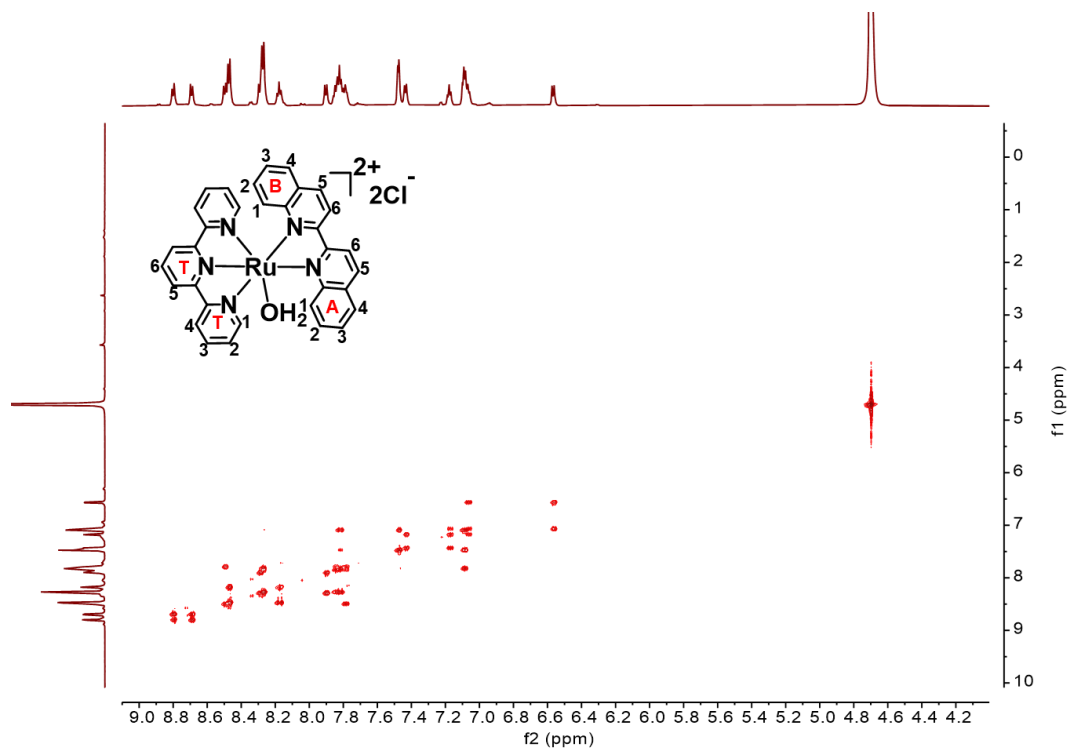
Figure S6. COSY NMR spectrum of Ru1-H$_2$O (700 MHz, D$_2$O).

2.5 Reference

[1] Jiang, Z. C.; Xiao, Y. Y.; Tong, X.; Zhao, Y., Selective Decrosslinking in Liquid Crystal Polymer Actuators for Optical Reconfiguration of Origami and Light-Fueled Locomotion. *Angewandte Chemie International Edition* **2019,** *58* (16), 5332-5337.

[2] Liao, Y., Design and applications of metastable-state photoacids. *Accounts of chemical research* **2017,** *50* (8), 1956-1964.

[3] Shafiq, Z.; Cui, J.; Pastor-Pérez, L.; San Miguel, V.; Gropeanu, R. A.; Serrano, C.; del Campo, A., Bioinspired underwater bonding and debonding on demand. *Angewandte Chemie* **2012,** *124* (18), 4408-4411.

[4] Weng, G.; Thanneeru, S.; He, J., Dynamic coordination of Eu–iminodiacetate to control fluorochromic response of polymer hydrogels to multistimuli. *Advanced Materials* **2018,** *30* (11), 1706526.

[5] Cui, J.; del Campo, A., Multivalent H-bonds for self-healing hydrogels. *Chemical Communications* **2012,** *48* (74), 9302-9304.

[6] Röttger, M.; Domenech, T.; van der Weegen, R.; Breuillac, A.; Nicolaÿ, R.; Leibler, L., High-performance vitrimers from commodity thermoplastics through dioxaborolane metathesis. *Science* **2017,** *356* (6333), 62-65.

[7] Bowman, C. N.; Kloxin, C. J., Covalent adaptable networks: reversible bond structures incorporated in polymer networks. *Angewandte Chemie International Edition* **2012,** *51* (18), 4272-4274.

[8] Jin, B.; Song, H.; Jiang, R.; Song, J.; Zhao, Q.; Xie, T., Programming a crystalline shape memory polymer network with thermo-and photo-reversible bonds toward a single-component soft robot. *Science advances* **2018,** *4* (1), eaao3865.

[9] An, Q.; Huang, T.; Shi, F., Covalent layer-by-layer films: chemistry, design, and multidisciplinary applications. *Chemical Society Reviews* **2018,** *47* (13), 5061-5098.

[10] Herder, M.; Lehn, J.-M., The photodynamic covalent bond: sensitized alkoxyamines as a tool to shift reaction networks out-of-equilibrium using light energy. *Journal of the American Chemical Society* **2018,** *140* (24), 7647-7657.

[11] Feringa, B. L., The art of building small: From molecular switches to motors (Nobel lecture). *Angewandte Chemie International Edition* **2017,** *56* (37), 11060-11078.

[12] Frisch, H.; Marschner, D. E.; Goldmann, A. S.; Barner-Kowollik, C., Wavelength-Gated Dynamic Covalent Chemistry. *Angewandte Chemie International Edition* **2018,** *57* (8), 2036-2045.

[13] Scott, T. F.; Schneider, A. D.; Cook, W. D.; Bowman, C. N., Photoinduced plasticity in cross-linked polymers. *Science* **2005,** *308* (5728), 1615-1617.

[14] Burnworth, M.; Tang, L.; Kumpfer, J. R.; Duncan, A. J.; Beyer, F. L.; Fiore, G. L.; Rowan, S. J.; Weder, C., Optically healable supramolecular polymers. *Nature* **2011,** *472* (7343), 334-337.

[15] Mobian, P.; Kern, J. M.; Sauvage, J. P., Light-driven machine prototypes based on dissociative excited states: photoinduced decoordination and thermal recoordination of a ring in a ruthenium (II)-containing [2] catenane. *Angewandte Chemie* **2004,** *116* (18), 2446-2449.

[16] Fan, W.; Tong, X.; Yan, Q.; Fu, S.; Zhao, Y., Photodegradable and size-tunable single-chain nanoparticles prepared from a single main-chain coumarin-containing polymer precursor. *Chemical Communications* **2014,** *50* (88), 13492-13494.

[17] Gerling, T.; Dietz, H., Reversible covalent stabilization of stacking contacts in DNA assemblies. *Angewandte Chemie* **2019,** *131* (9), 2706-2710.

[18] Truong, V. X.; Li, F. Y.; Ercole, F.; Forsythe, J. S., Wavelength-Selective Coupling and Decoupling of Polymer Chains via Reversible [2+2] Photocycloaddition of Styrylpyrene for Construction of Cytocompatible Photodynamic Hydrogels. *Acs Macro Letters* **2018,** *7* (4), 464-469.

[19] Marschner, D. E.; Frisch, H.; Offenloch, J. T.; Tuten, B. T.; Becer, C. R.; Walther, A.; Goldmann, A. S.; Tzvetkova, P.; Barner-Kowollik, C., Visible Light [2+2] Cycloadditions for Reversible Polymer Ligation. *Macromolecules* **2018,** *51* (10), 3802-3807.

[20] Frisch, H.; Bloesser, F. R.; Barner-Kowollik, C., Controlling Chain Coupling and Single-Chain Ligation by Two Colours of Visible Light. *Angewandte Chemie International Edition* **2019,** *58* (11), 3604-3609.

[21] Houck, H. A.; Blasco, E.; Du Prez, F. E.; Barner-Kowollik, C., Light-stabilized dynamic materials. *Journal of the American Chemical Society* **2019,** *141* (31), 12329-12337.

[22] Murayama, K.; Yamano, Y.; Asanuma, H., 8-Pyrenylvinyl adenine controls reversible duplex formation between serinol nucleic acid and RNA by [2+ 2] Photocycloaddition. *Journal of the American Chemical Society* **2019,** *141* (24), 9485-9489.

[23] Arai, T.; Tokumaru, K., Photochemical one-way adiabatic isomerization of aromatic olefins. *Chemical Reviews* **1993,** *93* (1), 23-39.

[24] Kovalenko, N. P.; Abdukadirov, A.; Gerko, V. I.; Alfimov, M. V. J. J. o. A. S., Some peculiarities of diarylethylenes with 3-pyrenyl fragments. *Journal of Applied Spectroscopy* **1980,** *32* (6), 607-612.

[25] Honda, S.; Oka, M.; Takagi, H.; Toyota, T., Topology-Reset Execution: Repeatable Postcyclization Recyclization of Cyclic Polymers. *Angewandte Chemie International Edition* **2019,** *58* (1), 144-148.

[26] Du, X.; Li, J.; Welle, A.; Li, L.; Feng, W.; Levkin, P. A., Reversible and Rewritable Surface Functionalization and Patterning via Photodynamic Disulfide Exchange. *Advanced Materials* **2015,** *27* (34), 4997-5001.

[27] Otsuka, H.; Nagano, S.; Kobashi, Y.; Maeda, T.; Takahara, A., A dynamic covalent polymer driven by disulfide metathesis under photoirradiation. *Chemical Communications* **2010,** *46* (7), 1150-1152.

[28] McBride, M. K.; Hendrikx, M.; Liu, D.; Worrell, B. T.; Broer, D. J.; Bowman, C. N., Photoinduced Plasticity in Cross-Linked Liquid Crystalline Networks. *Advanced Materials* **2017,** *29* (17), 1606509.

[29] Amamoto, Y.; Otsuka, H.; Takahara, A.; Matyjaszewski, K., Self-Healing of Covalently Cross-Linked Polymers by Reshuffling Thiuram Disulfide Moieties in Air under Visible Light. *Advanced Materials* **2012,** *24* (29), 3975-80.

[30] Amamoto, Y.; Kamada, J.; Otsuka, H.; Takahara, A.; Matyjaszewski, K., Polymers through Reshuffling of Trithiocarbonate Units. *Angewandte Chemie International Edition* **2011,** *50* (7), 1660-1663.

[31] Worrell, B. T.; McBride, M. K.; Lyon, G. B.; Cox, L. M.; Wang, C.; Mavila, S.; Lim, C.-H.; Coley, H. M.; Musgrave, C. B.; Ding, Y., Bistable and photoswitchable states of matter. *Nature communications* **2018,** *9*, 2804.

[32] Gordon, M. B.; French, J. M.; Wagner, N. J.; Kloxin, C. J., Dynamic bonds in covalently crosslinked polymer networks for photoactivated strengthening and healing. *Advanced Materials* **2015,** *27* (48), 8007-8010.

[33] Ji, S.; Cao, W.; Yu, Y.; Xu, H., Dynamic Diselenide Bonds: Exchange Reaction Induced by Visible Light without Catalysis. *Angewandte Chemie International Edition* **2014,** *53* (26), 6781-6785.

[34] Fan, F.; Ji, S.; Sun, C.; Liu, C.; Yu, Y.; Fu, Y.; Xu, H., Wavelength-Controlled Dynamic Metathesis: A Light-Driven Exchange Reaction between Disulfide and Diselenide Bonds. *Angewandte Chemie International Edition* **2018,** *57* (50), 16426-16430.

[35] Liu, C.; Zhang, Z.; Fan, Z.; He, C.; Tan, Y.; Xu, H., Adaptive Se-Te Metathesis Controlled by Cucurbituril-Based Host-Guest Interaction. *Chemistry – An Asian Journal* **2020,** *15* (24), 4321-4326.

[36] Liu, C.; Fan, Z.; Tan, Y.; Fan, F.; Xu, H., Tunable Structural Color Patterns Based on the Visible-Light-Responsive Dynamic Diselenide Metathesis. *Advanced Materials* **2020,** *32* (12), e1907569.

[37] Zayat, L.; Calero, C.; Albores, P.; Baraldo, L.; Etchenique, R., A new strategy for neurochemical photodelivery: Metal-ligand heterolytic cleavage. *Journal of the American Chemical Society* **2003,** *125* (4), 882-883.

[38] Sgambellone, M. A.; David, A.; Garner, R. N.; Dunbar, K. R.; Turro, C., Cellular Toxicity Induced by the Photorelease of a Caged Bioactive Molecule: Design of a Potential Dual-Action Ru(II) Complex. *Journal of the American Chemical Society* **2013,** *135* (30), 11274-11282.

[39] van Rixel, V. H. S.; Ramu, V.; Auyeung, A. B.; Beztsinna, N.; Leger, D. Y.; Lameijer, L. N.; Hilt, S. T.; Le Devedec, S. E.; Yildiz, T.; Betancourt, T.; Gildner, M. B.; Hudnall, T. W.; Sol, V.; Liagre, B.; Kornienko, A.; Bonnet, S., Photo-Uncaging of a Microtubule-Targeted Rigidin Analogue in Hypoxic Cancer Cells and in a Xenograft Mouse Model. *Journal of the American Chemical Society* **2019,** *141* (46), 18444-18454.

[40] Miguel, V. S.; Alvarez, M.; Filevich, O.; Etchenique, R.; del Campo, A., Multiphoton Reactive Surfaces Using Ruthenium(II) Photocleavable Cages. *Langmuir* **2012,** *28* (2), 1217-1221.

[41] Albani, B. A.; Peña, B.; Leed, N. A.; De Paula, N. A.; Pavani, C.; Baptista, M. S.; Dunbar, K. R.; Turro, C., Marked improvement in photoinduced cell death by a new tris-heteroleptic complex with dual action: singlet oxygen sensitization and ligand dissociation. *Journal of the American Chemical Society* **2014,** *136* (49), 17095-17101.

[42] Howerton, B. S.; Heidary, D. K.; Glazer, E. C., Strained ruthenium complexes are potent light-activated anticancer agents. *Journal of the American Chemical Society* **2012,** *134* (20), 8324-8327.

[43] Respondek, T.; Garner, R. N.; Herroon, M. K.; Podgorski, I.; Turro, C.; Kodanko, J. J., Light activation of a cysteine protease inhibitor: caging of a peptidomimetic nitrile with RuII (bpy) 2. *Journal of the American Chemical Society* **2011,** *133* (43), 17164-17167.

[44] Bahreman, A.; Limburg, B.; Siegler, M. A.; Bouwman, E.; Bonnet, S., Spontaneous formation in the dark, and visible light-induced cleavage, of a Ru-S bond in water: a thermodynamic and kinetic study. *Inorganic Chemistry* **2013,** *52* (16), 9456-69.

[45] Xie, C.; Sun, W.; Lu, H.; Kretzschmann, A.; Liu, J.; Wagner, M.; Butt, H.-J.; Deng, X.; Wu, S., Reconfiguring surface functions using visible-light-controlled metal-ligand coordination. *Nature communications* **2018,** *9*, 3842.

[46] Liu, J.; Xie, C.; Kretzschmann, A.; Koynov, K.; Butt, H. J.; Wu, S., Metallopolymer Organohydrogels with Photo-Controlled Coordination Crosslinks Work Properly Below 0° C. *Advanced Materials* **2020,** *32* (14), 1908324.

[47] Israelachvili, J. N., *Intermolecular and surface forces*. Academic press: 2011.

Chapter 3 Reconfigurable materials based on Ru-Se photodynamic bond

3.1 Introduction

Stimuli-responsive materials have potential applications in drug delivery,[1-3] manipulation of macroscopic devices,[4] information storage,[5] molecular switches,[6, 7] lithographies,[8] etc. These materials can respond to external stimuli, such as heat, light, electric or magnetic field, carbon dioxide, and pH. Among them, light, a noninvasive stimulus, has a high spatiotemporal resolution compared with other stimuli. Specific photoreactions of photoresponsive materials can be triggered by light irradiation, which results in changes in their physical or chemical properties such as polarity, orientation, or wettability.[9, 10]

To date, several photoresponsive compounds have been developed and used in materials science,[11, 12] nanotechnologies,[13-15] and biomedicine.[2, 3, 16, 17] For example, cis-trans isomerization of azobenzenes is used for information storage, lithography, and phytopharmacology;[12, 18-20] alkenes or overcrowded alkenes have been developed for self-locking and photoinduced surface functionalization;[21-23] the cleavage of coordination bonds or linkage of transition metal complexes can be used for drug delivery.[2, 3, 24, 25] Among these photoresponsive compounds, ruthenium (Ru) complexes are a class of photoresponsive metal complexes. Ru complexes show the ability of ligands to be selectively photosubstituted by solvent molecules under light irradiation. The photoreactions of Ru complexes can even be induced by long-wavelength light, which is attributed to their metal-to-ligand charge-transfer (MLCT) bands in the visible or near-infrared region, which is promising for biological applications compared with other responsive compounds.[26] More importantly, unlike most of the reported photoreactions of photoresponsive compounds that exhibit static and irreversible weakness, the photoreactions of some Ru complexes have reversible and dynamic properties that have already been used in supramolecular chemistry,[15] functional surface[27]

and hydrogels.[28] But the limitation of these applications are all based on Ru-thioethers compounds. Seeking a new photodynamic bond and make it to be capable in different functional applications is a challenge for Ru complexes. Here, we designed Ru-Se photodynamic bond that can be constructed for reconfigurable photoresponsive materials in different operating environments which has never been studied in reported Ru complexes applications. We demonstrate that the Ru-Se dynamic bonds function properly in different environments such as micelle solutions, surfaces and polymer gels. The Ru-Se photodynamic bond opens up a new avenue for the development of responsive, healable, switchable, and reconfigurable materials.

3.2 Results and Discussion

3.2.1 Photo-controlled assembly of amphiphiles with Ru-Se bonds

It is well known that reversible formation or morphology transition of the stimuli-responsive nanoparticles have attracted considerable interest in the functional assembly region. Our new Ru-Se dynamic bond was applied to control the self-assembly of amphiphiles (Figure 1). To demonstrate reversible, photoswitchable self-assembly morphologies, we synthesized the complex Ru2-H_2O that contained a hydrophobic hydrocarbon chain and a selenoether ligand SeOEG (Figure 1, S1-S13). SeOEG contained a hydrophilic oligo(ethylene glycol) chain, which can coordination with Ru2-H_2O in dark conditions. To prepare the amphiphilic assemblies of Ru2-SeOEG, Ru2-H_2O (2 mmol) and SeOEG (10 mmol) were dissolved in THF/H_2O (3/1, v/v, 0.4 mL) and reacted overnight. Then, 1.6 mL Milli-Q water was added dropwise to the mixture with a stirring rate of 300 rpm. Afterward, the micelle dispersion was dialyzed against 5 L Milli-Q water for 8 h using a dialysis tube (MW cutoff, 0.5 kDa).
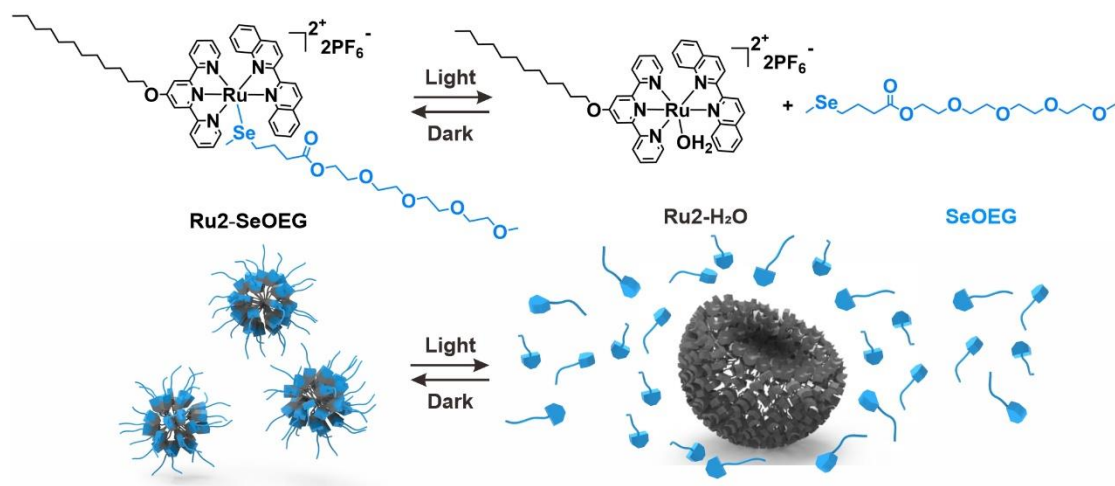
Figure 1. Chemical structures of Ru2-SeOEG, Ru2-H2O and SeOEG and schematic illustration of photo-controlled reversible morphology transitions. Different blocks represent different molecular groups, black, Ru2-H2O, blue, SeOEG ligands.

First, UV-vis absorption absorption spectroscopy was used to characterize the coordination and photosubstituion interconversions between Ru2-H2O and Ru2-SeOEG. The absorption band of the mixture was blue-shifted compared with that of Ru2-H2O, which showed that Ru2-SeOEG was formed via coordinating SeOEG with Ru2-H2O. As Ru2-SeOEG micelles solution was irradiated with green light (530 nm, 30 mW cm^{-2}), its absorption band shifted from 538 nm to 552 nm (Figure 2). Subsequently, the absorption band reverted when the sample was kept in the dark for 60 min. The absorption changes are in accordance with the dissociation and reformation Ru-Se bond that was studied in chapter 2. Therefore, SeOEG can reversibly coordinate to and dissociate from the Ru complex (Figure 1). In addition, the Ru2-SeOEG micelles could also perform stable enough in the PBS (10 mM) solution in the dark which endowed great potential in serval biological applications (Figure 3).
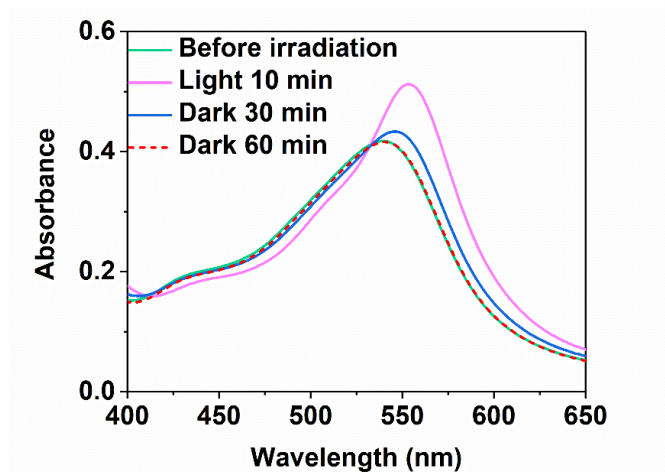
Figure 2. UV-vis spectra of Ru2-SeOEG micelle solution before irradiation, after green light (530 nm, 30 mW cm^{-2}) irradiation for 10 min, and after kept in the dark for 30 and 60 min. The spectral changes demonstrated that light irradiation induced dissociation Ru-Se bond and Ru-Se reformed in the dark.
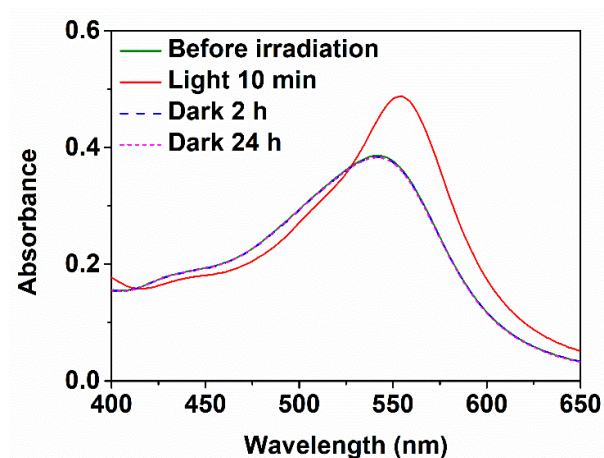
Figure 3. UV-Vis spectra of amphiphile Ru2-SeOEG in PBS (10 mM) before irradiation, after green light (530 nm, 30 mW cm^{-2}) irradiation for 10 min, and after kept in the dark for 2 and 24 h.

Transmission electron microscopy (TEM) fully characterized self-assembly behaviors with photo-controlled reversible morphology transitions based on Ru2-H$_2$O and SeOEG. First, TEM

showed that Ru2-SeOEG self-assembled into spheres with a diameter of ~5 nm (Figure 4a). The hydrodynamic diameter of Ru2-SeOEG assemblies measured using dynamic light scattering (DLS) was ~10 nm (Figure 5) due to hydrodynamic diameter higher than dry particle diameter. Meanwhile density function theory (DFT) simulation showed that the length of a Ru2-SeOEG molecule was ~2.5 nm (Figure 6). These results revealed that Ru2-SeOEG formed spherical micelles (Figure 4a).

Ru2-SeOEG micelles changed to bowl-shape large compound micelles with an average hydrodynamic diameter of ~350 nm after green light irradiation (530 nm, 30 mW cm^{-2}) for 10 min (Figure 4b). The bowl-shape large compound micelles reverted to spherical micelles after subsequent dark storage for 60 min (Figure 4c). Because SeOEG is water soluble, the bowl-shape large compound micelles should be mainly composed of Ru2-H$_2$O. The hydrodynamic diameters of the particles changed from ~10 nm to ~400 nm and recovered to ~10 nm (Figure 5).
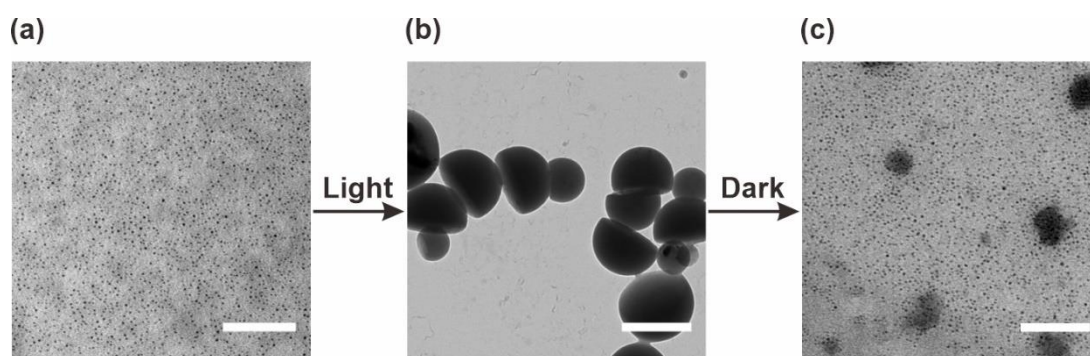
Figure 4. Photo-controlled self-assembly of amphiphiles with Ru-Se bonds. (a-c) Transmission electron microscopy (TEM) images of Ru2-SeOEG (a) before irradiation, (b) after green light irradiation for 10 min (530 nm, 30 mW cm^{-2}), and (c) subsequent kept in the dark for 60 min. Scale bars for (a) and (c): 100 nm; Scale bar for (b): 500 nm.
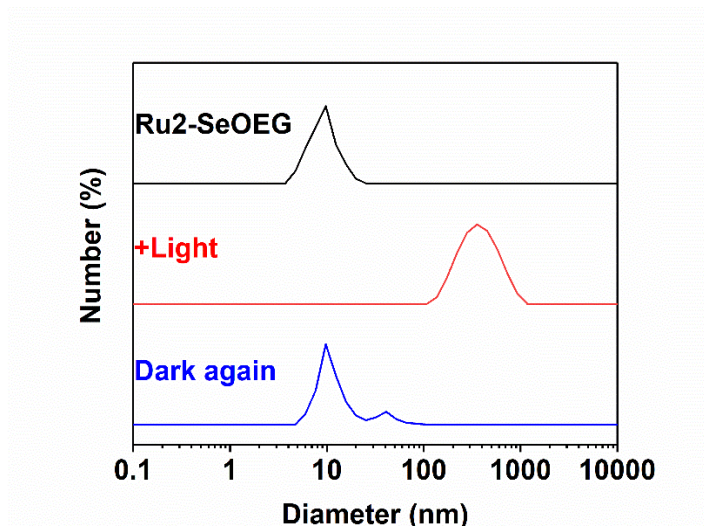
Figure 5. The hydrodynamic diameters of Ru2-SeOEG assemblies before irradiation, after light irradiation, and after dark storage measured by dynamic light scattering (DLS).
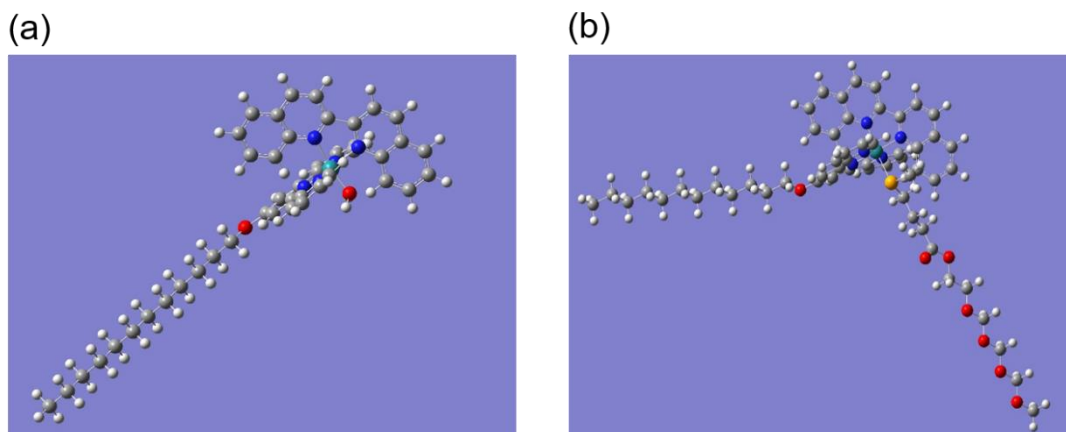
Figure 6. DFT calculations for potential conformation of (a) Ru2-H_2O and (b) Ru2-SeOEG. C gray, O red, N blue, H white, and Ru indigo.

More TEM images measured at tilting angles and scanning electron microscopy (SEM) could fully describe the morphology of bowl-shape large compound micelles after light irradiation owing to the formation of Ru2-H_2O (Figure 7 and 8). Moreover, cryo-scanning electron microscopy

(cryo-SEM) confirmed that the bowl-shape large compound micelles should exist in solution but not formed during drying processes (Figure 9).
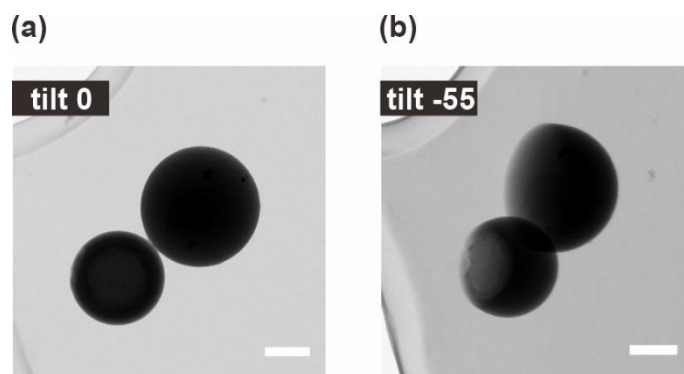
Figure 7. (a) and (b) TEM images of Ru2-SeOEG after green light irradiation measured at tilting angles of 0° (a) and -55° (b). Scale bars: 200 nm.
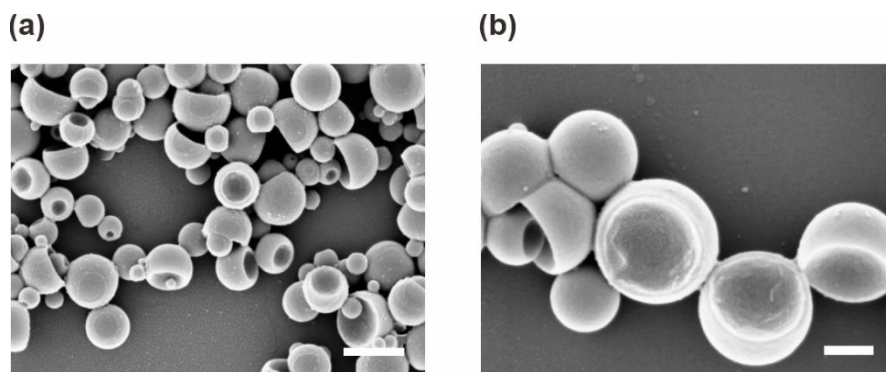
Figure 8. (a) and (b) Scanning electron microscopy (SEM) images of Ru2-SeOEG after green light irradiation. Scale bars for (a) and (b) are 1 μm and 200 nm, respectively.
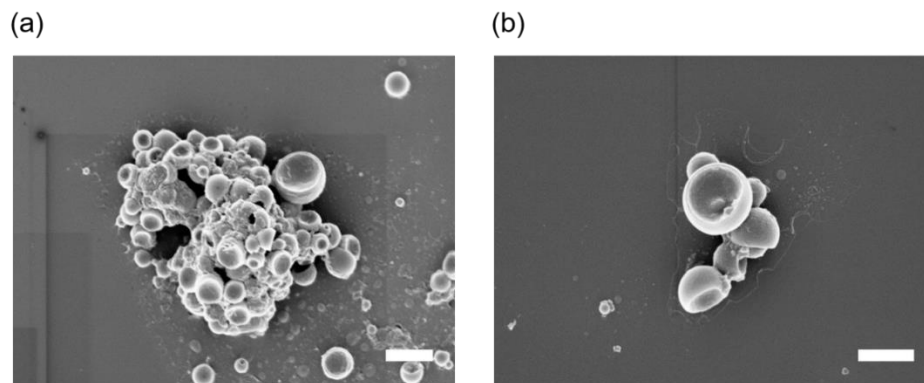
Figure 9. Cryo-SEM images of Ru2-SeOEG assemblies after green light irradiation. (a) Low magnification. Scale bar, 1 μm. (b) High magnification. Scale bar, 500 nm.

We interpret the photoinduced reversible morphology transitions using the packing parameter P of amphiphiles according to the theory proposed by Israelchvili et al. P equals to v/la, where v is the volume and l is the length of the hydrophobic chain and a represents the headgroup area (Eq. 1). Ru2-SeOEG formed micelles, indicating its P value was in the range of 0-0.33. After light irradiation, SeOEG was cleaved from Ru2-SeOEG. So, the molecular headgroup area a decreased. Therefore, P value increased dramatically, which should be the reason for the transition between micelles and bowl-shape large compound micelles.

$$P = \frac{v}{la} \qquad\qquad (\text{Eq. } 1)$$

3.2.2 Photoswitchable wettability based on Ru-Se bond

Smart surfaces are under intense investigation, especially the stimuli-responsive changes in wetting properties are potential in both fundamental research and industry. Our Ru-Se dynamic bonds are also applicable to switchable surfaces. (Figure 10). We synthesized Ru3-H$_2$O ([Ru(tpy-

COOH)(biq)(H$_2$O)](PF$_6$)$_2$, tpy-COOH = 6-(2,2':6',2''-terpyridin-4'-yloxy) hexanoic acid, biq = 2,2'-biquinoline) that contained a carboxylic group (Figure S14-S20) and a hydrophobic selenoether ligand SeC$_{12}$ (dodecyl 4-(methylselanyl) butanoate, Figure S14, S21-23).

To prepare Ru3-H$_2$O-grafted porous silica coating, a glass slide was held in the flame of a candle until a soot layer of a few micrometers thick was deposited. The candle-soot substrate was further performed by chemical vapor deposition method with tetraethoxysilane for 48 h. The substrate was subsequently heated at 600 °C for 4 h for removal of the carbon cores. As porous silica coating was prepared, which was modified with (3-aminopropyl)triethoxysilane (APTES). Ru3-H$_2$O was then grafted on the coating via amidation. The Ru3-H$_2$O-modified porous silica coating was fabricated by immersing the substrate into 10 mL dry DCM solution of Ru3-H$_2$O (100 mg, 0.097 mmol), EDC (68 mg, 0.355 mmol), and DMAP (40 mg, 0.327 mmol) for 24 h. (Figure 11).

To prepare hydrophilic Ru3-SeM-grafted coating (Figure 10a, left), Ru3-H$_2$O-grafted coating was immersed in an aqueous solution of SeM (10 mM) in the dark for 2 h. The static water contact angle of the Ru3-SeM-grafted coating was 29 ± 3° because SeM is hydrophilic (Figure 10b, left). To switch the wettability, the Ru3-SeM-grafted coating was irradiated with green light (530 nm, 30 mW cm^{-2}, 10 min) in water to remove SeM. The coating was then washed and immersed in an acetone/H$_2$O (v/v, 1/1) solution of SeC$_{12}$ in the dark for 2 h. Ru3-SeC$_{12}$-grafted coating was obtained (Figure 10a, right). Its static water contact angle was 105 ± 3° because SeC$_{12}$ ligand was hydrophobic (Figure 10b, right). To demonstrate that the wettability is switchable, the Ru3-SeC$_{12}$-grafted coating was irradiated with green light (530 nm, 30 mW cm^{-2}, 10 min) in acetone/H$_2$O to remove SeC$_{12}$. It was then washed and immersed in an aqueous solution of SeM in the dark for 2 h. The coating reverted to hydrophilic state. Furthermore, the wettability was switched for 5 cycles (Figure 9c), which showed that the hydrophilic-hydrophobic transitions were fully reversible.
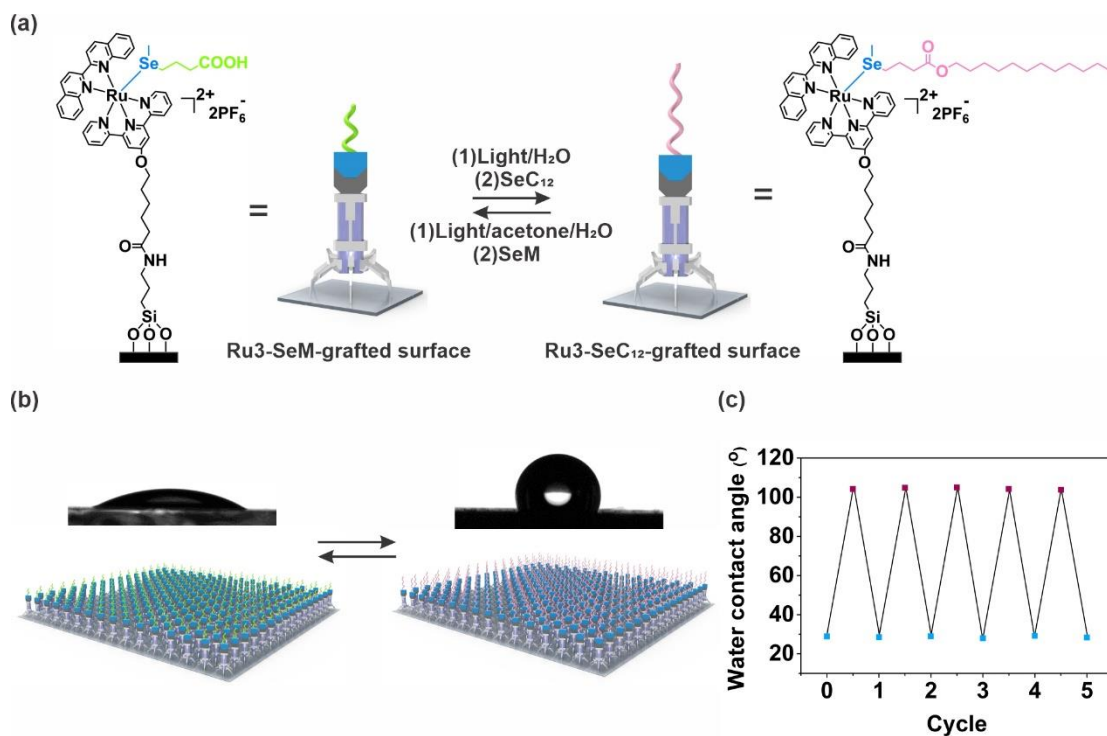
Figure 10. Photoswitchable wettability based on Ru-Se dynamic bond. (a) Schematic illustration of interconversion between a Ru3-SeM-grafted coating and a Ru3-SeC12-grafted coating. (b) Static water contact angles of Ru3-SeM-grafted and Ru3-SeC12-grafted coatings and schematic illustrations of the coatings. (c) Changes of static water contact angle as the coordinated ligands were converted between SeM and SeC12.
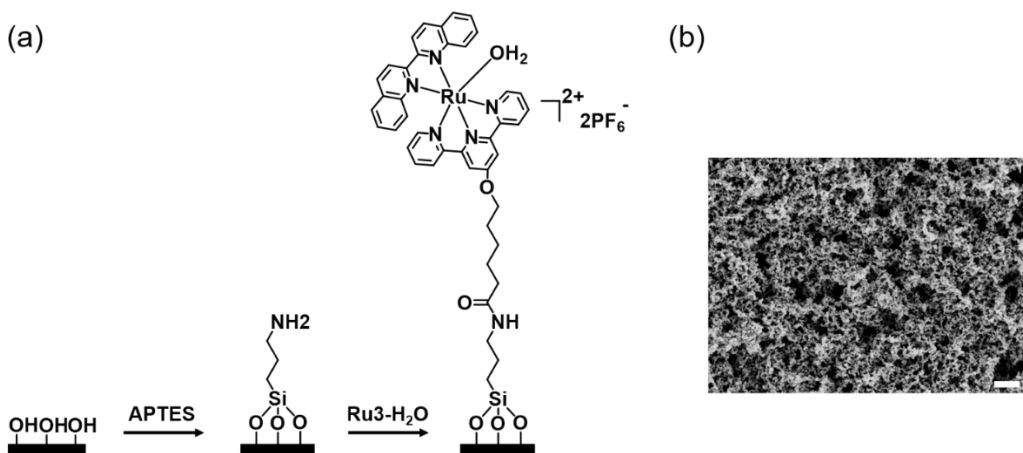
Figure 11. (a) Schematic illustration of preparation of Ru3-H$_2$O-grafted porous silica coating. (b) SEM image of Ru3-H$_2$O-grafted porous silica coating. Scale bar, 1 μm.

3.3.3 Photoinduced reversible gel-to-sol transitions using Ru-Se bond

Recently, a series of stimuli-responsive soft materials based on the disruption and reformation of dynamic interactions have been introduced and could be promising for biological materials. Our Ru-Se dynamic bond can be also used as reversible crosslinks for polymer gels (Figure 12). We synthesized a Ru complex Ru4-H$_2$O ([Ru(AAm-tpy)(biq)(H$_2$O)]Cl$_2$, AAm-tpy = N-(3-([2,2':6',2''-terpyridin]-4'-yloxy)propyl)acrylamide, biq = 2,2'-biquinoline) that contained a polymerizable acrylamide group (Figure S24-S27). We also synthesized a selenium ligand SeAAm (methyl 2-acrylamido-4-(methylselanyl)butanoate) that contained an acrylamide group (Figure S24, S28-S30).

To prepare polymer gels, [Ru(AAm-tpy)(biq)(Cl)]Cl (7.1 mg, 0.009 mmol) and SeAAm (15.6 mg, 0.045 mmol) were in 1.0 mL ethanol/H$_2$O (3/7, v/v) solution in the dark for 4 h to induce Ru-Se coordination. Then, the monomer HEA (97 mg, 0.84 mmol) and initiator VA-044 (2.9 mg, 0.009 mmol) were added to the mixture. The sample was placed in an oven at 50 °C for 12 h. The polymer gel was obtained after it was cooled to room temperature. The polymer gels could showe reversible gel-to-sol transitions under green light control (Figure 12).
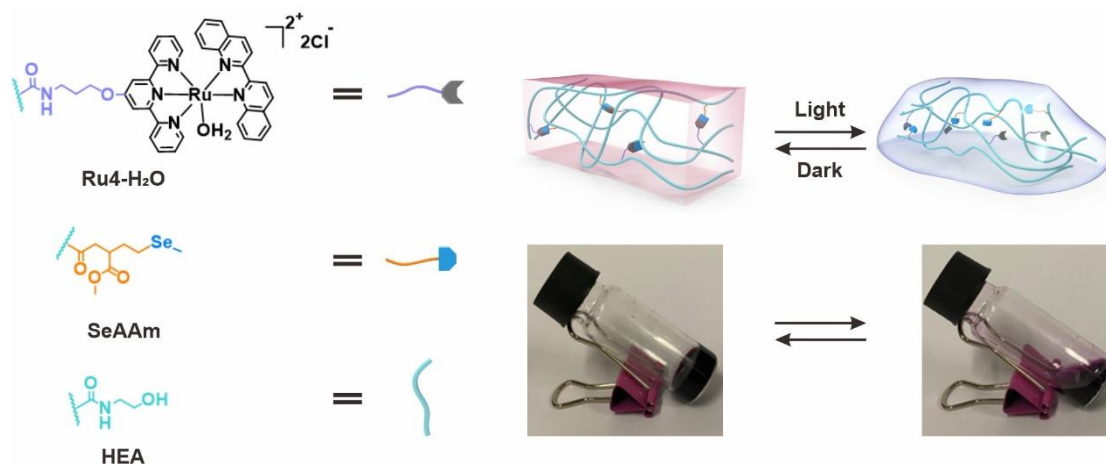
Figure 12. Photoinduced reversible gel-to-sol transitions of polymer gels with Ru-Se crosslinks. Schematic illustration and photographs of photoinduced reversible gel-to-sol transitions.

SEM was measured to observe the surface morphology of the polymer gels. It was clear that polymer gels with network structures formed via polymerization (Figure 13) and the connection of the network structure was acted by crosslinks based on Ru-Se dynamic bond crosslinks in the polymer gel (Figure 12).
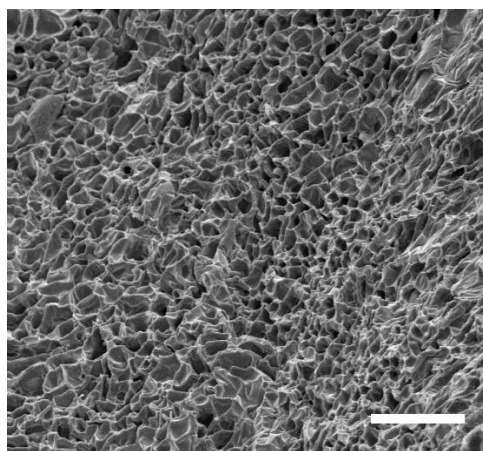
Figure 13. SEM image of the polymer gel networks. Scale bar: 1 µm.

Before further introducing the applications based on Ru-Se polymer gels, the photochemistry property was first illustrated. UV-vis absorption spectroscopy demonstrated that Ru-Se bonds in the polymer gel showed reversible dissociation/formation in the light irradiation/dark cycles (Figure 14). Photoinduced reversible dissociation/formation of Ru-Se crosslinks resulted in reversible gel-to-sol transitions (Figure 13). The polymer gel changed to sol after green light irradiation (530 nm, 30 mW cm^{-2}) for 10 min. The polymer gel reformed when the sol was kept in the dark for 120 min.
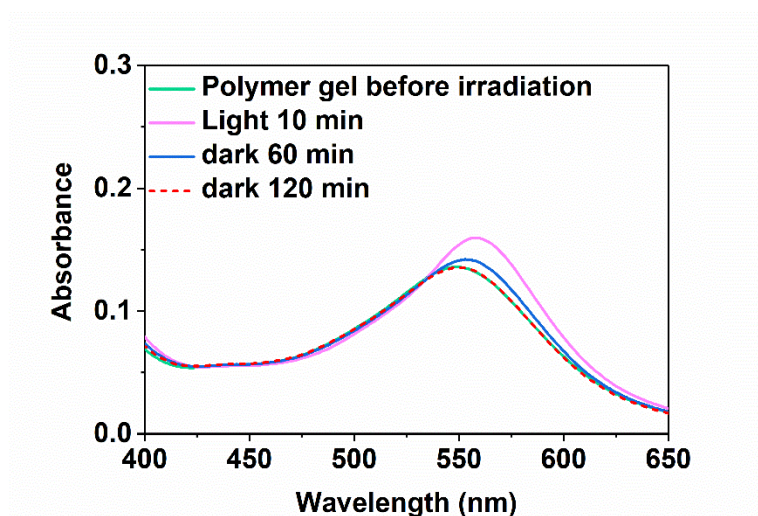
Figure 14. UV-vis absorption spectra of the polymer gel before irradiation, after green light (530 nm, 30 mW cm^{-2}) irradiation for 10 min, and after kept in the dark for 60 and 120 min. The spectral changes demonstrated that light irradiation induced dissociation Ru-Se bond and Ru-Se reformed in the dark.

It was important to deeply study the photoswitchable mechanical properties of Ru-Se polymer gels. The reversible gel-to-sol transitions were also studied using rheology (Figure 15). Initially, the storage modulus G' and loss modulus G'' of the polymer were 1.7-2.1 kPa and 0.07-0.25 kPa, respectively, in the angular frequency range 0.1-100 rad s^{-1}. G' was higher than G'', which

confirmed that the sample was a gel. After green light irradiation, G' and G'' decreased to 0.04-3.6

Pa and 0.16-12.7 Pa, respectively. G' became smaller than G'', which is in accordance with the fact

that the sample changed to sol after light irradiation. Subsequently, the polymer gel was kept in

the dark for 120 min. G' and G'' reverted and re-gelation occurred.
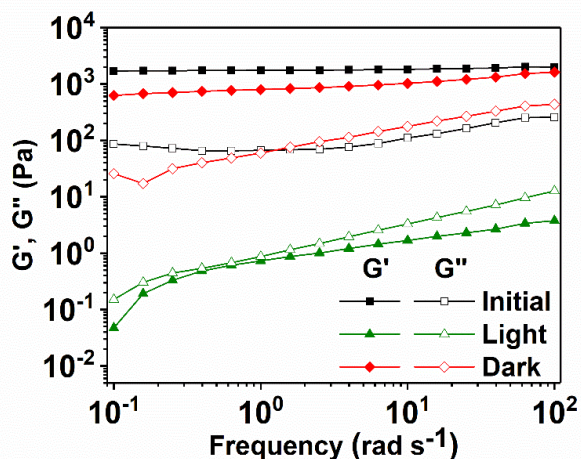
Figure 15. Rheology results of the polymer gel before irradiation, after green light irradiation, and subsequently stored in the dark. Storage modulus: G'; loss modulus: G''.

 Reshaping hydrogels is a basic requirement for photoresponsvie hydrogels application.

Photoinduced reversible gel-to-sol transitions were applied to reshaping the polymer gels (Figure

16a). To reshape a round polymer gel, it was irradiated with green light, transferred to a heart-

shaped mold, and kept in the dark. A heart-shaped polymer gel was obtained. The polymer gel was

also reshaped to a rectangle and a triangle. These results showed that the Ru-Se dynamic bond can

be applied to reconfigurable materials.
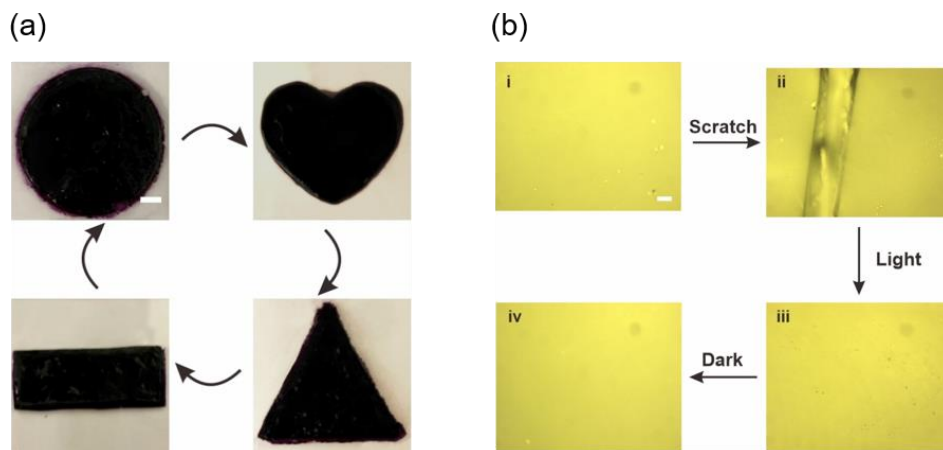
Figure 16. (a) Reshaping polymer gels for round, heart-shape, rectangle and triangle blocks. Scale bar: 2 mm. (b) Optical microscopy images of a polymer gel in the initial state, after scratching, after green light irradiation and subsequently kept in the dark for 2 h. Scale bar: 50 µm

At last, the polymer gel with Ru-Se dynamic bonds also exhibited healing ability based on photoinduced reversible gel-to-sol transitions (Figure 16b). To heal a scratched polymer gel, it was irradiated with green light (530 nm, 30 mW cm^{-2}) for 10 min to induce gel-to-sol transition. The sol flowed across the damaged area and re-gelation occurred in the dark. Thus, the Ru-Se bond is also a new dynamic bond for constructing healable materials.

3.3 Conclusion

In conclusion, after the deep characterization of Ru-Se photodynamic bond, we demonstrate that the new Ru-Se bond functions properly in different operating environments. We demonstrated photo-controlled assembly, photoswitchable wettability and photoinduced reversible gel-to-sol transitions using amphiphiles, surfaces and polymer gels that are constructed using Ru-Se bonds.

We anticipate more dynamic, reconfigurable, healable or responsive materials can be constructed using Ru-Se bonds. Our work opens an avenue for the development of photodynamic molecular systems, which is important for both the fundamental studies of dynamic bonds and the design of functional materials.

3.4 Supporting Information

Materials

RuCl$_3$•xH$_2$O (99.9%), 2,2'-biquinoline (98%), 4-(methylselanyl)butanoic acid (95%), 1-dodecanol (98%), 3,6,9,12-tetraoxatridecan-1-ol (98%), oxepan-2-one (98%), and potassium hydroxide (98%) were purchased from Sigma-Aldrich. 2-Amino-4-(methylseleno)butanoic acid (98%), N-(2-hydroxyethyl)acrylamide (98%), and 2,2'-azobis[2-(2-imidazolin-2-yl) propane] dihydrochloride (98%) (VA-044) were purchased from Tokyo Chemical Industry. 2,2':6',2''-Terpyridine (97%) and acryloyl chloride (97%) were purchased from Alfa Aesar. 4'-Chloro-2,2',6',2''-terpyridine (98%) was purchased from AEchem Scientific Corporation. All other solvents (HPLC grade) were purchased from Sigma-Aldrich or Fisher Scientific. Milli-Q water with a resistivity of 18.2 MΩ·cm was used in this study. Dialysis tubing (0.5K MWCO) was purchased from SERVA Electrophoresis GmbH, Germany.

Instruments and characterization

NMR spectra were recorded on Bruker Spectrospin NMR spectrometers (300 MHz or 700 MHz). UV-vis absorption spectra were measured on a Lambda 900 spectrometer (Perkin Elmer). The

molecular weights were determined using mass spectrometry (Bruker Time-of-flight MS Reflex III or Advion ASAP Atmospheric Solids Analysis). Photon flux was measured by Ophir 7Z02410 PD300 10pW-300mW power meter. Transmission electron microscopy (TEM) images were obtained on a JEOL 1400 transmission electron microscope. TEM images with different tilting angles were measured using an FEI Tecnai F20 transmission electron microscope. The hydrodynamic diameters of the assemblies were determined by dynamic light scattering (DLS) (ALV-7004, ALV GmbH). A laser diode (Qioptiq/Excelitas, iFLEX2000, $\lambda = 831$ nm, 40 mW) was used as the light source. The static water contact angles were measured with a contact angle meter (Dataphysics OCA35). Optical microscopy images were captured on an optical microscope (Zeiss) equipped with a CCD camera. Rheological characterization was carried out on an Advanced Rheometric Expansion System (ARES, Rheometric Scientific Company) with a parallel plate (PP 8 mm). The morphologies of Ru2-grafted porous silica coating, freeze-dried gel, and bowl-shaped assemblies were measured using scanning electron microscopy (SEM, LEO Gemini 1530).

Synthesis
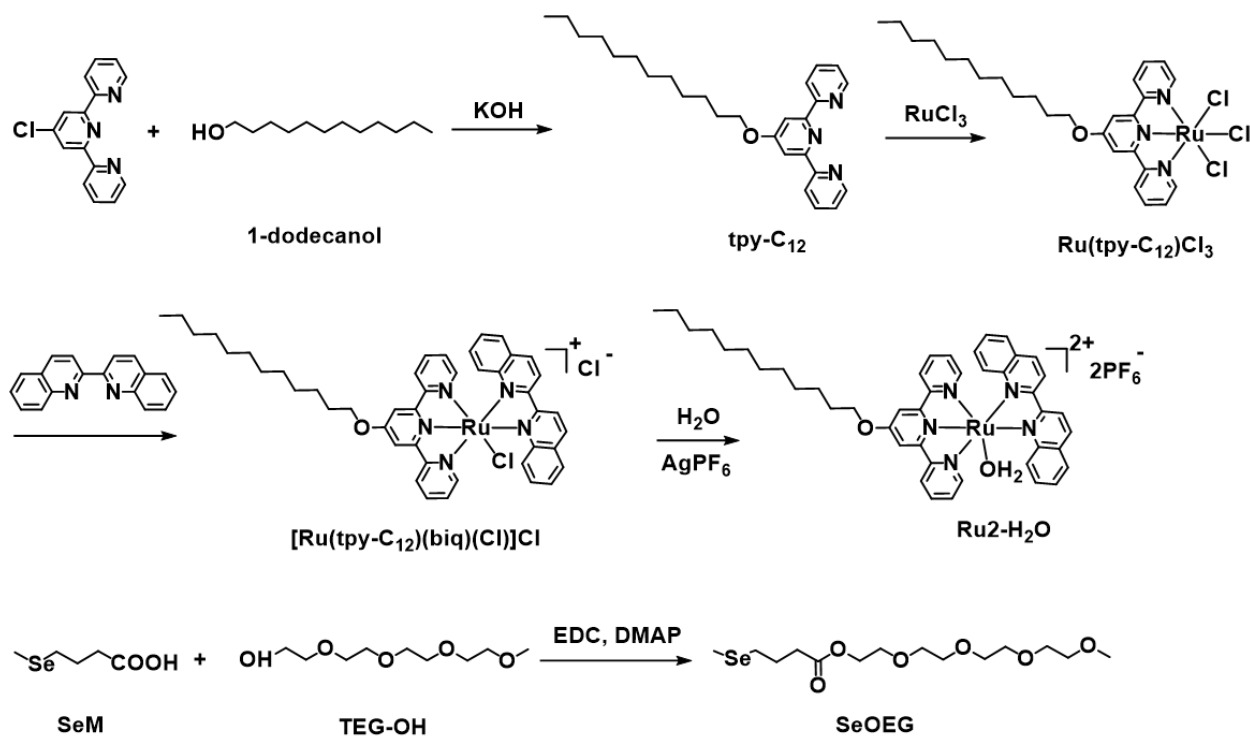
Figure S1. Synthetic routes for Ru2-H$_2$O and SeOEG.

Synthesis of 4'-(dodecyloxy)-2,2':6',2''-terpyridine (tpy-C$_{12}$) (Figure S1)

It was synthesized according to literature. ^{1}H NMR (300 MHz, CD$_2$Cl$_2$) (Figure S2) δ (ppm): 8.65 (d, J = 4.7 Hz, 2H), 8.60 (d, J = 8.0 Hz, 2H), 8.00 (s, 2H), 7.84 (dd, J = 8.0, 6.4 Hz, 2H), 7.32 (dd, J = 6.4, 4.7 Hz, 2H), 4.20 (t, J = 6.5 Hz, 2H), 1.91-1.77 (m, 2H), 1.55-1.42 (m, 2H), 1.38-1.21 (m, 16H), 0.86 (t, J = 6.9 Hz, 3H). ^{13}C NMR (75 MHz, CD$_2$Cl$_2$) (Figure S4) δ (ppm): 167.74, 157.42, 156.43, 149.42, 137.10, 124.24, 121.44, 107.59, 68.80, 32.32, 30.07, 30.04, 30.00, 29.98, 29.97, 29.75, 29.42, 26.31, 23.10, 14.28. MALDI-TOF (m/z): [M]$^+$, calculated for C$_{27}$H$_{35}$N$_3$O, 417.28, found, 417.60.

Synthesis of Ru(tpy-C$_{12}$)Cl$_3$ (Figure S1)

RuCl$_3$•xH$_2$O (220 mg, 0.84 mmol) and tpy-C$_{12}$ (317 mg, 0.76 mmol) were dissolved in 80 mL absolute ethanol under an argon atmosphere. The mixture was refluxed for 4 h. After cooled to room temperature, the mixture was filtrated. The filtrated brown powders were washed with ethanol and diethyl ether sequentially to obtain the product (312 mg, 66%).

Synthesis of [Ru(tpy-C$_{12}$)(biq)(Cl)]Cl (Figure S1)

Ru(tpy-C$_{12}$)(biq)Cl$_3$ (243 mg, 0.39 mmol) and 2,2'-biquinoline (biq, 100 mg, 0.39 mmol) were dissolved in 20 mL 1/1 ethanol/H$_2$O mixture. The mixture was degassed and refluxed overnight under an argon atmosphere. Afterwards, remove residue by filtration when the solution was hot. Then, the mixture was collected by evaporation under reduced pressure. The crude product was purified through column chromatography with silica gel (eluent: methanol/DCM = 1/10 to 1/5). Violet powders were obtained (125 mg, 40%). ^{1}H NMR (700 MHz, CD$_3$OD) (Figure S5) δ (ppm): 9.64 (d, J = 8.8 Hz, 1H), 8.93 (d, J = 8.9, 1H), 8.86 (d, J = 8.9, 1H), 8.70 (d, J = 8.6 Hz, 1H), 8.47 (d, J = 7.9 Hz, 2H), 8.29-8.24 (m, 3H), 8.21 (d, J = 8.7, 1H), 7.90-7.77 (m, 7H), 7.45 (dd, J= 8.8, 7.1 Hz, 1H), 7.29-7.23 (m, 3H), 6.89 (d, J = 8.8 Hz, 1H), 4.46 (t, J = 6.3 Hz, 2H), 2.01-1.94 (m, 2H), 1.65-1.59 (m, 2H), 1.50-1.31 (m, 16H), 0.90 (t, J = 6.6 Hz, 3H). ^{13}C NMR (175 MHz, CD$_3$OD) (Figure S7) δ (ppm): 166.81, 162.11, 159.55, 159.19, 158.87, 152.68, 152.02, 151.37, 137.80, 137.28, 135.91, 130.60, 130.34, 130.26, 129.21, 129.03, 128.98, 128.52, 128.34, 128.16, 126.80, 123.72, 123.62, 120.31, 120.24, 110.06, 69.87, 31.68, 29.42, 29.40, 29.35, 29.28, 29.06, 28.70, 28.62, 25.68, 22.31, 15.44. MALDI-TOF (m/z): [M]$^+$, calculated for C$_{45}$H$_{47}$ClN$_5$ORu, 810.25, found, 810.27.

Synthesis of Ru2-H$_2$O (Figure S1)

[Ru(tpy-C$_{12}$)(biq)(Cl)]Cl (34 mg, 0.04 mmol) and AgPF$_6$ (36 mg, 0.14 mmol) were dissolved in 5 mL 4/1 acetone/H$_2$O mixture. The mixture was degassed and refluxed overnight under an argon atmosphere. After the solution was cooled down to room temperature, the mixture was filtrated and concentrated to 1 mL by evaporation under reduced pressure. The dark purple product was obtained via precipitation by adding saturated KPF$_6$ solution (20 mg, 44%). ^{1}H NMR (700 MHz, CD$_3$OD) (Figure S8) δ (ppm): 9.04 (d, J = 8.4 Hz, 1H), 9.00 (d, J = 8.4 Hz, 1H), 8.79 (d, J = 8.4 Hz, 1H), 8.72 (d, J= 9.1 Hz, 1H), 8.61 (d, J = 8.4 Hz, 2H), 8.43 (m, 3H), 8.29 (d, J = 8.4 Hz, 1H), 8.06-7.97 (m, 4H), 7.92 (d, J = 7.0 Hz, 2H), 7.84 (d, J = 7.0 Hz, 1H), 7.51 (t, J = 7.0 Hz, 1H), 7.42 (t, J = 7.0 Hz, 2H), 7.38 (t, J = 8.4 Hz, 1H), 6.98 (d, J = 8.4 Hz, 1H), 4.57 (t, J = 6.3 Hz, 2H), 2.06-2.02 (m, 2H), 1.70-1.65 (m, 2H), 1.44-1.30 (m, 16H), 0.92 (t, J = 7.0 Hz, 3H). ^{13}C NMR (175 MHz, CD$_3$OD) (Figure S10) δ (ppm): 168.19, 162.36, 159.50, 159.49, 158.99, 153.69, 152.44, 150.89, 138.89, 138.62, 136.97, 132.02, 130.98, 129.77, 129.50, 129.33, 129.25, 128.49, 128.12, 127.99, 126.16, 124.43, 123.49, 120.97, 125.58, 111.09, 70.31, 31.68, 29.42, 29.35, 29.33, 29.30, 29.09, 28.67, 28.66, 25.65, 22.33, 13.02. MALDI-TOF (m/z): [M-2PF$_6$-H]$^+$, calculated for C$_{45}$H$_{47}$ClN$_5$ORu, 810.25, found, 810.27.

Synthesis of 2,5,8,11-tetraoxatridecan-13-yl-4-(methylselanyl)butanoate (SeOEG) (Figure S1)

4-(Methylselanyl)butanoic acid (SeM) (364 mg, 2 mmol) and 2,5,8,11-tetraoxatridecan-13-ol (TEG-OH) were dissolved in 5mL dry DCM. The solution was cooled down to 0 °C in an ice bath. EDC (500 mg, 2.5 mmol) and 4-DMAP (24.4 mg, 0.2 mmol) in 5 mL dry DCM were added dropwise into the mixture. The solution was stirred at room temperature overnight. The crude product was further purified through column chromatography with silica gel (eluent: ethyl acetate). Colorless oil was obtained (60 mg, 81%). ^{1}H NMR (300 MHz, CD$_2$Cl$_2$) (Figure S11) δ (ppm): 4.26

(t, J = 4.5 Hz, 2H), 3.74-3.67 (m, 12H), 3.56 (t, J = 5.7 Hz, 2H), 3.40 (s, 3H), 2.58-2.42 (m, 4H), 2.14 (s, 3H), 2.01-1.89 (m, 2H). ^{13}C NMR (75 MHz, CD$_2$Cl$_2$) (Figure S13) δ (ppm): 173.30, 72.29, 70.96, 70.94, 70.87, 70.86, 70.78, 63.92, 59.00, 33.69, 33.16, 24.55, 15.37. MALDI-TOF (m/z): [M]$^+$, calculated for C$_{14}$H$_{28}$O$_6$Se, 372.11, found, 372.42.
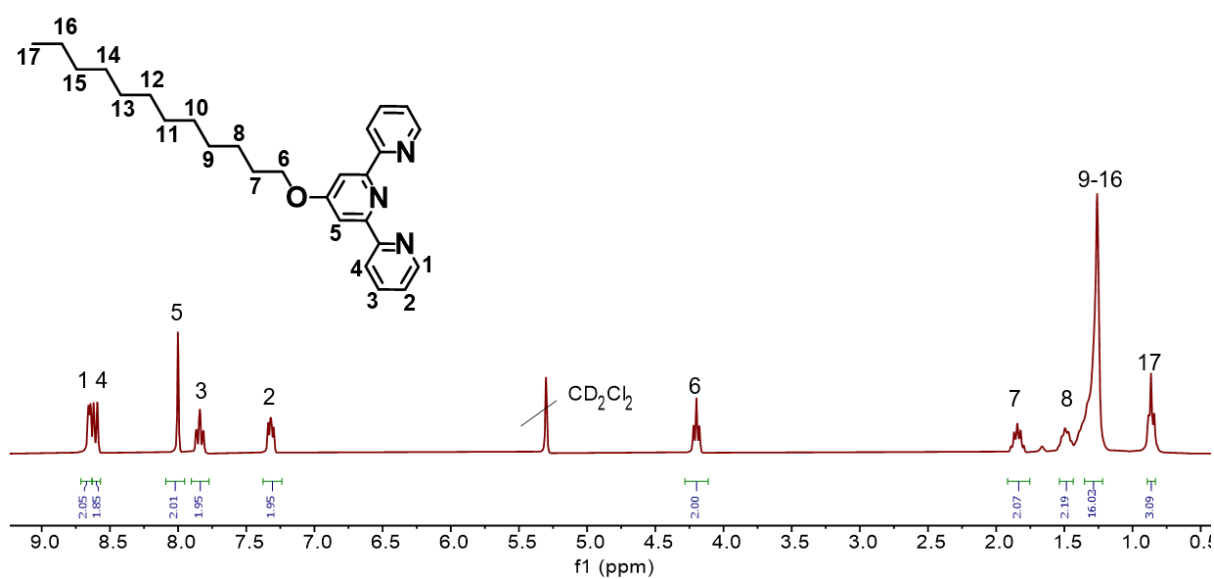
Figure S2. ^{1}H NMR spectrum of tpy-C$_{12}$ (300 MHz, CD$_2$Cl$_2$).
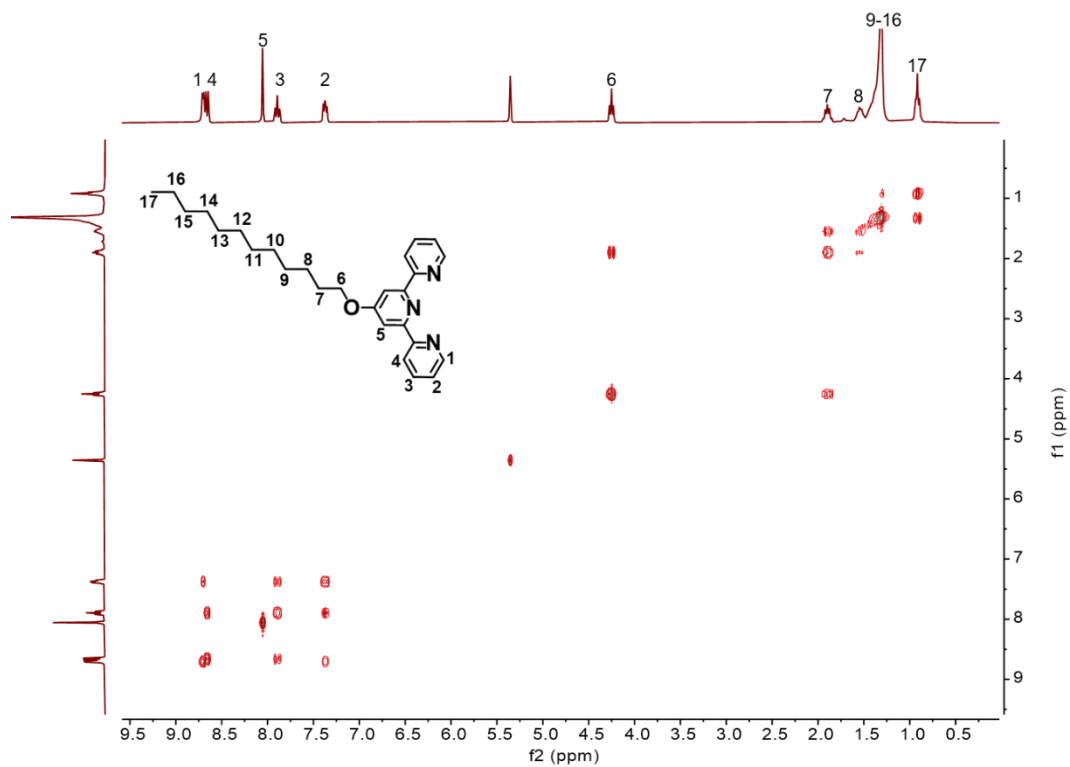
Figure S3. COSY NMR spectrum of tpy-C$_{12}$ (300 MHz, CD$_2$Cl$_2$).
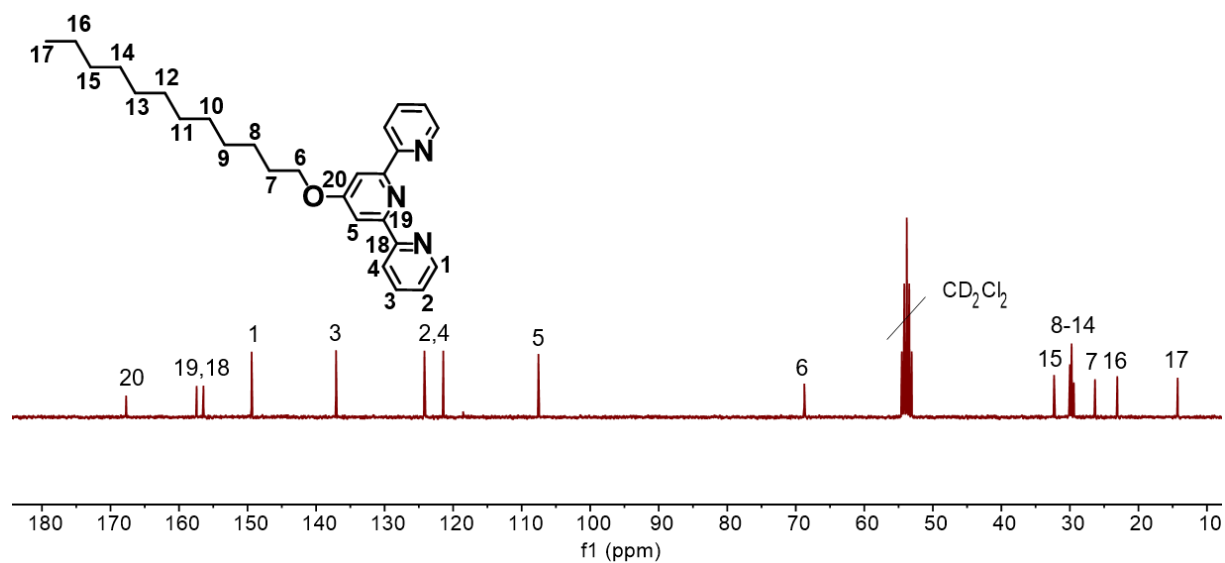
Figure S4. ^{13}C NMR spectrum of tpy-C$_{12}$ (75 MHz, CD$_2$Cl$_2$).
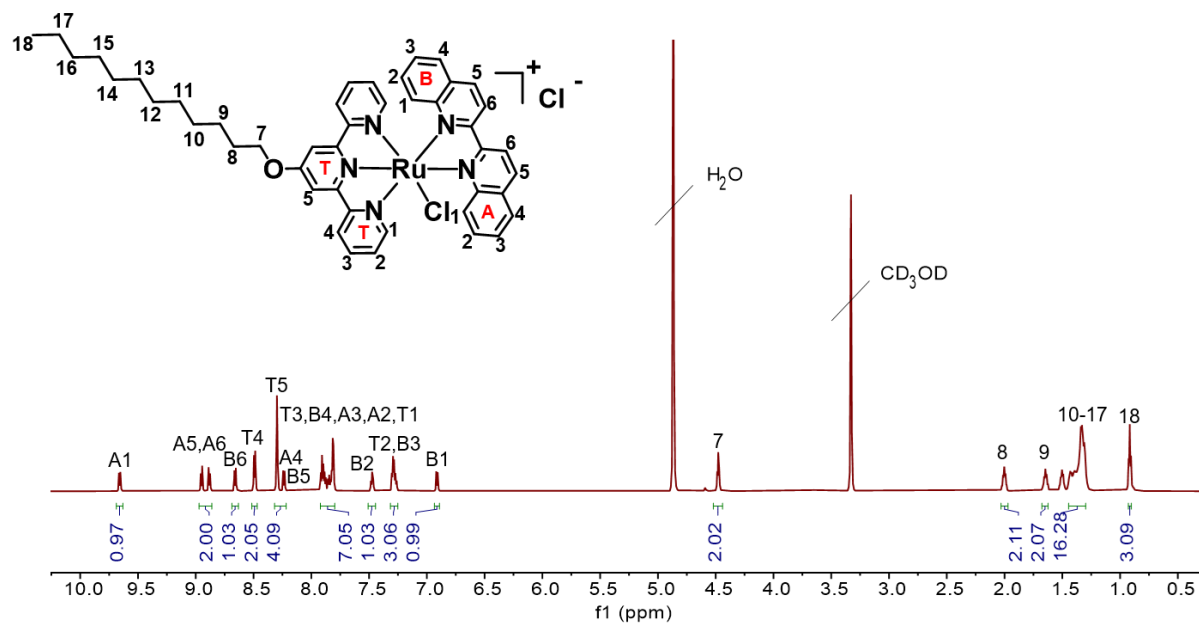
Figure S5. ^{1}H NMR spectrum of [Ru(tpy-C$_{12}$)(biq)(Cl)]Cl (700 MHz, CD$_3$OD).
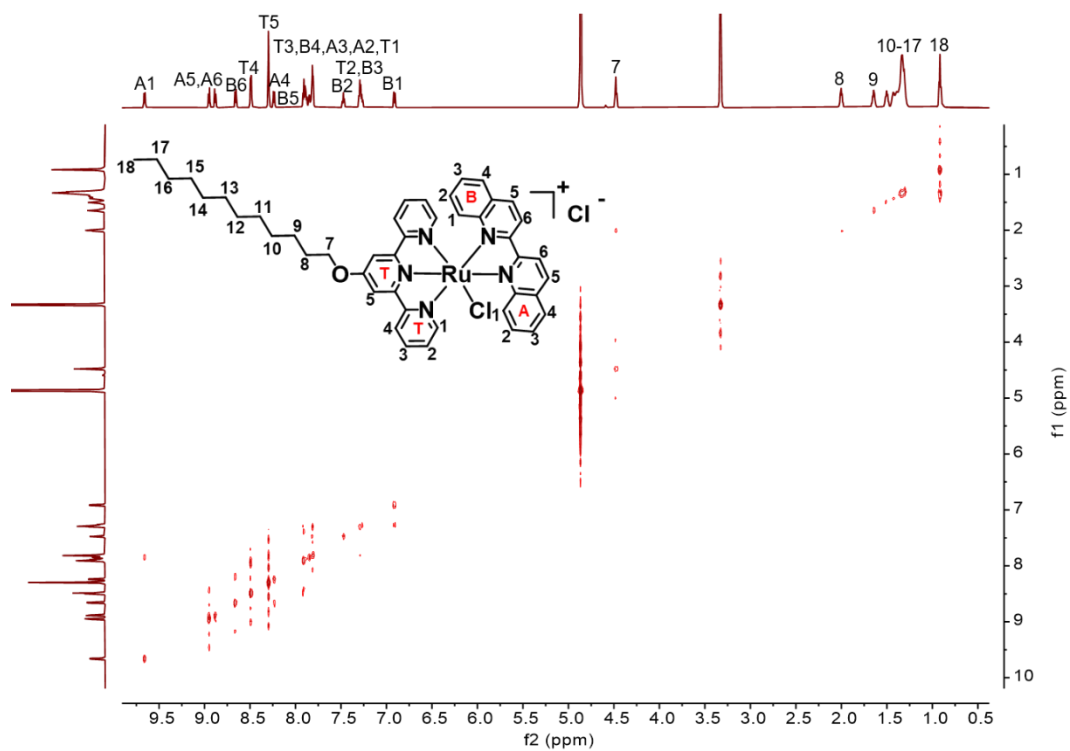
Figure S6. COSY spectrum of [Ru(tpy-C$_{12}$)(biq)(Cl)]Cl (700 MHz, CD$_3$OD).
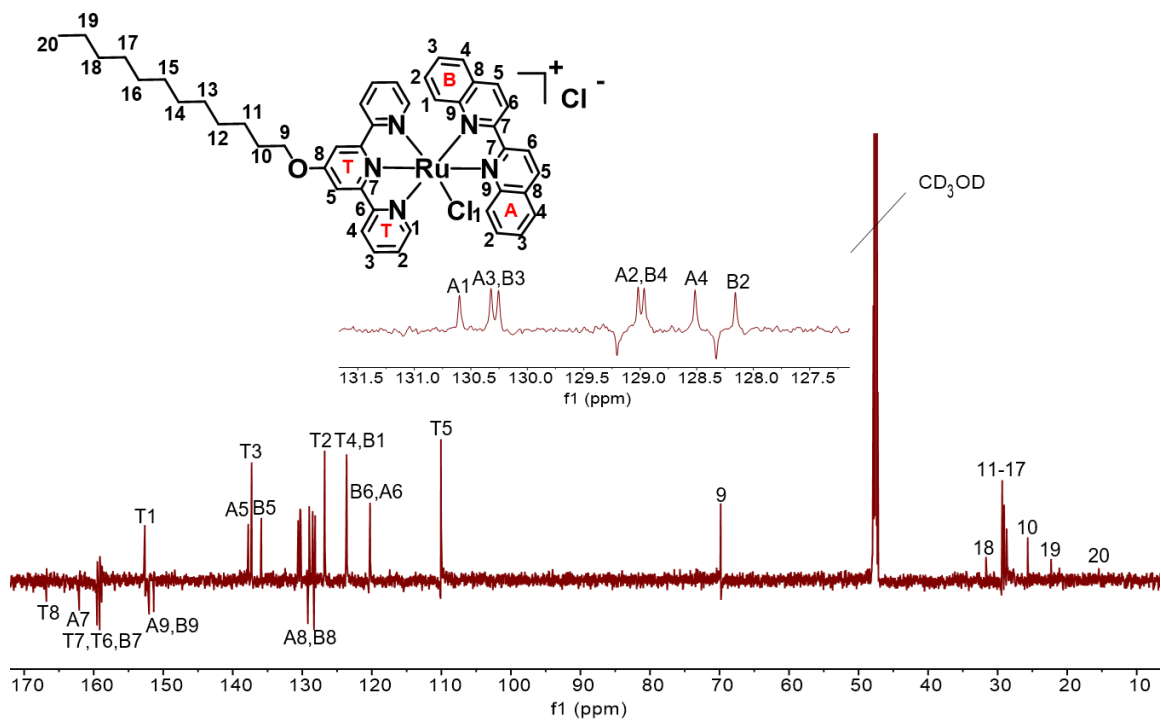
Figure S7. ^{13}C NMR spectrum of [Ru(tpy-C$_{12}$)(biq)(Cl)]Cl (175 MHz, CD$_3$OD).
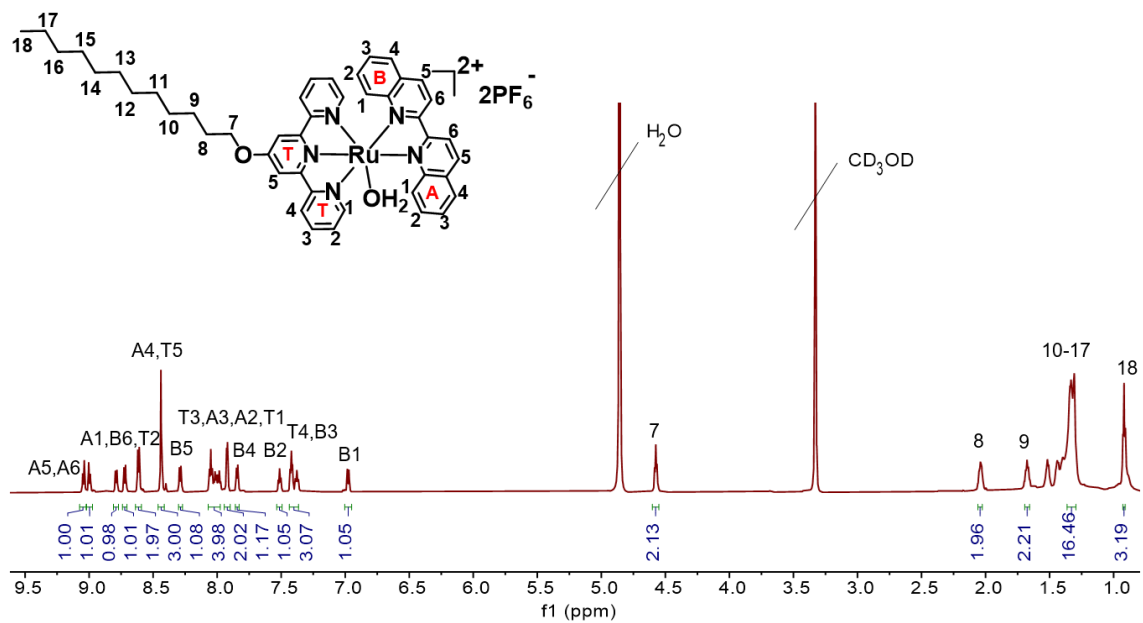
Figure S8. ^{1}H NMR spectrum of Ru2-H$_2$O (700 MHz, CD$_3$OD).

Figure S9. COSY spectrum of Ru2-H$_2$O (700 MHz, CD$_3$OD).

Figure S10. ^{13}C NMR spectrum of Ru2-H$_2$O (175 MHz, CD$_3$OD).
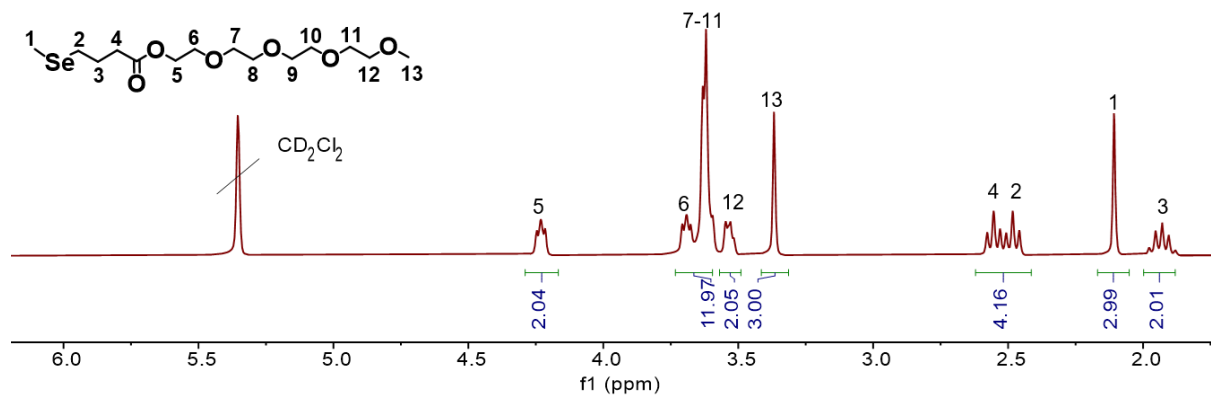
Figure S11. ^{1}H NMR spectrum of SeOEG (300 MHz, CD_2Cl_2).
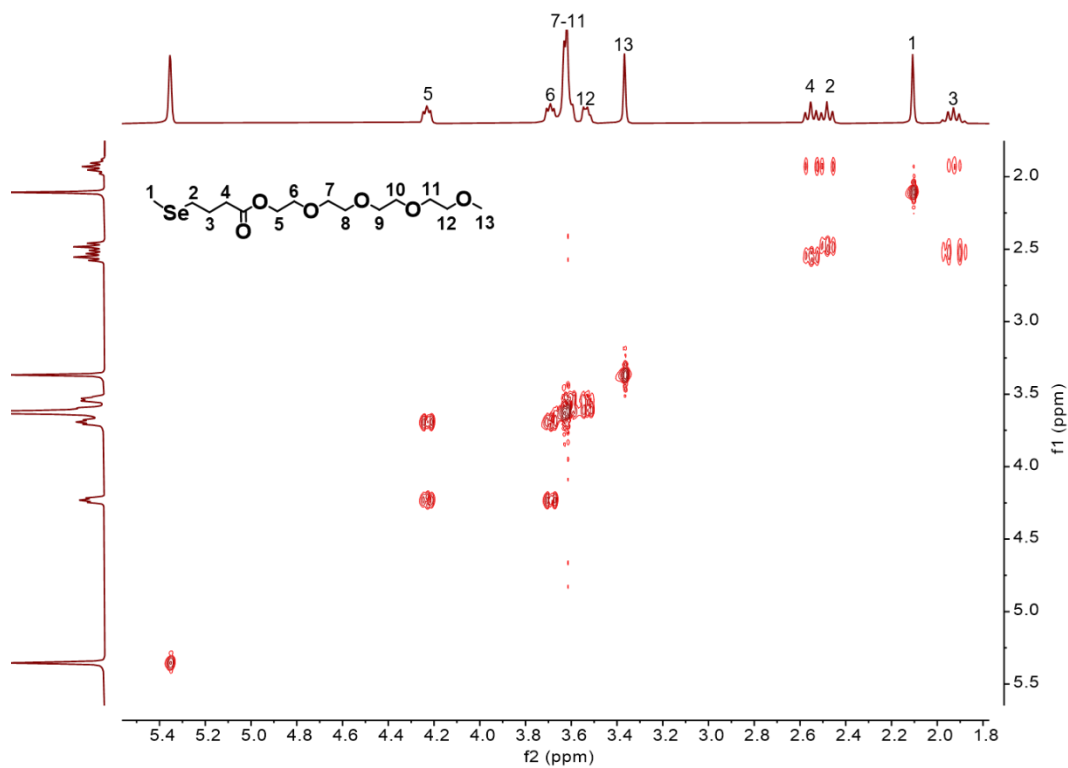
Figure S12. COSY NMR spectrum of SeOEG (300 MHz, CD_2Cl_2).
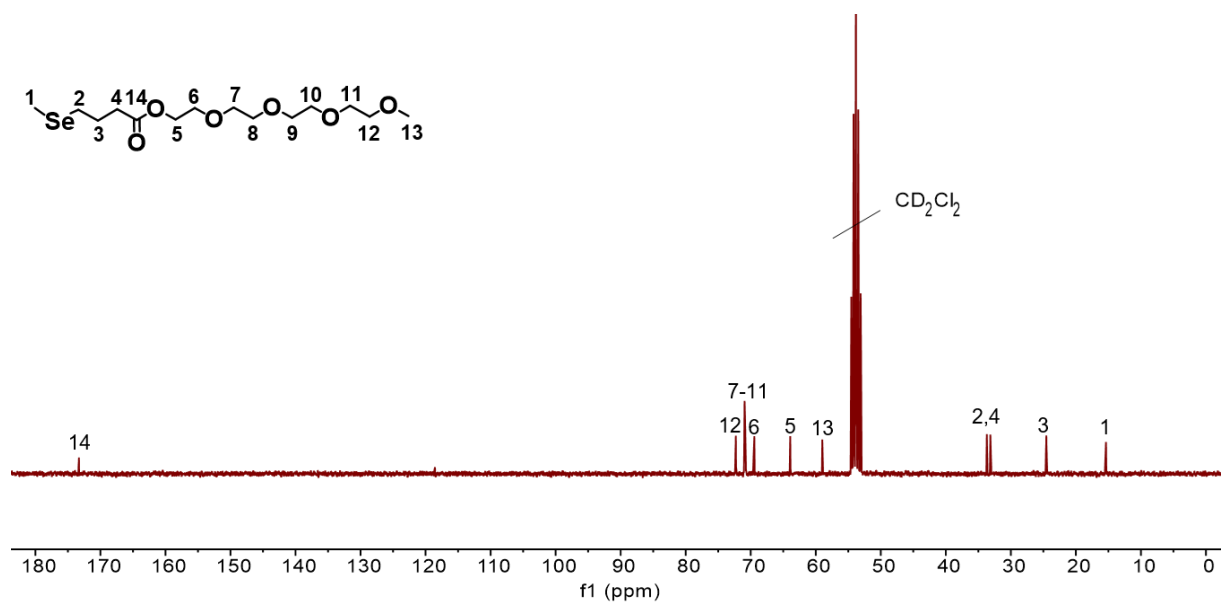
Figure S13. ^{13}C NMR spectrum of SeOEG (75 MHz, CD$_2$Cl$_2$).
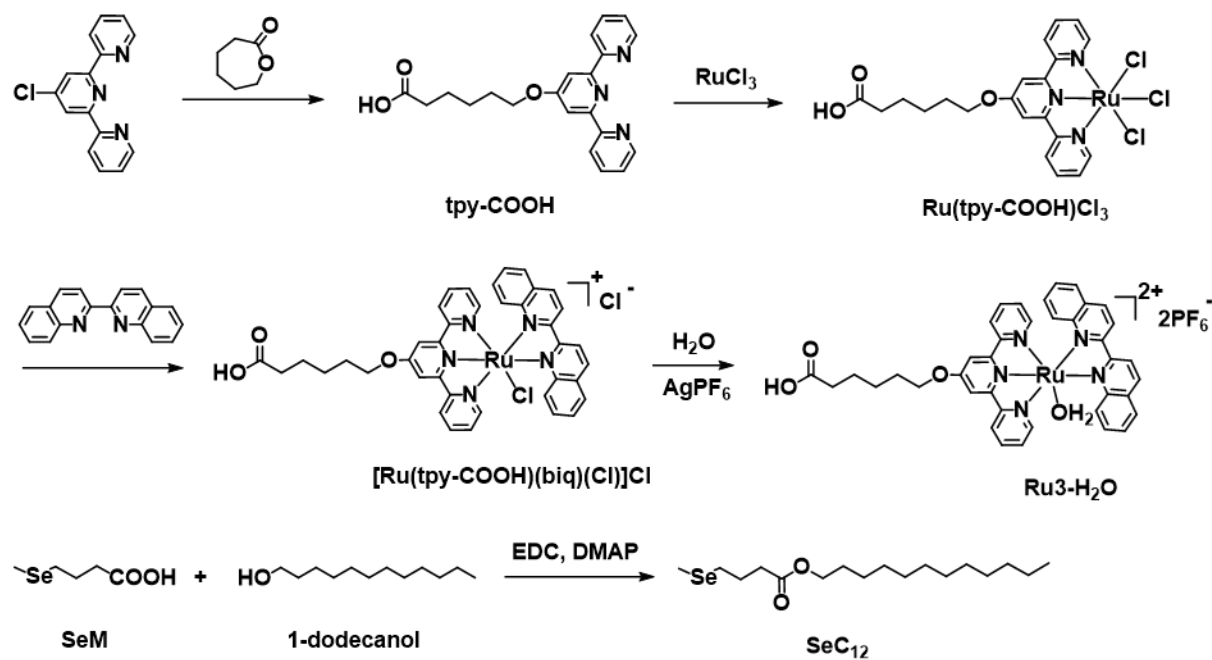
Figure S14. Synthetic routes for Ru3-H$_2$O and SeC$_{12}$.
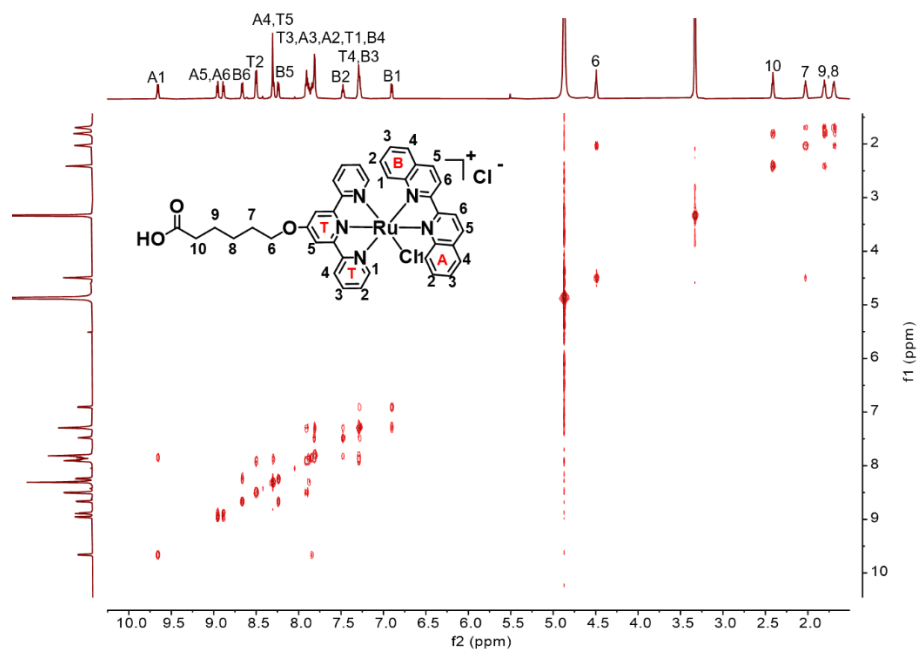
Synthesis of [Ru(tpy-COOH)(biq)(Cl)]Cl (Figure S14)

[Ru(tpy-COOH)(biq)(Cl)]Cl was synthesized according to literature.[27] ^{1}H NMR (700 MHz, CD$_3$OD) (Figure S15) δ (ppm): 9.64 (d, J = 8.8 Hz, 1H), 8.94 (d, J = 8.6 Hz, 1H), 8.87 (d, J = 8.6 Hz, 1H), 8.64 (d, J= 8.9 Hz, 1H), 8.51 (d, J = 8.4 Hz, 2H), 8.32-8.21 (m, 4H), 7.93-7.80 (m, 7H), 7.48 (t, J = 7.8 Hz, 1H), 7.29 (m, 3H), 6.89 (d, J = 9.1 Hz, 1H), 4.50 (t, J = 6.3 Hz, 2H), 2.41 (t, J = 6.3 Hz, 2H), 2.06-1.98 (m, 2H), 1.85-1.60 (m, 4H). ^{13}C NMR (175 MHz, CD$_3$OD) (Figure S17) δ (ppm): 166.74, 162.07, 159.51, 159.15, 158.86, 152.65, 152.02, 151.35, 149.70, 137.80, 137.30, 135.92, 130.60, 130.30, 129.21, 129.00, 128.95, 128.52, 128.31, 128.18, 126.80, 123.66, 120.35, 120.30, 110.11, 69.69, 33.88, 28.36, 25.31, 24.52. MALDI-TOF (m/z): [M-Cl]$^+$, calculated for C$_{39}$H$_{33}$ClN$_5$O$_3$Ru, 756.13, found, 756.11.

Synthesis of Ru3-H$_2$O (Figure S14)

[Ru(tpy-COOH)(biq)(Cl)]Cl was synthesized according to literature.[4] ^{1}H NMR (700 MHz, CD$_3$OD) (Figure S18) δ (ppm): 8.99 (dd, J = 9.1, 9.1 Hz, 2H), 8.74 (d, J = 9.1 Hz, 1H), 8.67 (d, J = 9.1 Hz, 1H), 8.60 (d, J = 8.4 Hz, 2H), 8.43-8.37 (m, 3H), 8.24 (d, J = 8.4 Hz, 1H), 8.03-7.78 (m, 7H), 7.47 (t, J = 7.2 Hz, 1H), 7.39-7.30 (m, 3H), 6.94 (d, J = 9.0 Hz, 1H), 4.57 (t, J = 6.3 Hz, 2H), 2.42 (t, J = 7.2 Hz, 2H), 2.10-2.02 (m, 2H), 1.86-1.68 (m, 4H). ^{13}C NMR (175 MHz, CD$_3$OD) (Figure S20) δ (ppm): 176.06, 168.12, 162.35, 159.52, 159.49, 159.00, 153.71, 152.42, 150.90, 138.90, 138.62, 136.99, 132.03, 131.01, 129.78, 129.51, 129.33, 129.27, 128.53, 128.13, 128.00, 126.15, 124.43, 123.47, 120.95, 120.56, 111.12, 70.07, 33.39, 28.28, 25.21, 24.32. MALDI-TOF (m/z): [M – 2PF$_6$ – H]$^+$, calculated for C$_{39}$H$_{35}$N$_5$O$_4$Ru, 739.17, found, 740.24.

Synthesis of SeC$_{12}$ (Figure S14)

4-(Methylselanyl)butanoic acid (SeM) (364 mg, 2 mmol) and 1-dodecanol (372.4 mg, 2 mmol) were dissolved in 5mL dry DCM. The solution was cooled to 0 °C in an ice bath. EDC (500 mg, 2.5 mmol) and 4-DMAP (24.4 mg, 0.2 mmol) in 5 mL dry DCM were added dropwise into the mixture. The solution was stirred at 0 °C for 2 h, and then kept stirring at room temperature overnight. The crude product was further purified through column chromatography with silica gel (eluent: DCM). Colorless oil was obtained (60 mg, 81%). ^{1}H NMR (300 MHz, CD$_2$Cl$_2$) (Figure S21) δ (ppm): 4.07 (t, J = 6.9 Hz, 2H), 2.55 (t, J = 7.2 Hz, 2H), 2.43 (t, J = 7.5 Hz, 2H), 2.10 (s, 3H), 1.96-1.86 (m, 2H), 1.60-1.59 (m, 2H), 1.41-1.25 (m, 18H), 0.91 (t, J = 6.3 Hz, 3H). ^{13}C NMR (75 MHz, CD$_2$Cl$_2$) (Figure S23) δ (ppm): 173.38, 64.84, 33.76, 33.31, 32.30, 30.02, 29.95, 29.91, 29.89, 29.73, 29.64, 29.02, 26.30, 24.63, 23.07, 15.38, 14.26. MALDI-TOF (m/z): [M]$^+$, calculated for C$_{17}$H$_{34}$O$_2$Se, 350.17, found, 350.52.
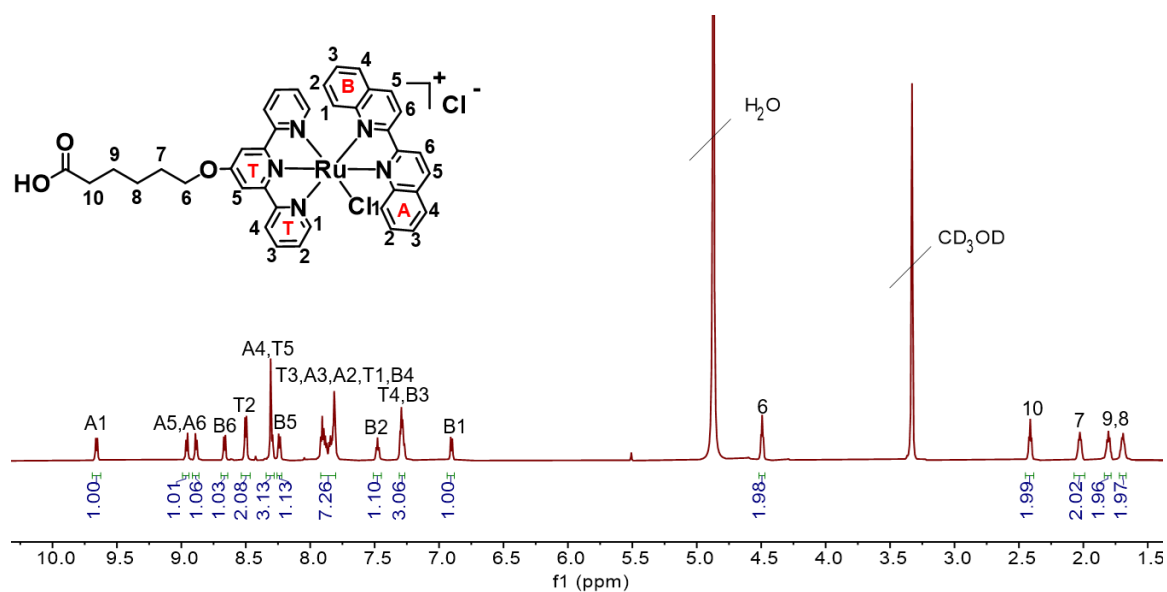
Figure S15. ^{1}H NMR spectrum of [Ru(tpy-COOH)(biq)(Cl)]Cl (700 MHz, CD$_3$OD).

Figure S16. COSY spectrum of [Ru(tpy-COOH)(biq)(Cl)]Cl (700 MHz, CD$_3$OD).
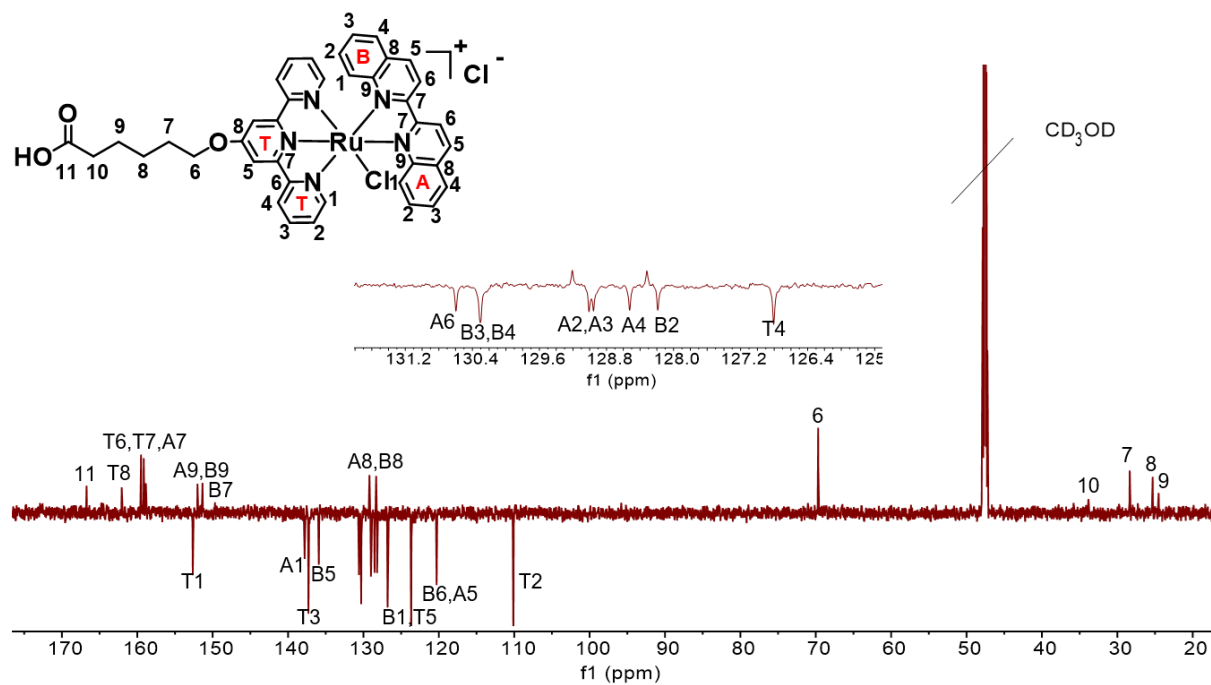
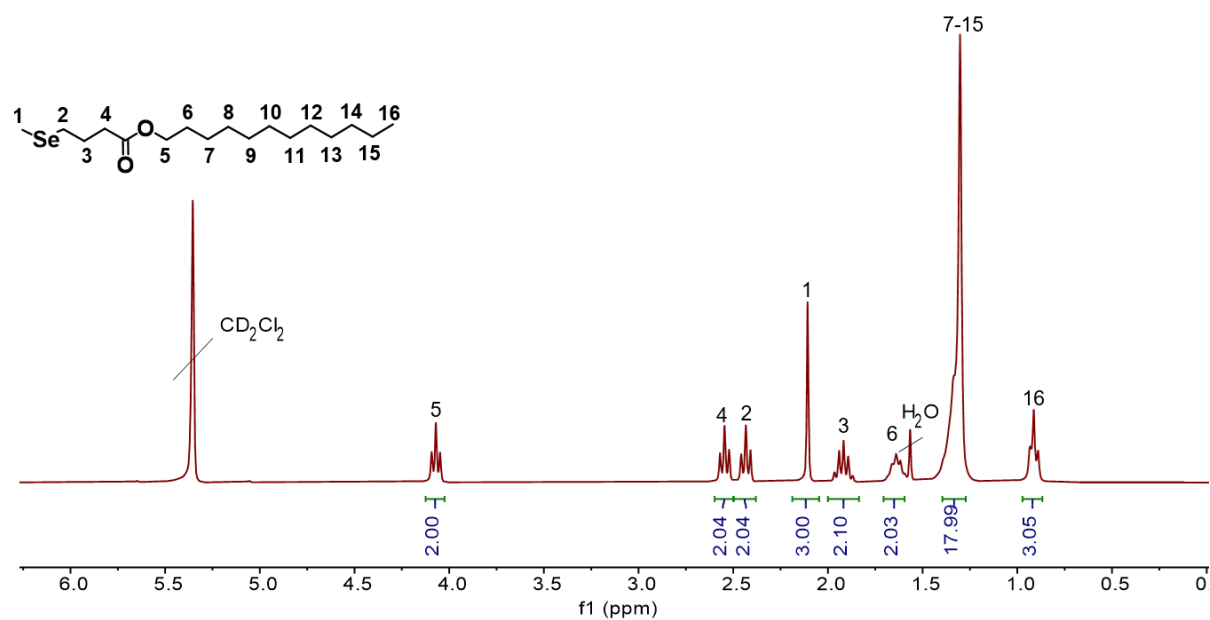**Figure S17.** ^{13}C NMR spectrum of [Ru(tpy-COOH)(biq)(Cl)]Cl (175 MHz, CD$_3$OD).
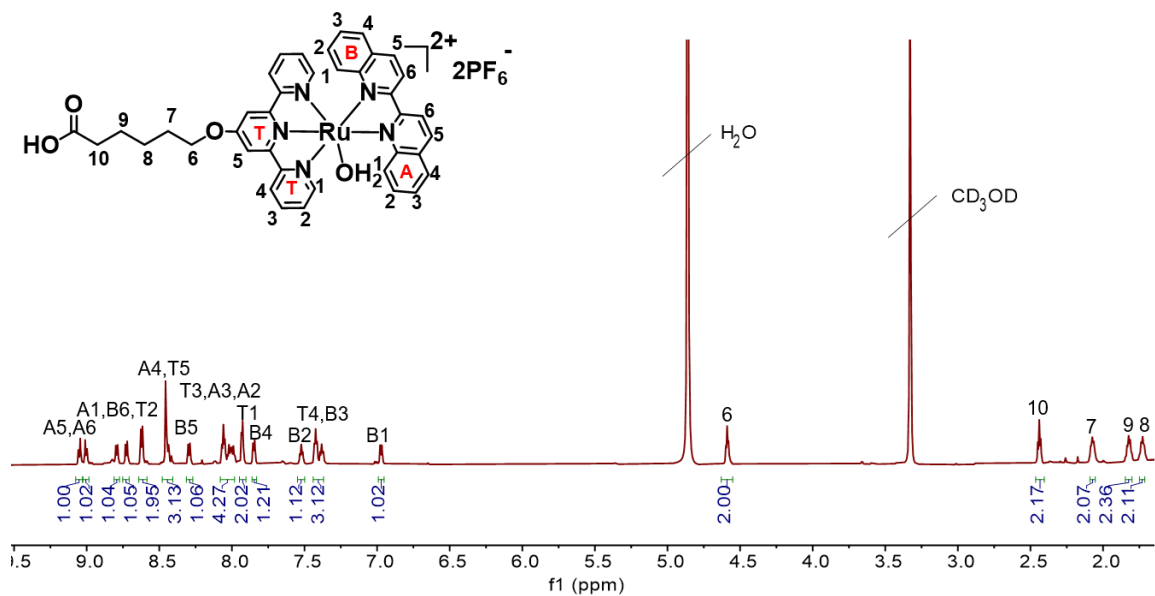
Figure S18. ^{1}H NMR spectrum of Ru3-H$_2$O (700 MHz, CD$_3$OD).
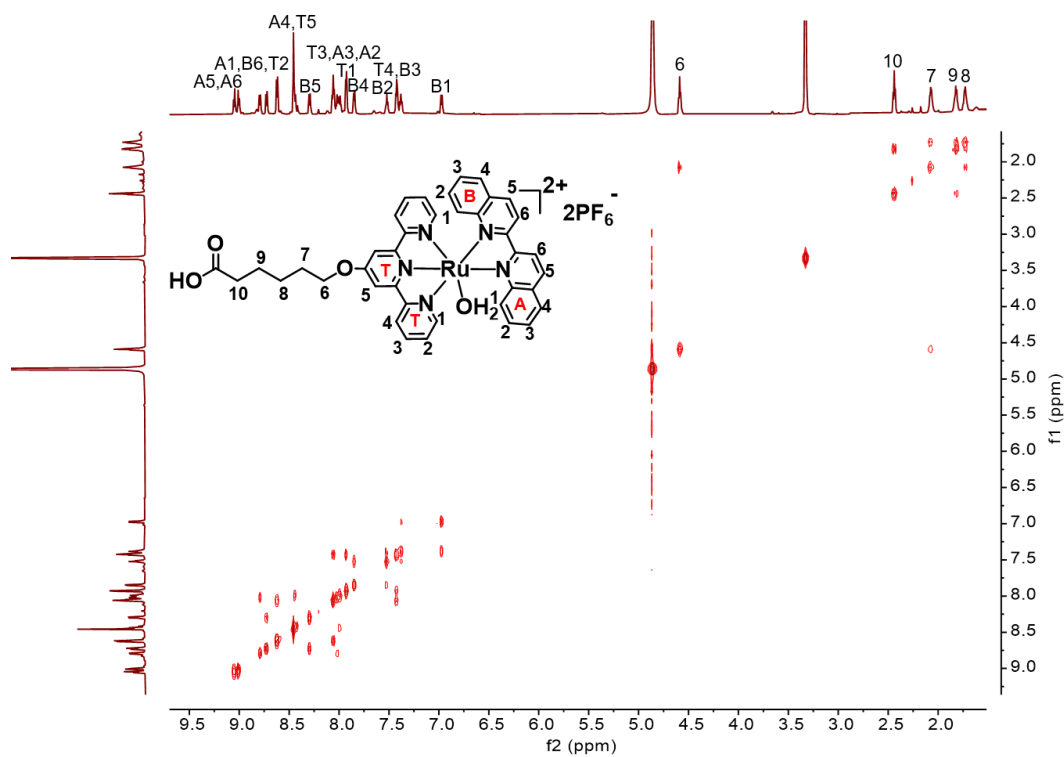
Figure S19. COSY spectrum of Ru3-H$_2$O (700 MHz, CD$_3$OD).
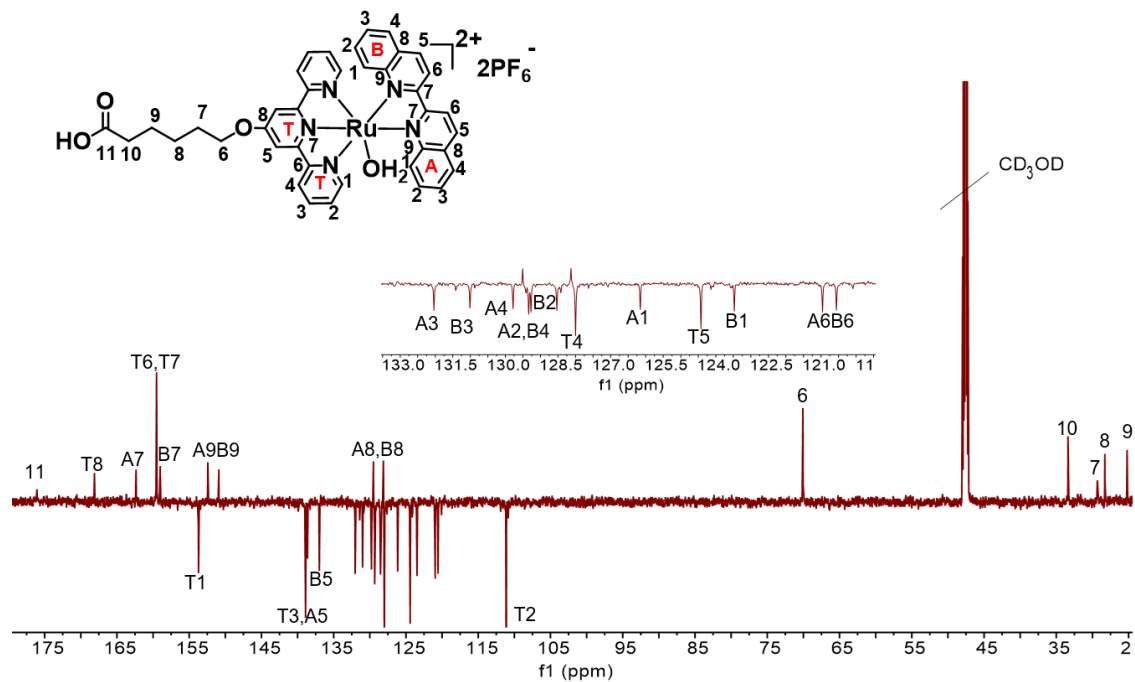
Figure S20. ^{13}C NMR spectrum of Ru3-H$_2$O (175 MHz, CD$_3$OD).

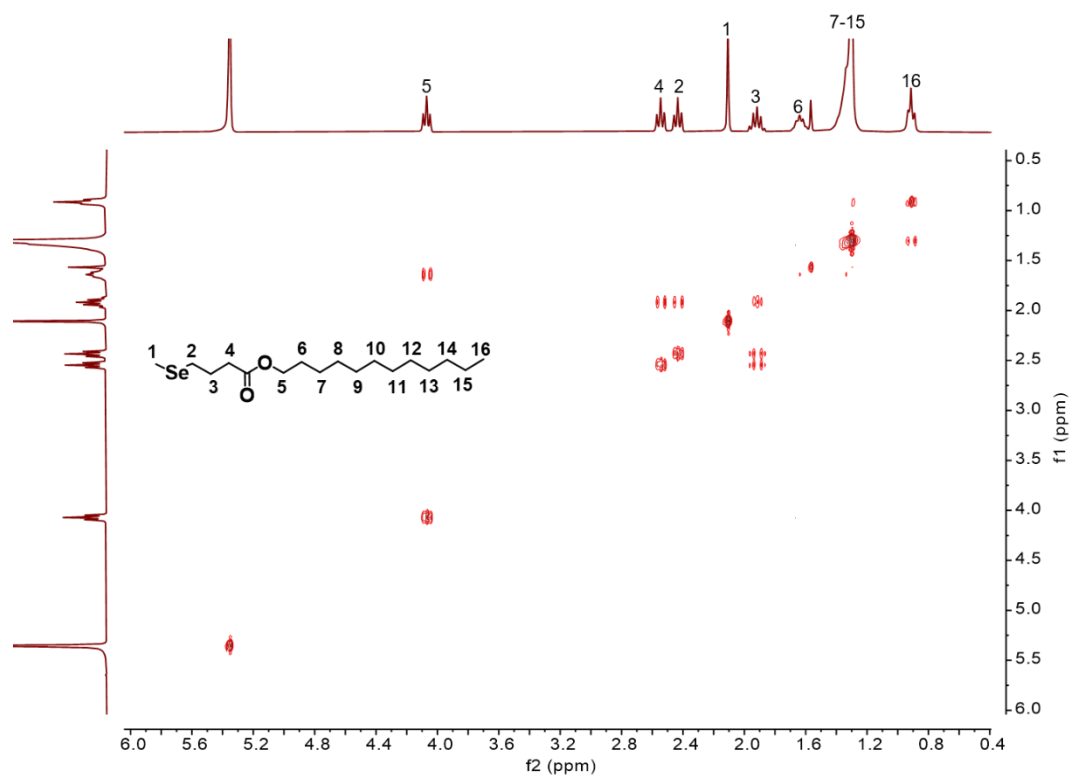**Figure S21.** ^{1}H NMR spectrum of SeC$_{12}$ (300 MHz, CD$_2$Cl$_2$).

Figure S22. COSY NMR spectrum of SeC$_{12}$ (300 MHz, CD$_2$Cl$_2$).
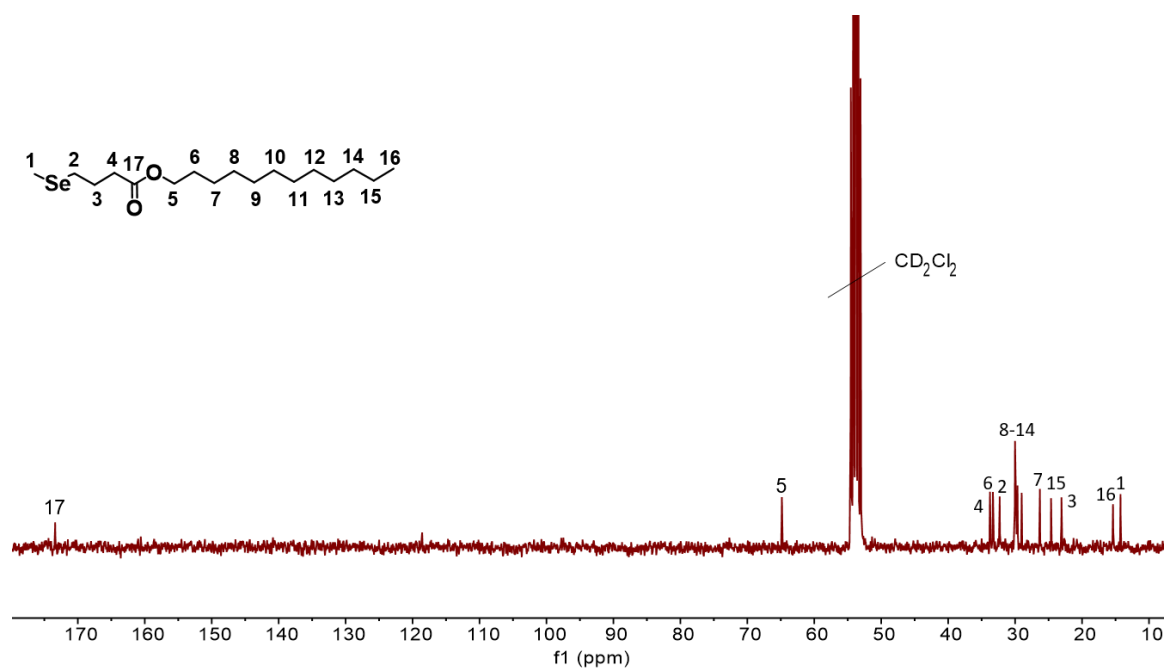
Figure S23. ^{13}C NMR spectrum of SeC$_{12}$ (75 MHz, CD$_2$Cl$_2$).
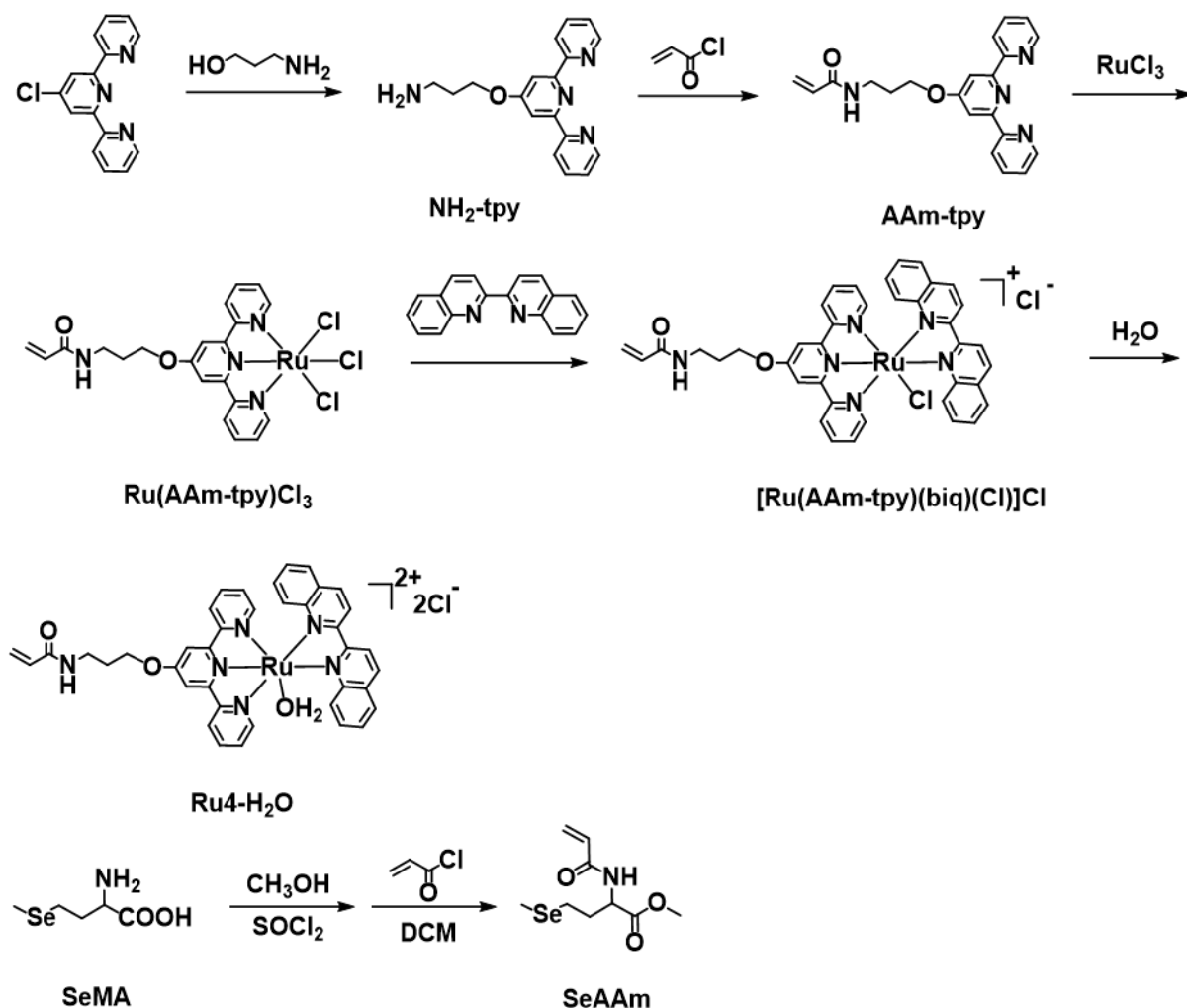
Figure S24. Synthetic routes for Ru4-H$_2$O and SeAAm.

Synthesis of [Ru(AAm-tpy)(biq)(Cl)]Cl (Figure S24)

[Ru(AAm-tpy)(biq)(Cl)]Cl was synthesized according to literature.[28] ^{1}H NMR (700 MHz, CD$_3$OD) (Figure S25) δ (ppm): 9.66 (d, J = 8.5 Hz, 1H), 8.94 (d, J = 8.4 Hz, 1H), 8.89 (d, J = 8.4 Hz, 1H), 8.66 (d, J = 8.9 Hz, 1H), 8.49 (d, J = 8.0 Hz, 2H), 8.31-8.25 (m, 3H), 8.22 (d, J = 8.9 Hz, 1H), 7.92-7.80 (m, 7H), 7.47 (dd, J = 8.8 Hz, 7.1Hz, 1H), 7.32-7.26 (m, 3H), 6.90 (d, J = 8.8 Hz, 1H),

6.34-6.26 (m, 2H), 5.72 (dd, J = 9.8 Hz, 1.9 Hz, 1H), 4.52 (t, J = 6.3 Hz, 2H), 3.61 (t, J = 7.0 Hz, 2H), 2.23 (m, 2H). ^{13}C NMR (175 MHz, CD$_3$OD) (Figure S27) δ (ppm): 166.54, 162.05, 162.99, 159.48, 159.18, 158.85, 152.65, 152.00, 151.35, 137.81, 137.30, 135.94, 130.68, 130.59, 130.35, 130.32, 129.21, 129.00, 128.96, 128.51, 128.31, 128.18, 126.82, 125.43, 123.68, 123.63, 120.33, 120.27, 110.11, 67.33, 35.84, 28.63. MALDI-TOF (m/z): [M-Cl]$^+$, calculated for C$_{39}$H$_{31}$ClN$_6$O$_2$Ru, 753.13, found, 752.94.

Synthesis of Ru4-H$_2$O (Figure S24)

Ru4-H$_2$O ([Ru(AAm-tpy)(biq)(H$_2$O)](Cl)$_2$) was prepared by hydrolysis of [Ru(AAm-tpy)(biq)(Cl)]Cl in water.

Synthesis of SeAAm (Figure S24)

Thionyl chloride (0.8 ml) was dissolved slowly in methanol (4 ml) at -5 ℃ and was stirred at room temperature for 1 h. Afterwards, 2-amino-4-(methylseleno)butanoic acid (SeMA) (0.6 g, 3 mmol) was added to the solution. The mixture was stirred at room temperature for 3 h and then refluxed for 40 min. After the solution was cooled to room temperature, the solvent was removed under reduced pressure. The white solid was redissolved in dry DCM (5 mL). N-(2-hydroxyethyl)acrylamide (0.3 mL, 3 mmol) was added dropwise at 0 ℃ and the solution was stirred at room temperature for 24 h . The crude product was purified through column chromatography with silica gel (eluent: methanol/DCM = 1/10). Colorless oil was obtained. (430 mg, 54.1%). ^{1}H NMR (300 MHz, CD$_2$Cl$_2$) (Figure S28) δ (ppm): 6.50-6.38 (m, 1H), 6.31-6.15 (m, 2H), 5.71 (dd, J = 9.4 Hz, 1.8 Hz , 1H), 4.76 (m, 1H), 3.77 (s, 3H), 2.60-2.53 (m, 2H), 2.28-2.10 (m, 2H), 2.01 (s, 3H). ^{13}C NMR (75 MHz, CD$_2$Cl$_2$) (Figure S30) δ (ppm): 172.68, 165.35, 130.84, 127.14, 52.72, 41.28, 33.26, 20.62, 4.20.
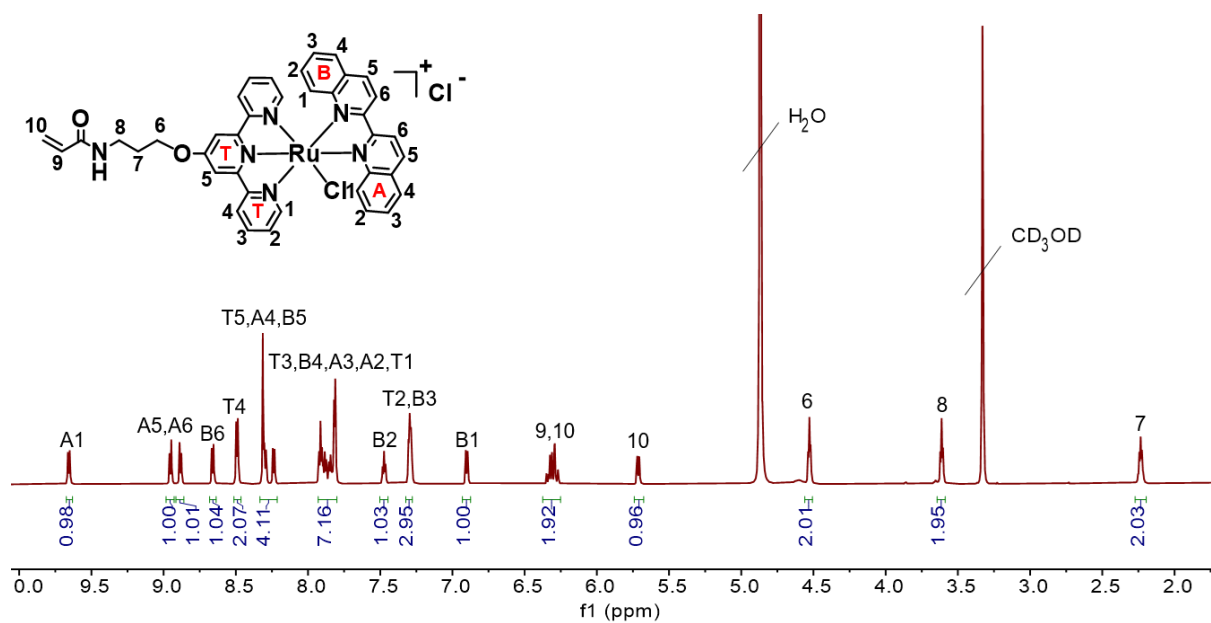
Figure S25. ^{1}H NMR spectrum of [Ru(AAm-tpy)(biq)(Cl)]Cl (700 MHz, CD$_3$OD).
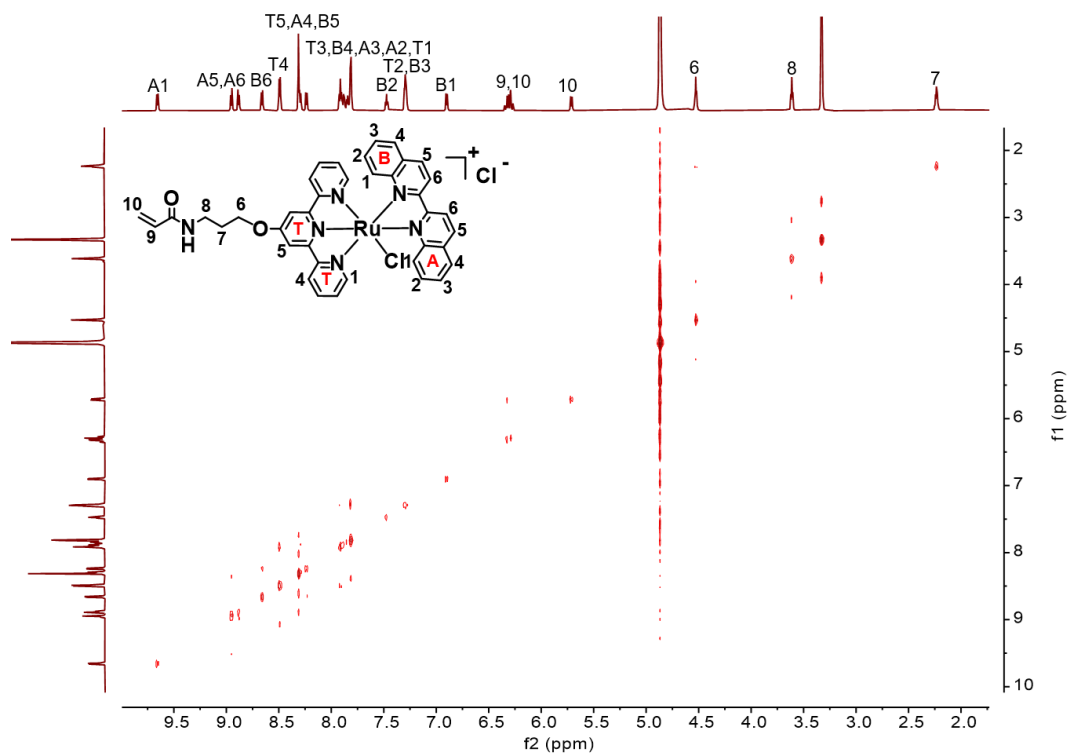
Figure S26. COSY NMR spectrum of [Ru(AAm-tpy)(biq)(Cl)]Cl (700 MHz, CD$_3$OD).
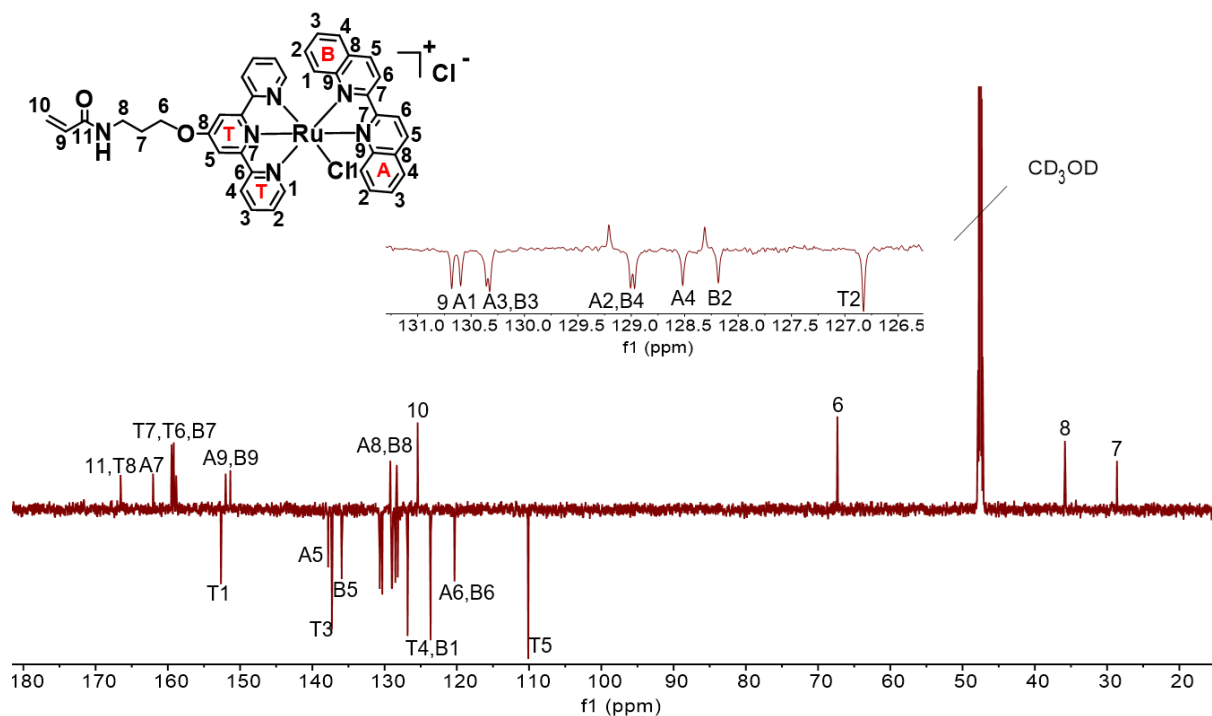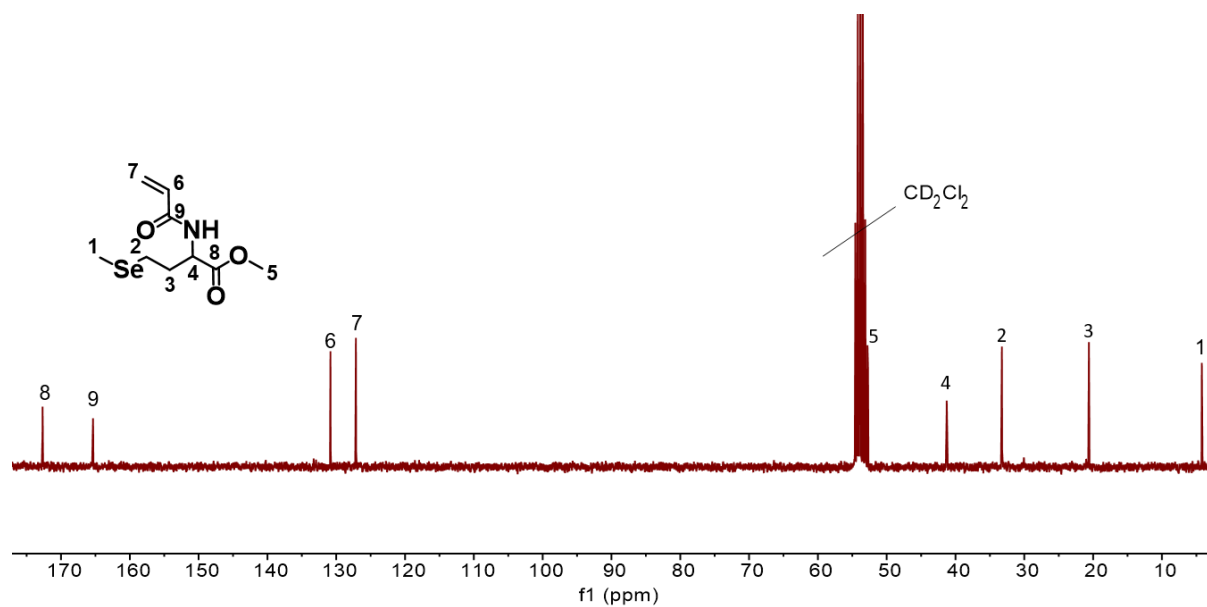
Figure S27. ^{13}C NMR spectrum of [Ru(AAm-tpy)(biq)(Cl)]Cl (175 MHz, CD$_3$OD).
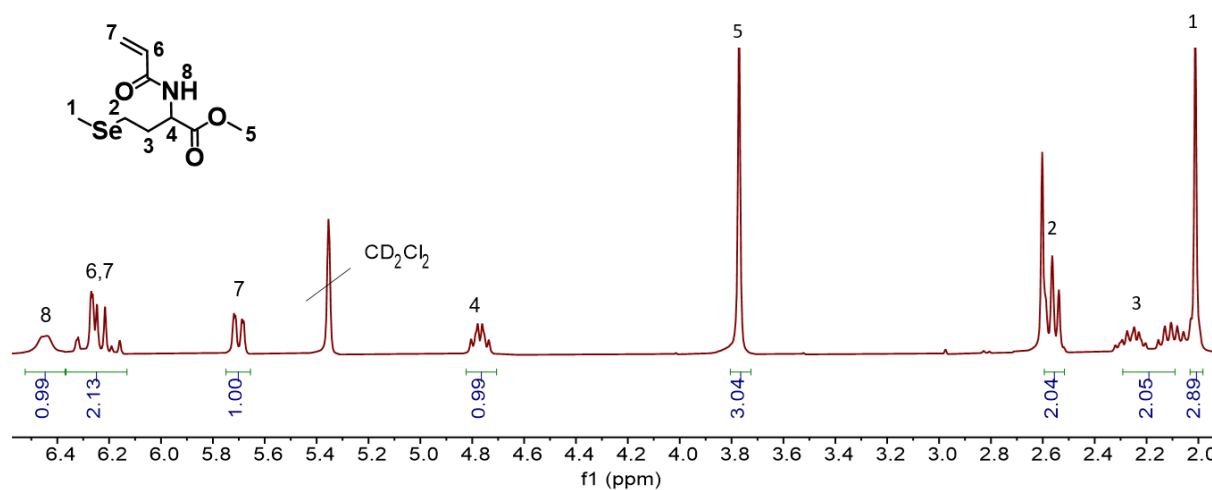
Figure S28. ^{1}H NMR spectrum of SeAAm (300 MHz, CD$_2$Cl$_2$).
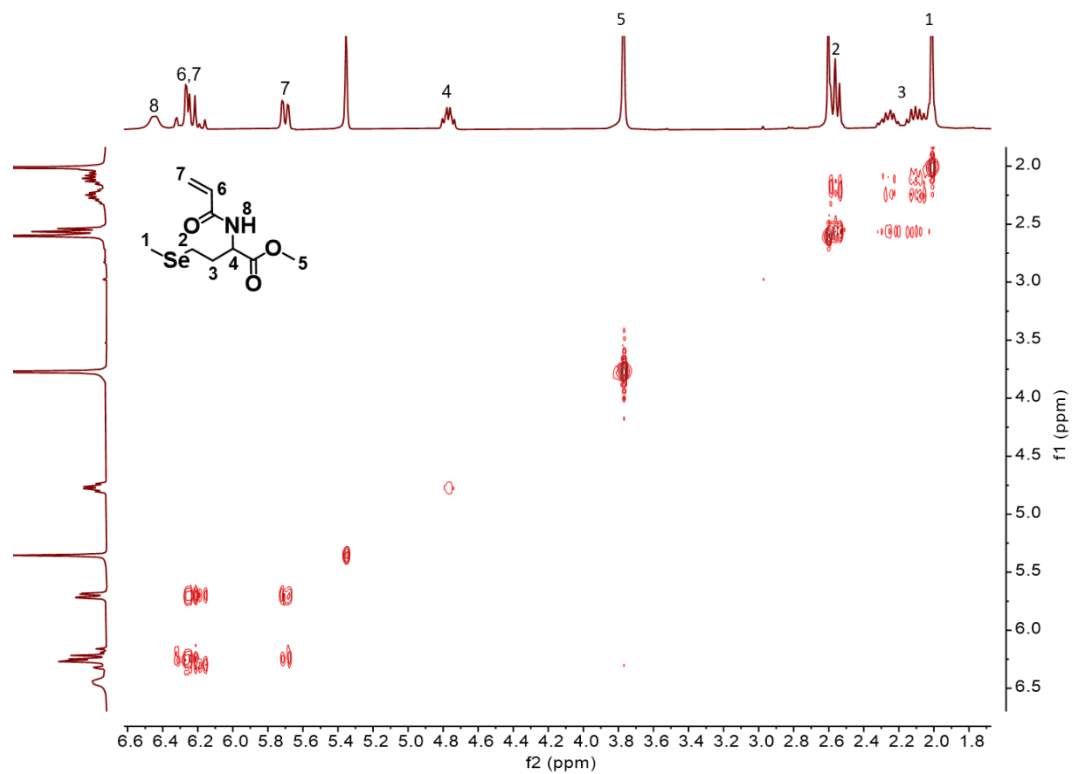
Figure S29. COSY NMR spectrum of SeAAm (300 MHz, CD$_2$Cl$_2$).

Figure S30. ^{13}C NMR spectrum of SeAAm (75 MHz, CD$_2$Cl$_2$).

3.5 Acknowledgements

3.6 Reference

[1] Hoffman, A. S., Hydrogels for biomedical applications. *Advanced drug delivery reviews* **2012,** *64*, 18-23.

[2] Sun, W.; Wen, Y.; Thiramanas, R.; Chen, M.; Han, J.; Gong, N.; Wagner, M.; Jiang, S.; Meijer, M. S.; Bonnet, S., Red-Light-Controlled Release of Drug–Ru Complex Conjugates from Metallopolymer Micelles for Phototherapy in Hypoxic Tumor Environments. *Advanced Functional Materials* **2018,** *28* (39), 1804227.

[3] Zeng, X.; Wang, Y.; Han, J.; Sun, W.; Butt, H. J.; Liang, X. J.; Wu, S., Fighting against Drug-Resistant Tumors using a Dual-Responsive Pt (IV)/Ru (II) Bimetallic Polymer. *Advanced Materials* **2020,** *32* (43), 2004766.

[4] Xiao, M.; Jiang, C.; Shi, F., Design of a UV-responsive microactuator on a smart device for light-induced ON-OFF-ON motion. *NPG Asia Materials* **2014,** *6* (9), e128.

[5] Holub, J.; Vantomme, G.; Lehn, J.-M., Training a constitutional dynamic network for effector recognition: Storage, recall, and erasing of information. *Journal of the American Chemical Society* **2016,** *138* (36), 11783-11791.

[6] Zhang, K.; Zhang, M.; Feng, X.; Hempenius, M. A.; Vancso, G. J., Switching light transmittance by responsive organometallic poly (ionic liquid) s: control by cross talk of thermal and redox stimuli. *Advanced functional materials* **2017,** *27* (41), 1702784.

[7] Meng, H.; Li, G., Reversible switching transitions of stimuli-responsive shape changing polymers. *Journal of Materials Chemistry A* **2013,** *1* (27), 7838-7865.

[8] Ionov, L.; Minko, S.; Stamm, M.; Gohy, J.-F.; Jérôme, R.; Scholl, A., Reversible chemical patterning on stimuli-responsive polymer film: Environment-responsive lithography. *Journal of the American Chemical Society* **2003,** *125* (27), 8302-8306.

[9] Gohy, J.-F.; Zhao, Y., Photo-responsive block copolymer micelles: design and behavior. *Chemical Society Reviews* **2013,** *42* (17), 7117-7129.

[10] Tian, Z.; Li, A. D., Photoswitching-enabled novel optical imaging: innovative solutions for real-world challenges in fluorescence detections. *Accounts of chemical research* **2013,** *46* (2), 269-279.

[11] Rack, J. J.; Winkler, J. R.; Gray, H. B., Phototriggered Ru (II)-dimethylsulfoxide linkage isomerization in crystals and films. *Journal of the American Chemical Society* **2001,** *123* (10), 2432-2433.

[12] Wu, S.; Duan, S.; Lei, Z.; Su, W.; Zhang, Z.; Wang, K.; Zhang, Q., Supramolecular bisazopolymers exhibiting enhanced photoinduced birefringence and enhanced stability of birefringence for four-dimensional optical recording. *Journal of Materials Chemistry* **2010,** *20* (25), 5202-5209.

[13] Balzani, V.; Credi, A.; Venturi, M., Light powered molecular machines. *Chemical Society Reviews* **2009,** *38* (6), 1542-1550.

[14] Balzani, V.; Clemente-León, M.; Credi, A.; Ferrer, B.; Venturi, M.; Flood, A. H.; Stoddart, J. F., Autonomous artificial nanomotor powered by sunlight. *Proceedings of the National Academy of Sciences* **2006,** *103* (5), 1178-1183.

[15] Bahreman, A.; Limburg, B.; Siegler, M. A.; Koning, R.; Koster, A. J.; Bonnet, S., Ruthenium polypyridyl complexes hopping at anionic lipid bilayers through a supramolecular bond sensitive to visible light. *Chemistry–A European Journal* **2012,** *18* (33), 10271-10280.

[16] Higgins, S. L.; Brewer, K. J., Designing Red-Light-Activated Multifunctional Agents for the Photodynamic Therapy. *Angewandte Chemie International Edition* **2012,** *51* (46), 11420-11422.

[17] Gulzar, A.; Gai, S.; Yang, P.; Li, C.; Ansari, M. B.; Lin, J., Stimuli responsive drug delivery application of polymer and silica in biomedicine. *Journal of Materials Chemistry B* **2015,** *3* (44), 8599-8622.

[18] Zhou, H.; Xue, C.; Weis, P.; Suzuki, Y.; Huang, S.; Koynov, K.; Auernhammer, G. K.; Berger, R.; Butt, H.-J.; Wu, S., Photoswitching of glass transition temperatures of azobenzene-containing polymers induces reversible solid-to-liquid transitions. *Nature chemistry* **2017,** *9* (2), 145-151.

[19] Chen, M.; Yao, B.; Kappl, M.; Liu, S.; Yuan, J.; Berger, R.; Zhang, F.; Butt, H. J.; Liu, Y.; Wu, S., Entangled Azobenzene-Containing Polymers with Photoinduced Reversible Solid-to-Liquid Transitions for Healable and Reprocessable Photoactuators. *Advanced Functional Materials* **2020,** *30* (4), 1906752.

[20] Trads, J. B.; Hüll, K.; Matsuura, B. S.; Laprell, L.; Fehrentz, T.; Görldt, N.; Kozek, K. A.; Weaver, C. D.; Klöcker, N.; Barber, D. M., Sign inversion in photopharmacology: Incorporation of cyclic

azobenzenes in photoswitchable potassium channel blockers and openers. *Angewandte Chemie International Edition* **2019,** *58* (43), 15421-15428.

[21] Muraoka, T.; Kinbara, K.; Aida, T., A self-locking molecule operative with a photoresponsive key. *Journal of the American Chemical Society* **2006,** *128* (35), 11600-11605.

[22] Zhang, Y.; Tamijani, A. A.; Taylor, M. E.; Zhi, B.; Haynes, C. L.; Mason, S. E.; Hamers, R. J., Molecular surface functionalization of carbon materials via radical-induced grafting of terminal alkenes. *Journal of the American Chemical Society* **2019,** *141* (20), 8277-8288.

[23] van Leeuwen, T.; Lubbe, A. S.; Štacko, P.; Wezenberg, S. J.; Feringa, B. L., Dynamic control of function by light-driven molecular motors. *Nature Reviews Chemistry* **2017,** *1* (12), 96.

[24] Wang, Z.; Wang, N.; Cheng, S.-C.; Xu, K.; Deng, Z.; Chen, S.; Xu, Z.; Xie, K.; Tse, M.-K.; Shi, P., Phorbiplatin, a highly potent Pt (IV) antitumor prodrug that can be controllably activated by red light. *Chem* **2019,** *5* (12), 3151-3165.

[25] Sun, W.; Li, S.; Haupler, B.; Liu, J.; Jin, S.; Steffen, W.; Schubert, U. S.; Butt, H. J.; Liang, X. J.; Wu, S., An Amphiphilic Ruthenium Polymetallodrug for Combined Photodynamic Therapy and Photochemotherapy In Vivo. *Advanced Materials* **2017,** *29* (6).

[26] Al-Afyouni, M. H.; Rohrabaugh, T. N.; Al-Afyouni, K. F.; Turro, C., New Ru (II) photocages operative with near-IR light: new platform for drug delivery in the PDT window. *Chemical science* **2018,** *9* (32), 6711-6720.

[27] Xie, C.; Sun, W.; Lu, H.; Kretzschmann, A.; Liu, J.; Wagner, M.; Butt, H.-J.; Deng, X.; Wu, S., Reconfiguring surface functions using visible-light-controlled metal-ligand coordination. *Nature communications* **2018,** *9*, 3842.

[28] Liu, J.; Xie, C.; Kretzschmann, A.; Koynov, K.; Butt, H. J.; Wu, S., Metallopolymer Organohydrogels with Photo-Controlled Coordination Crosslinks Work Properly Below 0° C. *Advanced Materials* **2020,** *32* (14), 1908324.

Chapter 4 Summary and Outlook

4.1 Summary

We successfully characterize a new dynamic bond containing Ru-Se which is responsive to visible light. The new photodynamic bond Ru-Se could form in the dark condition between Ru backbone and a selenoether ligand. When the mixture carrying Ru-Se bond was irradiated by visible light, the new Ru-Se bond was photocleaved. Moreover, this new bond could reversibly form and dissociate with dark and light irradiation transitions. These features have been fully characterized by nuclear magnetic resonance (NMR) and UV-vis spectroscopy. The thermodynamic and kinetic data for the thermal coordination and photosubstitution of Ru-Se model complexes are calculated.

We also designed and synthesized a few visible light responsive complexes containing the Ru-Se bonds for different functional applications. 1) An amphiphile with Ru-Se bonds showed reversible morphological transitions between spherical micelles and bowl-shaped assemblies in the dark/light irradiation cycles; 2) A surface substrate modified with Ru-Se compounds exhibited photoswitchable wettability; 3) A Ru-Se bond acted as crosslinks in polymer gel could undergo photoinduced reversible sol-gel transitions, which showed reshaping and self-healing properties. I expect this work could open avenues for both of fundamental studies of dynamic bonds and applications of functional materials.

4.2 Outlook

There are still several open questions and challenges for constructing new photodynamic bonds and reconfigurable photoresponsive materials based on Ru complexes. First, it will be better that the activated wavelength of designed Ru complexes can be red-shifted to near-infrared (NIR) region attributed by deep penetration of NIR light in biology applications. Although two-photon process or upconverting nanoparticle (UCNP) has been introduced for NIR light activation, both methods are inefficient non-linear optical processes. The photosubstituted ligands with modified functional groups should be taken into consideration.

Second, the complete characterization methods of photodynamic bonds need to be further investigated. The bond energy and activation energy determinations of photodynamic bonds still meet problems. This important factor could help us to understand whether the photodynamic bonds are reversibly controlled under the specific condition.

Third, in the thesis, only three photocontrolled Ru-Se complexes are designed for photoresponsive materials. We can expect more smart materials can be constructed by Ru complexes. We believe reconfigurable Ru complexes also have great potential to perform in lithology, actuators, and photoswitchable porous materials.

Publications

1. **<u>Jianxiong Han</u>**, Chaoming Xie, Yun-Shuai Huanga, Manfred Wagner, Wendong Liu, Xiaolong Zeng, Jiahui Liu, Shijie Sun, Kaloian Koynov, Hans-Jürgen Butt and Si Wu*. Ru-Se Coordination: A New Dynamic Bond for Visible Light-Responsive Materials. *Journal of the American Chemical Society, 2021, 143, 12736−12744.*

2. **<u>Jianxiong Han</u>**, Yun-shuai Huang, Ni Yang, and Si Wu*. Reconfigurable Materials Based on Photocontrolled Metal–Ligand Coordination. *Advanced Intelligent System, 2020, 2, 2000112*

3. Xiaolong Zeng, Yufei Wang, **<u>Jianxiong Han</u>**, Wen Sun, Hans-Jürgen Butt, Xing-Jie Liang*, Si Wu*. Fighting against Drug‐Resistant Tumors using a Dual‐Responsive Pt (IV)/Ru (II) Bimetallic Polymer. *Advanced Materials, 2020, 32, 2004766.*

4. Wen Sun, Yan Wen, Raweewan Thiramanas, Mingjia Chen, **<u>Jianxiong Han</u>**, Ningqiang Gong, Manfred Wagner, Shuai Jiang, Michael S. Meijer, Sylvestre Bonnet, Hans-Jürgen Butt, Volker Mailänder,* Xing-Jie Liang,* and Si Wu*. Red-Light-Controlled Release of Drug-Ru Complex Conjugates from Metallopolymer Micelles for Phototherapy in Hypoxic Tumor Environments. *Advanced Functional Materials, 2018, 28, 1804227*

Acknowledgment

During my PhD period, a lot of nice people really helped me a lot to finish this nice journey. Here is my deepest appreciation to all of you.

First of all, I would like to give my biggest respect and sincerely acknowledge my supervisor for giving me the chance to study in your group as a Ph.D. student. During the past 4 years, you are always kind, warm and patient to all group members. I sincerely appreciate your scientific guidance, enthusiasm discussion and encouragement. I really wish to be a better man like you in both scientific area and daily life.

Then, I would like to appreciate my project leader with your guidance to a new and challenging research area. You always help me to solve my problems with your rich experience. Without your suggestions and comments, I cannot finish the project by myself. I really want to learn from your critical and cautious attitude on everything even tiny details.

I would like to thank my colleagues and collaborators who support me during the past time. I appreciate for the helpful NMR measurements and discussions, for his help on organic synthesis, for his SEM measurements and discussions. Their kind assistances make progress on my project.

Additionally, I am grateful to the members of our sub-group

. I will never forget the happy time we experienced together. You brought me a lot of joy and gave me encouragement during the past years.

In the end, I would like sincerely appreciate my family. I can always have your motivating words when I feel depressed. Thank you very much for your endless love, warm support and encouragement.